Fundamental Study on Development of Micro Actuators Driven by Liquid Crystals

Chunbo Liu

A dissertation submitted to
Kochi University of Technology
in partial fulfillment of the requirements
for the degree of

Doctor of Philosophy

Special Course for International Students
Department of Engineering
Graduate School of Engineering
Kochi University of Technology
Kochi, Japan

March 2007

Abstract

Liquid crystal is the state between solid and liquid, so it has properties of both of the two materials: the fluidity like general liquid and the anisotropy like solid. Because of the special properties, liquid crystal technology has a major effect on many areas of science and engineering, as well as device technology. The most common and successful application of liquid crystal technology is liquid crystal displays (LCD). This field has grown into a multi-billion dollar industry, and many significant scientific and engineering discoveries have been made. But as one state of materials, liquid crystal should be applied on more fields like the other three states, so it is important to explore new applying field. In this dissertation as an attempt, we propose novel micro-actuator driven by liquid crystalline materials.

An actuator is the mechanism by which an agent acts upon an environment. The agent can be either an artificial intelligent agent or any other autonomous being (human, other animal, etc). It can be used to cause a device to be turned on or off, adjusted or moved. For example, the motor and mechanism that moves the head assembly on a disk drive or an arm of a robot all can be called an actuator. Micro-actuator, as its name suggests, is actuator whose size is very small, usually within nano or micro-meter. Until now, there are many kinds of micro-actuator are developed in order to satisfy different application request of the industry, science and technology field. For example, on the space flight filed, electromagnetic, thermomechanical, and piezoelectric actuators are widely used. The demands which people request from the micro-actuator are: micro size, high efficiency in converting one kind of energy into mechanical work, better adaptability to the work surrounding, short response time, easy to realize accurate control etc. The actuators discussed as examples above can satisfy one or two of the requests. If we can develop one kind of micro-actuator which can satisfy more than three requests above, it must become excellent one. Micro-actuator driven by liquid crystal is a challenge to the goal and the advantages of it are:

1. Driven by low voltage
2. Simple structure and micro- or nano-meter size
3. Ever-changing shape
4. Realize of micromanipulation

The role of the liquid crystals in the actuators is to convert electric energy into kinetic energy. When electric energy is applied to liquid crystals, the rotation of the constitutive rod-like molecules occurs, and then liquid crystalline flow will be induced. The flow

can be utilized as the kinetic source of the actuators. As fundamental research, in this dissertation, transient behaviors of a nematic liquid crystal between two parallel plates under an electric field have been investigated numerically by using the Leslie-Ericksen theory as a constitutive equation and we focus our attention on the effect of various parameters, such as the twist angle ϕ_w (the difference of angle ϕ between the upper plate and the lower plate), an applied voltage and its waveform, and the size of the actuator, on the performance of the actuators to identify the optimized parameters. We have used the Crank-Nicolson scheme for the time integration, and a finite difference scheme for spatial discretization. The material constants, such as viscosity coefficients, elastic constants, and dielectric constants of 5CB (4-n-pentyl-4'- cyano-biphenyl) have been employed in this computation.

At first, we discuss about our simulation results of the liquid crystalline flows, induced by the imposition of the electric field, between fixed parallel plates. Imposition of an electric field on a liquid crystal induces flow (so called back-flow), whose profile and magnitude depend strongly on the twist angle of the director; when the twist angle is 0 deg, the induced flow is planar and the velocity profile between plates is S-shaped and anti-symmetric with respect to the center plane of the two plates. With increasing the twist angle, the flow has an out of plane component, and finally the profile becomes unidirectional when the twist angle reaches 180 deg and the magnitude of the shear stress decreases with the increasing of the twist angle.

With the increment of the applied voltage, the shear stress acting on the plate, the velocity, and the flow rate are increased and the response is improved. The effect of the gap of the plates is large; when the gap is reduced to 5 μm, for example, the response is so high that the physical quantities become maxima within a couple of milliseconds. However, if the electric field intensity is kept constant, the effect of the gap is negligible. The tilt angle has comparatively little effect.

The simplest way to take the force out of the liquid crystal is through the bounding plate, so as a next step, one of the plates of the cell is set to be free, thus the upper plate will move freely when the induced liquid crystalline flow shear stress is exerted on it. In addition to this, this time, in order to induce continuous flow with liquid crystal, we use AC power supply in stead of the DC one in this step, from the results it can be say that the upper plate can be driven to move continuously by the induced liquid crystalline flow, and by changing the frequency of the AC power supply, smoother movement of the upper plate can be achieved. In addition to this, the frequency and the duty also have effect on the moving velocity of the plate, for a specific liquid crystalline cell which is

decided by the gap of the two plates and the orientation conditions, we always can find an optimum applied voltage including the magnitude and the waveform to achieve the fastest velocity of the upper plate. The gap is also an important factor that is must be considered when to design the actuator. When the gap is smaller than 60 μm, the rotate angle range of the director can be controlled by the selecting parameters such as the voltage, the frequency, etc, but in the case that the gap is larger than 60μm, it is impossible to do this. We also did experiments together with the simulation, and the results are in well agreement.

In this dissertation, we discussed the possibility of applying the liquid crystalline materials to the filed of micro-actuator through the simulation of liquid crystalline flow induced by the imposition of the electric filed between parallel plates. It is found from the results obtained in this study that liquid crystalline micro-actuators with arbitrary characteristics can be developed by controlling properly applied voltage, size of actuators, and anchoring conditions.

List of content

Chapter 1: General introduction

1.1 Liquid crystal

1.1.1 Introduction

It is well known that there are three common states of materials: solid, liquid and gas. For example, water is solid below 0°C, liquid between 0°C and 100°C, and gas above 100°C. However, this simplified classification is not good for all the materials. For some materials, the fourth state exists such as liquid crystal. Liquid crystal is state which is sometimes observed to occur between the solid and the liquid state.

As showing in the figure 1-1, the distinguishing characteristic of the liquid crystalline state is the tendency of the molecules to point along a common axis, called the director (showing in the figure 1-1 by red arrow). This is in contrast to molecules in the liquid phase, which have no intrinsic order, and in the solid state, molecules are highly ordered in position and orientation. The first observations of liquid crystalline behavior were made towards the end of the last century, and several thousands of organic compounds are known now to form liquid crystals. An essential requirement for liquid crystal phase to occur is that the molecule must be highly geometrically anisotropic in shape, like a rod or a disc [1]. Discussion of liquid crystal in this dissertation is restricted to small long-rod molecule.

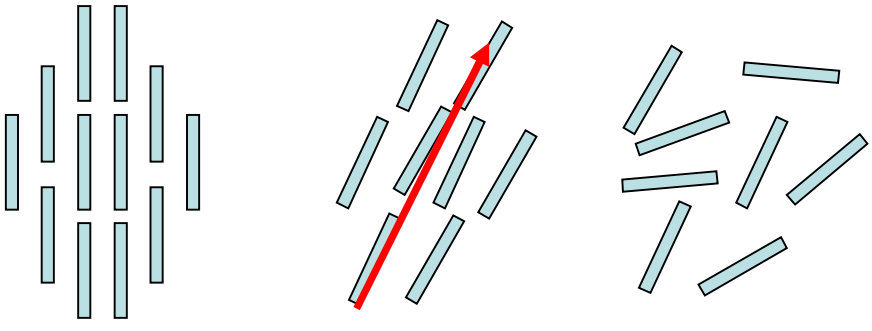

Figure 1-1 Liquid crystal state

1.1.2 Liquid crystalline phases

The various liquid crystalline phases can be characterized by the type of ordering that is present. The ordering can be distinguished into positional order (whether or not molecules are arranged in any sort of ordered lattice) and orientational order (whether or not molecules are pointing in the same direction), and moreover order can be either short-range (only between molecules close to each other) or long-range (extending to larger, sometimes macroscopic, dimensions).

Thermotropic liquid crystals [2]

Thermotropic phases are those that occur in a certain temperature range. Most liquid crystal of this kind will have an isotropic phase at high temperature. That is, heating will eventually drive them in to a conventional liquid phase characterized by random and isotropic molecular ordering (little to no long-range order), and fluid-like flow behavior. Under other conditions (for instance, lower temperature), the liquid crystal might inhabit one or more phases with significant anisotropic orientational structure and long-range orientational order while still having an ability to flow. At too low temperature, most liquid crystal materials will form a conventional (though anisotropic) crystal. Many thermotropic liquid crystals exhibit a variety of phases as temperature is changed. Until now, there are four kinds of thermotropic liquid crystals have been found.

1. Nematic phase

One of the most common liquid crystalline phases is the nematic, where the molecules have no positional order, but they do have long-range orentational order. Thus, the molecules flow and are randomly distributed as in a liquid, but they all point in the same direction (within each domain). Most nematics are uniaxial: they have one axis that is longer and preferred, with the other two being equivalent (can be approximated as cylinders). Some liquid crystals are biaxial nametics, meaning that in addition to orienting their long axis, they also orient along a secondary axis.

2. Smectic phase

The smectic phase is one where in addition to the orientation order; the mesogens are grouped into layers, enforcing long-range positional order in one direction. In the smetic

A phase, the molecules point perpendicular to the layer planes, whereas in the smectic C phase, the molecules are tilted with respect to the layer planes.

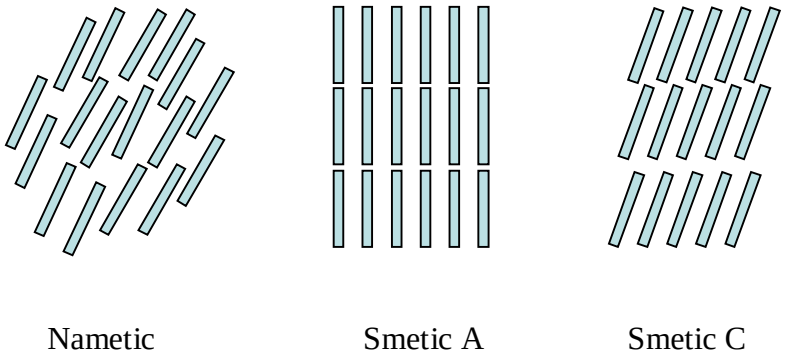

Figure 1-2 Array of the liquid crystalline molecule

3. Chiral phases

The chiral nematic phase exhibits chirality (handedness). This phase is often called the cholesteric phase because it was first observed for cholesterol derivatives. Only chiral molecules (i.e.: those that lack inversion symmetry can give rise to such a phase. This phase exhibits a twisting of the molecules along the director, with the molecular axis perpendicular to the director. The finite twist angle between adjacent molecules is due to their asymmetric packing, which results in longer-range chiral order. An important characteristic of chiral phase is the pitch which refers to the distance (along the director) over which the mesogens undergo a full 360° twist (but note that the structure repeats itself every half-pitch, since the positive and negative directions along the director are equivalent). The pitch may be varied by adjusting of liquid crystals; the pitch is on the same order as the wavelength of visible light. This causes these systems to exhibit unique optical properties, such as selective reflection. These properties are exploited in a number of optical applications.

4. Discotic phases

Disk-shaped mesogens can orient themselves in a layer-like fashion known as the discotic nematic phase. If the disks pack into stacks, the phase is called a discotic columnar. The columns themselves may be organized in to rectangular or hexagonal arrays. Chiral discotic phases, similar to the chiral nematic phase, are also known.

Lyotropic liquid crystals

Different from the thermotropic liquid crystals, a lyotropic liquid crystal consists of two or more components that exhibit liquid-crystalline properties in certain concentration ranges. In the lyotropic phases, solvent molecules fill the space around the compounds to provide fluidity to the system. In contrast to the thermotropic liquid crystals, these lyotropics have another degree of freedom of concentration that enables them to induce a variety of different phases [3].

1.2 Characteristic of liquid crystal

1.2.1 Fluidity and anisotropy

Liquid crystal is the state between solid and liquid, it has properties of a both a fluid and a crystalline material, that is fluidity like general liquid and directivity like solid (crystal). This is because the special structure of the liquid crystal molecules, the most common liquid crystal molecules are long-rod shaped, consisting of atoms with different values of the electronegativity. The molecule has polarity and the dipole moment of a chemical bonding is a vector and therefore, a compensation or increase of the bond moments in a molecule can be observed. As a result of the polar of the liquid crystal molecules, the anisotropy of optical, dielectric and diamagnetic are shown. Utilizing the fluidity of the liquid crystal, we can feed it into vessels of any shape, in addition to this, the anisotropy including mainly the optical and electrical anisotropy. These are the most important factors that the liquid crystal has been successfully applied on the display field.

1.2.2 Electric field effects

The response of liquid crystal molecules to an electric field is the major characteristic utilized in industrial applications. The ability of the director to align along an external field is caused by the electric nature of the molecules. Permanent electric dipoles result when one end of a molecule has a net positive charge while the other end has a net negative charge. When an external electric field is applied to the liquid crystal, the dipole molecules tend to orient themselves along the direction of the field. In the following diagram, the black arrows represent the electric field vector and the red

arrows show the electric force on the molecule. Even if a molecule does not form a permanent dipole, it can still be influenced by an electric field. In molecules such that an induced electric dipole results. While not as strong as permanent dipoles, orientation with the external field still occurs [4].

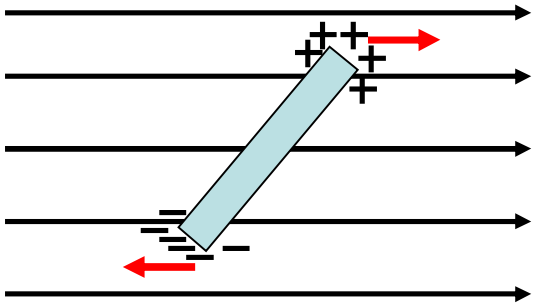

Figure 1-3 Dipole of the liquid crystal

As explained above, when an electric field is imposed to liquid crystal, the molecules will begin to rotate towards the direction of electric field. If there are some obstacles such as interface, the competition between orientation produced by interface anchoring and by electric field effects is often exploited in liquid crystal. Consider the case in which liquid crystal molecules are aligned parallel to the interface and an electric field is applied perpendicular to the cell as in the following diagram. At first, as the electric field increases in magnitude, no change in alignment occurs. However at a threshold magnitude of electric field, deformation occurs. Deformation occurs where the director changes its orientation from one molecule to the next. The occurrence of such a change from an aligned to a deformed state is called a Freedericksz transition and can also be produced by the application of a magnetic field of sufficient strength. This will be stated in detail in next chapter.

1.2.3 Backflow induced by the electric field [5-8]

Because the liquid crystal has the fluidity and dielectric anisotropy at same time, so the rotation of the molecules induced by the imposition of an electric field will induce liquid crystal flow. The flow, which is called the backflow, is always supposed to be the main cause of decrease in the contrast for optical devices, such as liquid crystal displays

(LCDs). Therefore, until recently, the application of the backflow had not received wide attention.

1.3 Applications of liquid crystals

Liquid crystal technology has had a major effect many areas of science and engineering, as well as device technology. Applications for this special kind of material are still being discovered and continue to provide effective solutions to many different problems.

1.3.1 Established applications

1. Liquid crystal displays

The most common application of liquid crystal technology is liquid crystal displays (LCD). This field has grown into a multi-billion dollar industry, and many significant scientific and engineering discoveries have been made.

2. Liquid crystal thermometers

As demonstrated earlier, chiral nematic (cholesteric) liquid crystals reflect light with a wavelength equal to the pitch. Because the pitch is dependent upon temperature, the color reflected also is dependent upon temperature. Liquid crystals make it possible to accurately gauge temperature just by looking at the color of the thermometer. By mixing different compounds, a device for practically any temperature range can be built.

1.3.2 New applications

1. Optical Imaging

An application of liquid crystals that is only now being explored is optical imaging and recording. In this technology, a liquid crystal cell is placed between two layers of photoconductor. Light is applied to the photoconductor, which increases the material's conductivity. This causes an electric field to develop in the liquid crystal corresponding to the intensity of the light. The electric pattern can be transmitted by an electrode,

which enables the image to be recorded. This technology is still being developed and is one of the most promising areas of liquid crystal research.

2. Other liquid crystal applications

Liquid crystals have a multitude of other uses. They are used for nondestructive mechanical testing of materials under stress. This technique is also used for the visualization of radio frequency (RF) waves in waveguides. They are used in medical applications where, for example, transient pressure transmitted by a walking foot on the ground is measured. Low molar mass (LMM) liquid crystals have applications including erasable optical disks, full color "electronic slides" for computer-aided drawing (CAD), and light modulators for color electronic imaging. In this article, we propose a novel idea that develops micro-actuators driven by liquid crystalline materials.

1.4 Micro-actuator

1.4.1 Introduction

An actuator is the mechanism by which an agent acts upon an environment. The agent can be either an artificial intelligent agent or any other autonomous being (human, other animal, etc). It can be used to cause a device to be turned on or off, adjusted or moved. For example, the motor and mechanism that moves the head assembly on a disk drive or an arm of a robot all can be called an actuator. Micro-actuator, as its name suggests, is actuator whose size is very small, usually within nano or micro-meter. Until now, there are many kinds of micro-actuator are developed in order to satisfy different application request of the industry, science and technology field, among these, the actuator utilized in the space flight filed is the most advanced, below we will summarize them simply.

1.4.2 Categories of micro-actuator[9]

1. Electrocmagnetic

Electromagnetism arises from electric current moving through a conducting material. Attractive or repulsive forces are generated adjacent to the conductor and proportional to the current flow. Structures can be built which gather and focuses electromagnetic

forces, and harness them to create motion. Electromagnetic devices have found wide ranging applications in spacecraft, an important advantage of electromagnetic devices is their high efficiency in converting electrical energy into mechanical work.

2. Thermomechanical

Thermomechanical systems use the physical expansion or contraction that occurs in materials as they undergo temperature changes within their phase (solid, liquid and gas). Thermomechanical actuators are, by their very nature, affected by changes in temperature. Therefore, performance and energy consumption of these devices will be directly related to the surrounding temperature.

3. Piezoelectric

Piezoelectric motion arises from the dimensional changes generated in certain crystalline materials when subjected to an electric field or to an electric charge. Structures can be built which gather and focus the force of the dimensional changes, and harness then to create motion. Piezo materials operate with high force and speed, and return to a neutral position when unpowered.

In addition to these, there are many kinds of micro-actuator such as magnetostrictive, electrostatic and shape memory, etc. From discussion above we can give conclusion below: the demand which people request from the micro-actuator are: micro size, high efficiency in converting one kind of energy into mechanical work, better adaptability to the work surrounding, short response time, easy to realize accurate control etc. The actuator discussed as examples above can satisfy one or two of the requests exhibited above, if we can develop one kind of micro-actuator which can satisfy more than three requests above, it must become excellent one. Micro-actuator driven by liquid crystal is a challenge to the goal.

1.4.3 Advantages of micro-actuator driven by liquid crystal

1. Driven by low voltage.

To drive the micro-actuator, only 3~10volts is needed, it is very low compare to electromagnetic actuator and it is safe to human or animals, so this kind of micro-actuator can be used in medical mechanism.

2. Simple structure and micro- or nano-meter size [10]

In the liquid crystalline actuator, the energy source (usually the electrode) can be used to be execution part, that is to say take out the force induced by backflow out of the liquid crystal trough the electrode, so the structure of the actuator can be designed to be very simple. At the same time, the aim to reduce exterior size of the actuator can be easily achieved.

3. Ever-changing shape

Liquid crystal has the properties of liquid such as fluidity and no regular shape, so if it is used to make actuator, there is no requirement for the shape of the actuator. This can offers more flexibility to the designer and bring up the efficiency of the actuator.

4. Realize of micromanipulation

The input energy of the liquid crystalline actuator is electricity and output is velocity of the execute part, so by using Leslie-Ericksen theory (details in chapter 2), the micromanipulation of the actuator can be realized perfectly.

Chapter 2: Foundation of theory

2.1 Introduction

In this chapter the continuum theory of nematic liquid ctystal is discussed. Many of the most important physical phenomena exhibited by the nematic phase, such as its unusual flow properties or its response to electric and magnetic fields can be studied by regarding the liquid crystal as continuous medium. The foundations of the continuum model were laid in the late 1920s by Ossen [11] and Zöcher [12] who developed a static theory which proved to be quite successful. The subject lay dormant for nearly thirty years afterwards until Frank [13] reexamined Ossen's treatment and presented it as a theory of curvature elasticity. Dynamical theories were putforward by Anzelius [14] and Ossen, but the formulation of general conservation laws and constitutive equations describing the mechanical behavior of the nematic state is due to Ericksen [15-16] and Leslie [17]. Other continuum theories have been proposed, but it turns out that the Erickson-Leslie approach (usually be called L-E theory) is the one that is most widely used in discussing the nematic state.

The L-E theory is rather complex since it contains both viscous and elastic stresses. It can best be understood by considering viscous and elastic effects separately. If elastic effects are neglected, the L-E equations reduce to Erickson's transversely isotropic fluid, while in the absence of flow the elastic stresses are just those of the Frank-Ossen theory. Below we will give simple introduction of these three theories.

2.1.1 Erickson's transversely isotropic fluid

In the absence of elastic stresses, the stress tensor for a flowing nematic is given by (Erickson 1960, 1961)

$$\sigma = 2\mu\mathbf{D} + 2\mu_1\mathbf{D}:\mathbf{nnnn} + \mu_2(\mathbf{nn}\cdot\mathbf{D} + \mathbf{D}\cdot\mathbf{nn}) \qquad (2\text{-}1)$$

Where μ , μ_1 and μ_2 are constant viscosities, and $\mathbf{D} = \frac{1}{2}(\nabla\mathbf{v} + (\nabla\mathbf{v})^T)$ is the symmetric part of the velocity gradient tensor, $\mathbf{n}$ is a unit vector, presents director of the liquid crystal.

Since the director $\mathbf{n}$ can be influenced by the flow, an additional dynamic equation must be provided to couple $\mathbf{n}$ to the velocity gradient. The most general relationship that gives $\partial\mathbf{n}/\partial t$ in terms of $\mathbf{n}$ and $\nabla\mathbf{n}$ that satisfies frame invariance, as well as the constraint that the director is a unit vector $\mathbf{n}\cdot\mathbf{n}=1$, and that is linear in $\nabla\mathbf{n}$, is

$$D\mathbf{n}/Dt - \mathbf{n}\cdot\boldsymbol{\omega} - \lambda(\mathbf{n}\cdot\mathbf{D} - \mathbf{nnn}:\mathbf{D}) = \mathbf{0} \qquad (2\text{-}2)$$

Where $D\mathbf{n}/Dt$ is the substantial time derivative of the director $\mathbf{n}$, namely $D\mathbf{n}/Dt \equiv \partial\mathbf{n}/\partial t + \mathbf{v}\cdot\nabla\mathbf{n}$, and $\boldsymbol{\omega} \equiv \tfrac{1}{2}(\nabla\mathbf{v} - (\nabla\mathbf{v})^T)$ is the anti-symmetric part of the velocity gradient. The term $-\mathbf{nnn}:\mathbf{D}$ is included in Equation (10-3) to satisfy the constraint $\mathbf{n}\cdot\mathbf{n}=1$. The coefficient λ is called the reactive parameter, or tumbling parameter; it controls the rotation of the director in a flow field. For molecules of roughly baculiform shape (the usual case), $\lambda > 0$, while for nematics composed of disc-like molecules or particles, one expects $\lambda < 0$.

2.1.2 Frank-Ossen theory

The orientatin of the director at a wall or bounding surface, the so-called anchoring condition, can be controlled by chemical treatment, or rubbing of, the surface (de Gennes and Prost 1993). A director orientation that is orthogonal to the surface is called homeotropic alignment. A thin film of lecithin (a surfactant) on glass often produces homeotropic anchoring (Haller and Huggins 1972; Creagh and Kmetz 1972; de Gennes and Prost 1993). Buffering a surface after it has been coated with a thin film, such as polyimide, usually produces nearly parallel orientation in the direction of buffing, although there is often a 2-3° pre-tilt in the direction normal to the surface. Buffering is used to establish the desired anchoring conditions in liquid –crystal displays.

Director and orientations can differ from one surface to another. If the alignments imposed at two different surfaces are not parallel to each other, then the director alignment varies spatially from one surface to the other (see Fig2-1). Spatial variations in the director field disrupt somewhat the molecular packing and thus incur a free-energy penalty, the minimization of which determines the equilibrium or static dependence of the director **n** on position **x**. If the change of the director orientation is small over the length a molecule (which for small-molecule nematics is usually the case), then the excess free energy density W_d produced by that gradient can be obtained from the low-order Frank continuum theory.

$$W_d = K_1(\nabla \cdot \mathbf{n})^2 + K_2(\mathbf{n} \cdot \nabla \times \mathbf{n})^2 + K_3(\mathbf{n} \times \nabla \times \mathbf{n})^2 \qquad (2\text{-}3)$$

Here $\nabla \cdot \mathbf{n}$ and $\nabla \times \mathbf{n}$ are the divergence and the curl of **n**. The three contributions to W_d are associated with the three independent modes of distortion: spray, twist and bend, depicted in Fig.2-1. Terms of higher order than quadratic in $\nabla \mathbf{n}$ are only required if spatial distortions become severe. The frank constants, K_1, K_2 and K_3 are of the order *u/a*, where *a* is the molecular length scale and u is *a* nematic interaction energy parameter.

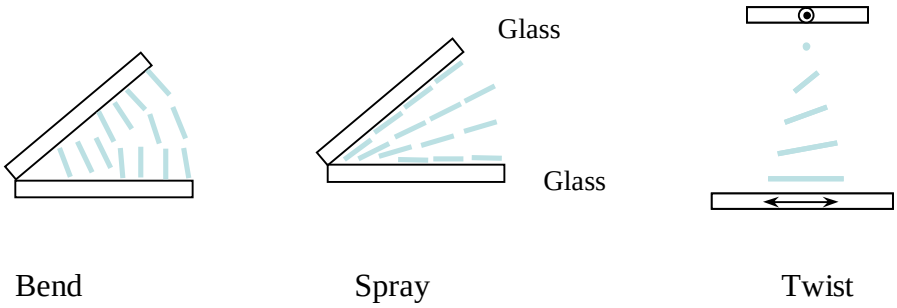

Figure 2-1 Three types of distortion in nematics

2.1.3 Leslie-Erickson theory [18-20]

In a flowing liquid crystal, both the viscous stresses and Frank elastic stresses are normally important. Thus, the Erickson theory for the viscous stresses must somehow be combined with the Frank theory for the elastic stresses. This was accomplished by Leslie, who developed what are now called "the Leslie-Erickson equations." The viscous stress tensor σ is

$$\sigma = \alpha_1 \mathbf{nnnn} : \mathbf{D} + \alpha_2 \mathbf{nN} + \alpha_3 \mathbf{Nn} + \alpha_4 \mathbf{D} + \alpha_5 \mathbf{nn} \cdot \mathbf{D} + \alpha_6 \mathbf{D} \cdot \mathbf{nn} \qquad (2\text{-}4)$$

Here, we have six viscosities $\alpha_1 - \alpha_6$. Only five of these are independent, however, since Parodi's (1970) relationship expresses one of the viscosities in terms of the others:

$$\alpha_6 = \alpha_2 + \alpha_3 + \alpha_5 \tag{2-5}$$

Relationships between the Leslie viscosities and Erickson viscosities is

$$\mu = \frac{\alpha_4}{2} \tag{2-6}$$

$$\mu_1 = \frac{\alpha_1}{2} - \frac{(\alpha_2 + \alpha_3)(\alpha_6 - \alpha_5)}{2(\alpha_2 - \alpha_3)} \tag{2-7}$$

$$\mu_2 = \frac{(\alpha_2\alpha_6 - \alpha_3\alpha_5)}{(\alpha_2 - \alpha_3)} \tag{2-8}$$

$\mathbf{N}$ is the rotation rate of $\mathbf{n}$ relative to that of the background fluid, defined as

$$\mathbf{N} \equiv D\mathbf{n}/Dt - \mathbf{n}\cdot\boldsymbol{\omega} \tag{2-9}$$

If the director field is uniform, Eq. (2-2) can be used to express $\mathbf{N}$ in terms of $\mathbf{D}$ and $\mathbf{n}$, and then Eq. (2-4) reduces to Erickson's equation (2-1).

However, if the director field is not uniform, Frank distortional stresses influence the rate of rotation of the director, and a new equation for $D\mathbf{n}/Dt$ (or, equivalently for $\mathbf{N}$) is required to replace Erickson's equation (2-3). This is obtained from the balance of angular momentum, which gives

$$\mathbf{h} - \mathbf{nn}\cdot\mathbf{h} - \gamma_2(\mathbf{n}\cdot\mathbf{D} - \mathbf{nnn}\cdot\mathbf{D}) - \gamma_1\mathbf{N} = \mathbf{0} \tag{2-10}$$

The vector $\mathbf{h}$ is the so-called molecular field; it is produced by the same director gradients that produce the distortional energy, the spray, twist, and bend portions of $\mathbf{h}$ are

$$\mathbf{h}_S = K_1\nabla(\nabla\cdot\mathbf{n}) \tag{2-11}$$

$$\mathbf{h}_T = -K_2[(\mathbf{A}\nabla)\times\mathbf{n} + \nabla\times(\mathbf{An})] \tag{2-12}$$

$$\mathbf{h}_B = K_3[\mathbf{B}\times(\nabla\times\mathbf{n}) + \nabla\times(\mathbf{n}\times\mathbf{B})] \tag{2-13}$$

Here $\mathbf{A} \equiv \mathbf{n}\cdot(\nabla\times\mathbf{n})$ and $\mathbf{B} \equiv \mathbf{n}\times(\nabla\times\mathbf{n})$

Chapter 3: Numerical solution techniques

3.1 Introduction

Computer simulation is now an integral part of contemporary basic and applied science and is approaching a role equal in importance to the traditional experimental and theoretical approaches. Hence, the ability 'to compute' is part of the essential repertoire of research scientists and educators. Why is computer simulation becoming important in physics? One reason is that most of out analytical tools such as differential calculus are best suited to the analysis of linear problem. However, many natural phenomena are non-linear, and small changes in a variable can produce large rather than small changes in another variable. Since non-linear problems can be solved by analytical schemes only in special cases, the computer gives us a new tool to explore non-linear phenomena. Another reason for the importance of computer simulation is our interest in systems with many degrees of freedom or with many variables.

Computer simulations are sometimes referred to as computer experiments since they share much in common with laboratory experiments. The computer program simulates the physical system and defines the computer experiment. Such a computer experiment serves as a bridge between laboratory experiments and theoretical calculations. Computer simulations, like laboratory experiments, are not substitutes for thinking but are tools which we can use to understand complex phenomena.

The space discretization approach used in this thesis is the easiest one for simple geometries which named finite difference scheme. There are two kinds of time advance schemes used in this simulation. They are the Runge-Kutta and the Crank-Nicholson schemes.

3.2 Space discretization

3.2.1 Finite difference scheme [21]

A finite difference is a mathematical expression of the form of $f(x+a)-f(x+b)$. The starting point is the conservation equation in differential form. The solution domain

is covered by a grid. At each grid point, the differential equation is approximated by replacing the partial derivatives by approximations in terms of the nodal values of the functions. The result is one algebraic equation per grid node, in which the variable value at that and a certain number of neighbor nodes appear as unknowns.

The first step in obtaining a numerical solution is to discretize the geometric domain. In finite difference discretization scheme the grid is usually locally structured, each grid node may be considered the origin of a local coordinate system, whose axes coincide with grid lines. This also implies that two grid lines belonging to the same family. Figure 3.1 (a) shows examples of one-dimensional (1D) and (b) shows two-dimensional (2D) Cartesian grids used in finite difference schemes [22].

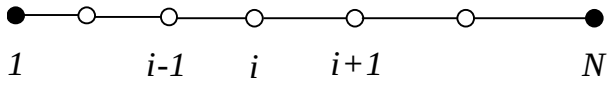

(a) One dimention

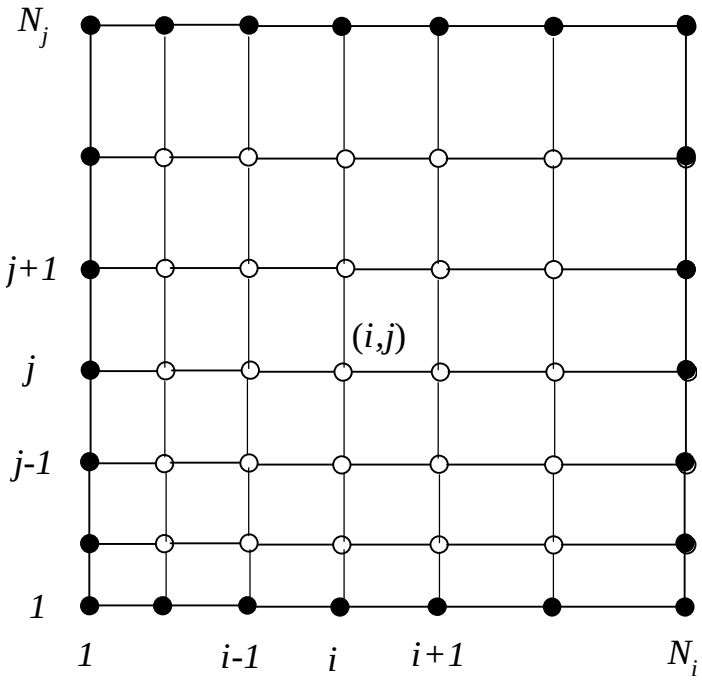

(b) Two dimension

Fig. 3-1 Finite difference scheme

Each node is uniquely identified by a set of indices, which are the indices of the grid lines that intersect at (*i*, *j*). The neighbor nodes are defined by increasing or reducing one of the indices by unity.

From the known value to request the unknown value, there are many kinds of schemes of approximation. They are all on the base of Taylor series expansion.

Any continuous differentiable function $\phi(x)$ can, in the vicinity of x_i, be expressed as a Taylor series:

$$\begin{aligned}\phi(x) = \phi(x_i) + (x - x_i)\left(\frac{\partial \phi}{\partial x}\right)_i + \frac{(x - x_i)^2}{2!}\left(\frac{\partial^2 \phi}{\partial x^2}\right)_i \\ + \frac{(x - x_i)^3}{3!}\left(\frac{\partial^3 \phi}{\partial x^3}\right)_i + \cdots + \frac{(x - x_i)^n}{n!}\left(\frac{\partial^n \phi}{\partial x^n}\right)_i + H\end{aligned} \tag{3-1}$$

Where *H* means "higher order terms". By replacing *x* by x_{i+1} or x_{i-1} in this equation, one obtains expressions for the variable values at these points in terms of the variable and its derivatives at x_i and this can be extended to any other point near *x*.

Here we only consider the first derivative, so there are three kinds of schemes can be get to compute the approximate value at the just point through the point near it, they are the forward-(FDS), backward-(BDS), and central- (CDS).

$$\phi_{i+1} = \left(\frac{\partial \phi}{\partial x}\right)_i (x_{i+1} - x_i) + \phi_i \tag{3-2}$$

$$\phi_i = \left(\frac{\partial \phi}{\partial x}\right)_i (x_i - x_{i-1}) + \phi_{i-1} \tag{3-3}$$

$$\phi_{i+1} = \left(\frac{\partial \phi}{\partial x}\right)_i (x_{i+1} - x_{i-1}) + \phi_{i-1} \tag{3-4}$$

The terms that were deleted from the right hand sides are called the truncation errors; they measure the accuracy of the approximation and determine the rate at which the error decreases as the spacing between points is reduced. In this study we use the CDS to do the space discretization, from the point of accuracy, it is better than the FDS and BDS.

3.3 Time advance scheme

3.3.1 Runge-Kutta scheme

The Runge-Kutta scheme was developed around 1900 by the German mathematician C.Runge and M.W.Kutta, it is a trade-off between accuracy and complexity of calculation which depends heavily on the chosen interval of the value known and the request one. In general as the interval is decreased the calculation takes longer but is more accurate. However, if it is decreased too much the slight rounding that occurs in the computer (because it cannot represent real numbers exactly) begins to accumulate enough to cause significant errors. For many higher order systems, it is very difficult to make the Euler approximation effective. For this reason more accurate and more elaborate techniques were developed.

The formula for the Euler scheme is

$$y_{n+1} = y_n + h \cdot f(x_n, y_n) \tag{3-5}$$

Which advances a solution from x_n to x_{n+1}, the formula is unsymmetrical: it advances the solution through an interval *h*, but uses derivative information only at the beginning of that interval. That means that the step's error is only one power of *h* smaller than the correction.

Consider, however, the use of a step like (3-5) to take a "trial" step to the midpoint of the interval. Then use the value of both *x* and *y* at that midpoint to compute the "real" step across the whole interval. Figure 3-2 illustrates the idea [23]. In equations,

$$\begin{aligned} k_1 &= h \cdot f(x_n, y_n) \\ k_2 &= h \cdot f(x_n + \frac{h}{2}, y_n + \frac{k_1}{2}) \\ y_{n+1} &= y_n + k_2 + O(h^3) \end{aligned} \tag{3-6}$$

As indicated in the error term, this symmetrization cancels out the first-order error term, making the scheme second order.

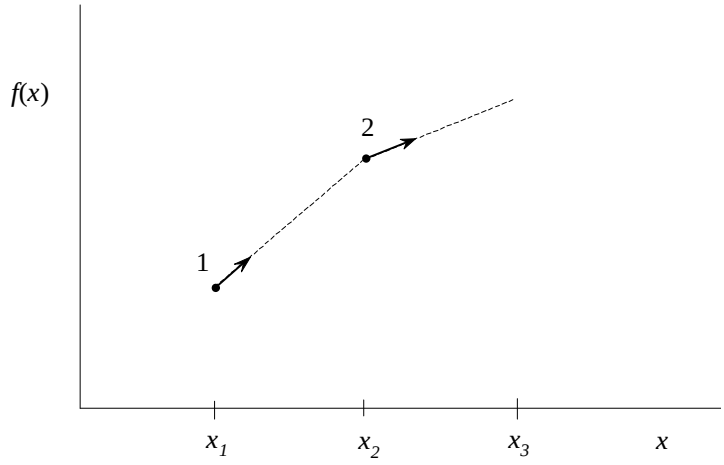

(a) Euler's scheme. In this simplest scheme for integrating an ODE, the derivative at the starting point of each interval is extrapolated to find the next function value. First-order accuracy.

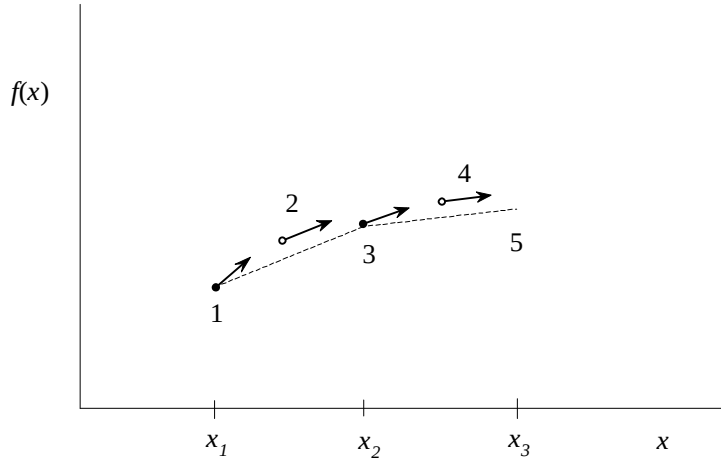

(b) Midpoint scheme. Second-order accuracy is obtained by using the initial derivative at each step to find a point halfway across the interval, then using the midpoint derivative across the full width of the interval. In the figure, filled dots represent final function values, while open dots represent function values that are discarded once their derivatives have been calculated and used.

Fig. 3-2 Principle of the Runge-Kutta scheme

Same as above, we can think about many ways to evaluate the right-hand side $f(x, y)$ that all agree to first order, but that have different coefficients of higher-order error terms. Adding up the right combination of these, we can eliminate the error terms order by order. That is the basic idea of the Runge-Kutta scheme. There are many schemes proposed these years on the base of this idea in order to solve particular problem. In this thesis, the two order Runge-Kutta scheme was used.

3.3.2 Crank-Nicholson scheme

The Euler scheme is termed an explicit scheme because we are able to write down an explicit solution for y_{n+1} in terms of "known" values at y_n. Inspection of our approximation for y'_n shows the error term is of order Dh^2 in our step formula. This shows that the Euler scheme is a first order scheme. It is easy to know that two-order Runge-Kutta scheme is also an explicit scheme, just replace x_n in (3-6) with t_n.

Below we will introduce the usually used implicit scheme, in contrast to the explicit, implicit schemes have y_{n+1} on both sides: $y_{n+1} = h(y_n, y_{n+1}, t_n, Dt)$. Implicit schemes are computationally more expensive for a single step than explicit schemes, but offer advantages in terms of stability and/or accuracy in many circumstances. Often the computational expense per step is more than compensated by the advantage that it is possible to take larger steps.

Before the Crank-Nicholson scheme, in order to compare, it is better to refer to the backward and forward Euler scheme. To put it simple, from the formula below it is easy to know that the forward Euler scheme is explicit (formula 3-7) and the backward is implicit (formula 3-8).

$$y_{n+1} = y_n + \Delta t \cdot f(t_n, y_n) \tag{3-7}$$

$$y_{n+1} = y_n + \Delta t \cdot f(t_{n+1}, y_{n+1}) \tag{3-8}$$

Both the forward and the backward Euler scheme are first order, here if we use central differences rather than the forward or the backward difference Euler, we may obtain a second order scheme due to cancellation of the terms of $O(Dt^2)$. Using the same discretisation of t we obtain

$$y_{n+1} - y_n = \frac{1}{2}\Delta t[\, f(t_{n+1}, y_{n+1}) + f(t_n, y_n)] \tag{3-9}$$

Like the Backward Euler, the scheme is implicit and it is not, in general, possible to write an explicit expression for y_{n+1} in terms of y_n. This is Crank-Nicholson scheme that is second order. Formal proof that the Crank-Nicholson scheme is second order accurate is slightly more complicated due to the linear interpolation to approximate $f(t_{n+1/2},y_{n+1/2})$. The overall approach is much the same, however, with a requirement for Taylor Series expansions about t_n

$$\begin{aligned} y_{n+1} &= y_n + \frac{dy}{dt}\Delta t + \frac{1}{2}\frac{d^{2y}}{dt^2}\Delta t^2 + O(\Delta t^3) \\ &\quad y_n + f_n\Delta t + \frac{1}{2}\left(\frac{\partial f}{\partial t} + f\frac{\partial f}{\partial y}\right)\Delta t^2 + O(\Delta t^3) \end{aligned} \tag{3-10}$$

$$\begin{aligned} f_{n+1} &= f_n + \frac{\partial f}{\partial t}\Delta t + \frac{\partial f}{\partial y}\Delta y + O(\Delta t^2) + O(\Delta y^2) \\ &\quad f_n + \frac{\partial f}{\partial t}\Delta t + \frac{\partial f}{\partial y}\frac{dy}{dt}\Delta t + O(\Delta t^2) \\ &\quad f_n + \left(\frac{\partial f}{\partial t} + f\frac{\partial f}{\partial y}\right)\Delta t + O(\Delta t^2) \end{aligned} \tag{3-11}$$

From formula (3-10) and (3-11) we can get (3-12), from the formula it is easy to know that the Crank-Nicholson scheme is second-order accurate.

$$\begin{aligned} \frac{1}{2}(f(t_n, y_n) + f(t_{n+1}, y_{n+1}))\Delta t = \frac{1}{2}\Bigg(& f_n + f_n + \left(\frac{\partial f}{\partial t} + f\frac{\partial f}{\partial y}\right)\Delta t + O(\Delta t^2)\Bigg)\Delta t \\ & f_n\Delta t + \frac{1}{2}\left(\frac{\partial f}{\partial t} + f\frac{\partial f}{\partial y}\right)\Delta t^2 + O(\Delta t^3) \end{aligned} \tag{3-12}$$

The figure 3-3 [24] shows the different between the backward, forward scheme and the Crank-Nicholson scheme.

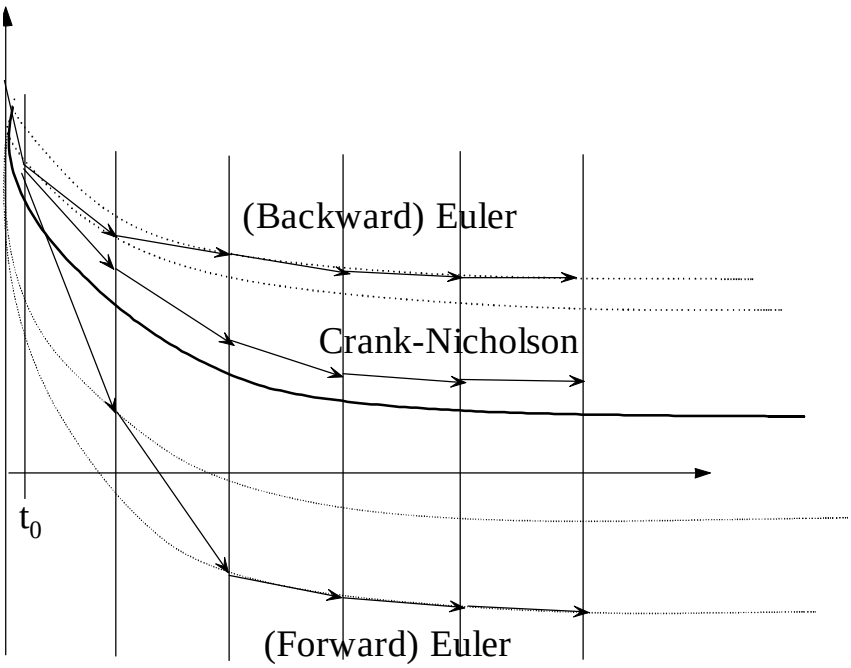

Fig. 3-3 Contrast of Crank-Nicholson to Backward and Forward scheme

Chapter 4: Simulation results

4.1 Introduction

In this thesis, the most common nematic liquid crystalline compound 5CB (4-n-pentyl-4'-cianobiphenyl) is used to do the simulation. 5CB, consists of thirty-eight atoms, is a comprehensive presentation of the temperature evolution of "linear" and "nonlinear" dielectric relaxation in the isotropic phase of nematic liquid crystal. Along with the development of the liquid crystal display, 5CB is becoming more and more familiar to common people. As described above, 5CB belong to the thermotropic liquid crystal, it can become to real liquid when the temperature is high enough and of course turn to crystal along with the decrease of the temperature. The chemical structure is like below:

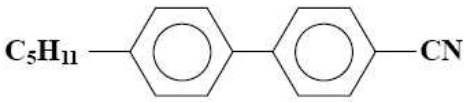

Because of the chemical structure, 5CB molecule shows long rod-like shape which is the typical structure of liquid crystalline molecule. The representative parameter including of viscosity, elastic and dielectric constants of 5CB is shown in table 4-1:

Table 4-1 Material constants of 5CB [25]

(Pa·s)						(N)			(F/m)	
α_1	α_2	α_3	α_4	α_5	α_6	K_1	K_2	K_3	$\varepsilon_{//}$	$\varepsilon_{\perp}$
$\times 10^{-2}$						$\times 10^{-12}$				
0	-8.6	-0.4	8.9	5.9	-3.1	6.37	3.81	8.60	15.7	5.7

From the table we can see that the value of parallel dielectric constant is three times larger than the one of perpendicular direction, so when the electric field is imposed to the 5CB, the molecules will rotate to the direction parallel to the electric field, along this process, because liquid crystal has the fluidity, flow (usually called backflow) will be

reduced along the area. This is the fundamental principle of the backflow, show in figure 4-1.

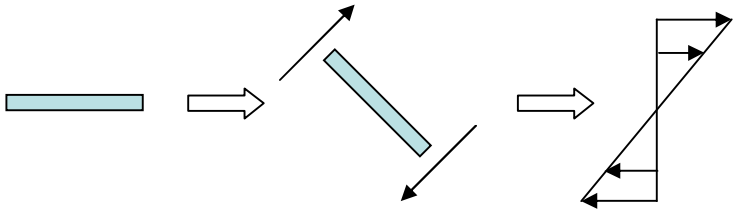

Fig. 4-1 Principle of backflow

4.2 Numerical simulation

4.2.1 Governing equations [26-30]

The governing equations of liquid crystalline isothermal flow under the electric field are as follows:

Continuity equation

$$\nabla \cdot \mathbf{v} = 0 \tag{4-1}$$

Momentum equation

$$\rho\left\{\frac{\partial \mathbf{v}}{\partial t} + (\mathbf{v} \cdot \nabla)\mathbf{v}\right\} = \mathbf{F} + \nabla \cdot (-p\mathbf{I} + \boldsymbol{\tau}) \tag{4-2}$$

Here $\mathbf{v}$ is the velocity vector of the liquid crystalline flow; ρ is the density of the liquid crystal, p is the pressure, $\mathbf{I}$ is unit tensor. $\mathbf{F}$ is the external force, in this simulation, because the electric field is used, so $\mathbf{F}$ is expressed by the formula below:

$$\mathbf{F} = \left[(\varepsilon_{\perp}\mathbf{E} + \varepsilon_a(\mathbf{n} \cdot \mathbf{E})\mathbf{n}) \cdot \nabla\right]\mathbf{E} \tag{4-3}$$

In here, $\mathbf{E}$ is the electric field strength, $\varepsilon_{\perp}$ is the dielectric constant of the perpendicular direction, and ε_{α} is the dielectric anisotropy, expressed as below:

$$\varepsilon_\alpha = \varepsilon_\parallel - \varepsilon_\perp \tag{4-4}$$

n is an unit vector, describes the change of the unique variable of liquid crystal: director.

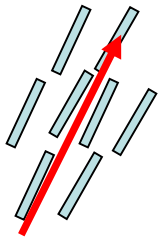

Figure 4-2 Director of the liquid crystal **n**

τ is the stress tensor, according the L-E theory, it can be expressed by the formula below:

$$\begin{aligned}\boldsymbol{\tau} = {} & \alpha_1 \mathbf{nnn}\cdot\mathbf{A}\cdot\mathbf{n} + \alpha_2 \mathbf{nN} + \alpha_3 \mathbf{Nn} + \alpha_4 \mathbf{A} + \alpha_5 \mathbf{nn}\cdot\mathbf{A} \\ & + \alpha_6 \mathbf{A}\cdot\mathbf{nn} - \frac{\partial F}{\partial \nabla \mathbf{n}}\cdot(\nabla\mathbf{n})^T\end{aligned} \tag{4-5}$$

Here $\alpha_1 \ldots \alpha_6$ are the viscosity constants of liquid crystal, because of the existence of the director **n,** six viscosity constants are needed to express the influence of the viscosity to the liquid crystalline flow. **N** is the rotation rate of **n** relative to that of the background fluid, defined as

$$\mathbf{N} = \frac{D\mathbf{n}}{Dt} - \boldsymbol{\Omega}\cdot\mathbf{n} \tag{4-6}$$

Ω is vorticity tensor, defined as

$$\Omega = \frac{1}{2}\left\{(\nabla\mathbf{v})^T - \nabla\mathbf{v}\right\} \tag{4-7}$$

A is the deformation velocity tensor, defined as

$$\mathbf{A} = \frac{1}{2}\left\{(\nabla \mathbf{v})^T + \nabla \mathbf{v}\right\} \tag{4-8}$$

F is the unit energy density, according to the Frank - Ossen theory, can be described as below

$$F = \frac{1}{2}\left\{K_1(\nabla \cdot \mathbf{n})^2 + K_2(\mathbf{n} \cdot \nabla \times \mathbf{n})^2 + K_3|\mathbf{n} \times \nabla \times \mathbf{n}|^2\right\} \tag{4-9}$$

K_1, K_2 and K_3 are the elastic constants.

Angular momentum equation

$$\mathbf{n} \times \left\{\mathbf{G} - \frac{\partial F}{\partial \mathbf{n}} + \nabla \cdot \left(\frac{\partial F}{\partial \nabla \mathbf{n}}\right) + \gamma_1 \mathbf{N} + \gamma_2 \mathbf{A} \cdot \mathbf{n}\right\} = \mathbf{0} \tag{4-10}$$

G is the unit volume external force imposed on the director, defined as

$$\mathbf{G} = \varepsilon_\alpha \mathbf{n} \cdot \mathbf{EE} \tag{4-11}$$

γ_1 and γ_2 are the viscosity constant.

$$\gamma_1 = \alpha_3 - \alpha_2$$

$$\gamma_2 = \alpha_6 - \alpha_5$$

4.2.2 Coordinate system and the expansion of the equations

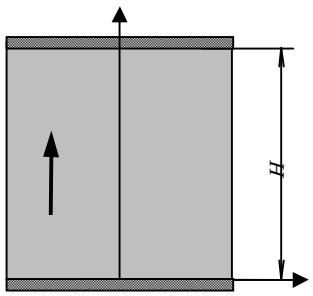

Fig. 4-3 Coordinate system

Like showing in the figure 4-3, there is liquid crystal (5CB) between the two plates whose gap is H, at the time $t = 0$s, electric field of strength E is imposed along the Y direction, so the vector **E** is become like below,

$$\mathbf{E} = (0, E, 0)^T \tag{4-12}$$

The director at this situation is a three-dimensional vector, defined as

$$\mathbf{n} = (n_x, n_y, n_z)^T \tag{4-13}$$

In this case, the Y direction component of the velocity is 0, so

$$\mathbf{v} = (u, 0, w)^T \tag{4-14}$$

By using formula 4-12, 4-13 and 4-14, the governing equations (mainly the momentum and the angular momentum equation) can be expanded as below [31-33]

$$\begin{aligned}\rho\frac{\partial u}{\partial t} &= \alpha_1\left\{\frac{\partial}{\partial y}\left(n_x^2 n_y^2\right)\frac{\partial u}{\partial y}+\frac{\partial}{\partial y}\left(n_x n_y^2 n_z\right)\frac{\partial w}{\partial y}+n_x n_y^2\left(n_x\frac{\partial^2 u}{\partial y^2}+n_z\frac{\partial^2 w}{\partial y^2}\right)\right\}+\frac{\alpha_4}{2}\frac{\partial^2 u}{\partial y^2}\\ &+\alpha_2\frac{\partial}{\partial y}\left(n_y\frac{\partial n_x}{\partial t}\right)+\alpha_3\frac{\partial}{\partial y}\left(n_x\frac{\partial n_y}{\partial t}\right)-\frac{\alpha_2-\alpha_5}{2}\left(2n_y\frac{\partial n_y}{\partial y}\frac{\partial u}{\partial y}+n_y^2\frac{\partial^2 u}{\partial y^2}\right)\\ &+\frac{\alpha_3+\alpha_6}{2}\left\{2n_x\frac{\partial n_x}{\partial y}\frac{\partial u}{\partial y}+\frac{\partial}{\partial y}\left(n_x n_z\right)\frac{\partial w}{\partial y}+n_x^2\frac{\partial^2 u}{\partial y^2}+n_x n_z\frac{\partial^2 w}{\partial y^2}\right\}\end{aligned} \tag{4-15a}$$

$$\begin{aligned}\rho\frac{\partial w}{\partial t} &= \alpha_1\left\{\frac{\partial}{\partial y}\left(n_x n_y^2 n_z\right)\frac{\partial u}{\partial y}+\frac{\partial}{\partial y}\left(n_y^2 n_z^2\right)\frac{\partial w}{\partial y}+n_y^2 n_z\left(n_x\frac{\partial^2 u}{\partial y^2}+n_z\frac{\partial^2 w}{\partial y^2}\right)\right\}+\frac{\alpha_4}{2}\frac{\partial^2 w}{\partial y^2}\\ &+\alpha_2\frac{\partial}{\partial y}\left(n_y\frac{\partial n_z}{\partial t}\right)+\alpha_3\frac{\partial}{\partial y}\left(n_z\frac{\partial n_y}{\partial t}\right)-\frac{\alpha_2-\alpha_5}{2}\left(2n_y\frac{\partial n_y}{\partial y}\frac{\partial w}{\partial y}+n_y^2\frac{\partial^2 w}{\partial y^2}\right)\\ &+\frac{\alpha_3+\alpha_6}{2}\left\{\frac{\partial}{\partial y}\left(n_x n_z\right)\frac{\partial u}{\partial y}+2n_z\frac{\partial n_z}{\partial y}\frac{\partial w}{\partial y}+n_x n_z\frac{\partial^2 u}{\partial y^2}+n_z^2\frac{\partial^2 w}{\partial y^2}\right\}\end{aligned} \tag{4-15b}$$

$$\gamma_1\frac{\partial n_x}{\partial t} = n_y\left\{2\left(K_3-K_2\right)\frac{\partial n_x}{\partial y}\frac{\partial n_y}{\partial y}-\alpha_2\frac{\partial u}{\partial y}\right\}+\left\{K_2+\left(K_3-K_2\right)n_y^2\right\}\frac{\partial^2 n_x}{\partial y^2} \tag{4-16a}$$

$$\gamma_1 \frac{\partial n_y}{\partial t} = n_y \Delta\varepsilon E^2 - \alpha_3 \left(n_x \frac{\partial u}{\partial y} + n_z \frac{\partial w}{\partial y} \right) - (K_3 - K_2) n_y \left\{ \left(\frac{\partial n_x}{\partial y} \right)^2 + \left(\frac{\partial n_y}{\partial y} \right)^2 - \left(\frac{\partial n_z}{\partial y} \right)^2 \right\} + \left\{ K_1 + (K_3 - K_2) n_y^2 \right\} \frac{\partial^2 n_y}{\partial y^2} \quad \text{(4-16b)}$$

$$\gamma_1 \frac{\partial n_z}{\partial t} = n_y \left\{ 2(K_3 - K_2) \frac{\partial n_y}{\partial y} \frac{\partial n_z}{\partial y} - \alpha_2 \frac{\partial w}{\partial y} \right\} + \left\{ K_2 + (K_3 - K_2) n_y^2 \right\} \frac{\partial^2 n_z}{\partial y^2} \quad \text{(4-16c)}$$

4.2.3 Computation parameters

In this simulation, we choose the parameters relate closely to the function of the micro-actuator, they are the voltage applied, the gap between the two plates, and director orientation which expressed by the twist and tilt angles. As showing the figure 4-4, twist angle is defined as the difference of the angle ϕ between the two plates, and angle θ is the tilt angle. In order to satisfy the advantage of low voltage driven and micro-size, the voltage alternative range is chose from 0V to 10V, and the gap of the two plates is 10-100. As to the director orientation, in order to find out the optimum condition fro micro-actuator, we choose the range 1- 45 deg of the tilt angle and 0 -180 deg of the twist angle to describe all the probability of the director [34-38].

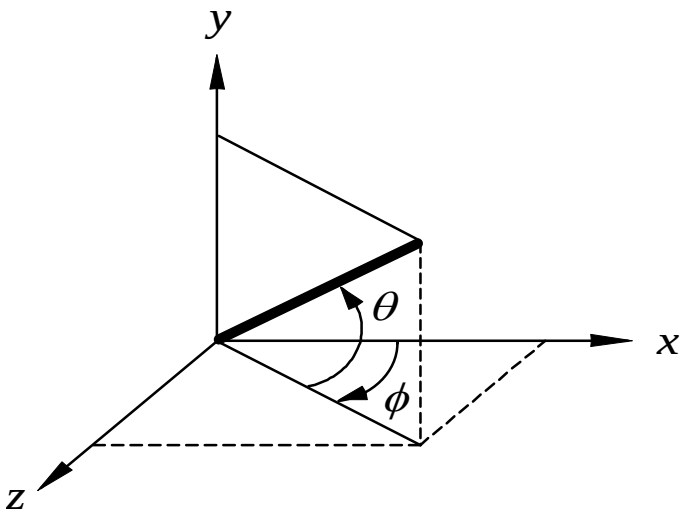

Fig. 4-4 Coordinate of the director

4.3 Numerical simulation [39-45]

4.3.1 Boundary and initial conditions

As boundary condition, the velocity at the plate is set as 0 μm/s, the director orientation is set as below: the tilt angle is from 0deg to 45 deg with an interval of 5 deg and the twist angle is from 0 deg to 180 deg with an interval of 60 deg. The initial condition is: velocity field is 0 μm/s at t = 0, orientation field is the steady solution of the one dimension equation without the electric field.

4.3.2 Numerical simulation

In order to discrete the equation 4-15 to 4- 16, the two-order central difference scheme in the space direction and two-order Runge-Kutta scheme in the time direction are used. $\Delta y = H/100$ and $\Delta t = 10^{-9}$ s is the unit of the space and time separately. The density of the liquid crystal used (5CB) is be set as same as water- $\rho = 1000 kg/m^3$.

4.4 Results and discussion

The simulation is divided into two cases; the two plates are both set to be fixed and fix the lower one in the same time free the upper one. In the first case, we can utilize the backflow directly, for example, to drive the particles placed between the two plates; in the second case, we can use the upper plate which is be set to be free as a medium to turn the flow into the kinetic energy, that is the movement of the plate. Both of them can be used to develop micro-actuator.

4.4.1 In the case of the upper plate being fixed

The coordination system is shown in figure 4-5(a), both upper and lower plates are fixed, and liquid crystal is filled between the two parallel plates, here we also give two examples of the different orientation field in figure 4-5(b) and (c), both of the tilt angle is 1 deg and twist angle are 0 and 180 deg, the electric field is exposed along the y direction.

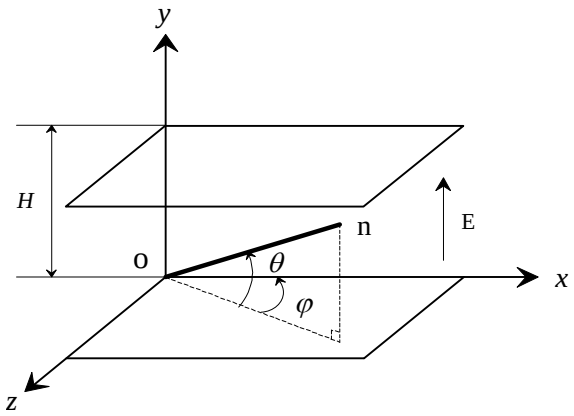

(a) Flow geometry

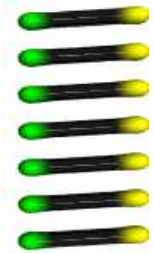

(b) 0 deg twist and 1deg tilt angle

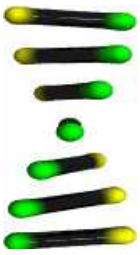

(c) 180 deg twist angle and 1 deg tilt angle

Fig. 4-5 Flow geometry and orientation of the director

1. The velocity profile between the two plates

The effect of the twist angle (Parameter: E = 5V, H = 50μm, θ = 1°)

(1) Twist angle φ = 0°

Figure 4-6 shows the time series of profiles from the steady state of electric field off to on, (a) is the angular velocity profiles of the director and (b) is the induced velocity profiles at the same time. From the figures, we can see that when the electric field is applied, within 0.36 s, the angular velocity of the director increases and because the anchoring effect, the director near the plates rotates slowly than the one in the middle. Along with the closer of the director to 90 deg, the angular velocity in the middle becomes decreasing from 0.36 s, in contrast, the rotate velocity near the plates keep on increasing. At t = 0.48 s, the angular velocity of the director near the plates becomes larger than the one in the middle. Because the backflow is induced by the rotation of the director basically, so the change tendency of the flow velocity is same as the angular velocity, from t = 0 s to 0.36 s, the velocity increases and keeps as anti-symmetry S-shape. After 0.36 s, the velocity becomes decreasing quickly, but the S-shape is kept all along and the maximum of the velocity is 30μm/s. In the case the twist angle is 0 deg, the director component of Z direction is 0, so there is no velocity is induced in Z direction.

(2) Twist angle φ = 90°

The computation results of the twist angle 90 deg is shown in figure 4-7, when the twist angle is larger than 0 deg, there is director component in Z direction, so the flow in Z direction is also induced this time. Figure (a) is the angular velocity profiles and (b), (c) is the X-direction, Z-direction velocity separately. As shown as the figure, the director takes the same action when the electric field is imposed as the case when the twist angle is 0 deg, but the induced velocity is different completely. The anti-symmetry of the velocity profiles break down and in the X-direction, the minus velocity field expands over the midline to the lower half part, at the same time, in Z-direction, the plus velocity field exceeds half part. Another different point is the velocity profiles shape of the 90 deg twist angle changes with the time, so in both X-direction and Z-direction there are fields whose velocity direction changes with time.

(3) Twist angle φ = 180°

Figure 4-8 shows the time series of profiles for 180 deg twist angle. Same as 0 and 90 deg twist angel, the angular velocity of the director increases for 0.36 s, then begins to decrease. The X-direction velocity profile becomes to symmetry when the twist angle increases to 180 deg, and the one-direction flow does not change along time, the maximum value is 65μm/s. For Z-direction, same as the X-direction of 0 deg twist angle, the anti-symmetry S-shape velocity profile is achieved and the maximum value is also near to the 0 deg twist angle,-35μm/s.

Through we give both the X-direction and Z-direction velocity profiles in the case of twist angle is larger than 0 deg, it is very difficult to compound them to form three-dimensional image of the induced backflow in brain, so in figure 4-9, we give an example of three-dimension figure of the velocity profile, twist angle is 180 deg.

Summary

From the account above, we can give conclusion below: the velocity profile shape will change with the changing of the twist angle, in X-direction, the profile will change from anti-symmetric to asymmetric when the twist angle reach 90 deg, and to symmetric as the twist angle reaches 180 deg. As the same time, the magnitude of the maximum velocity increases with the increasing of the twist angle.

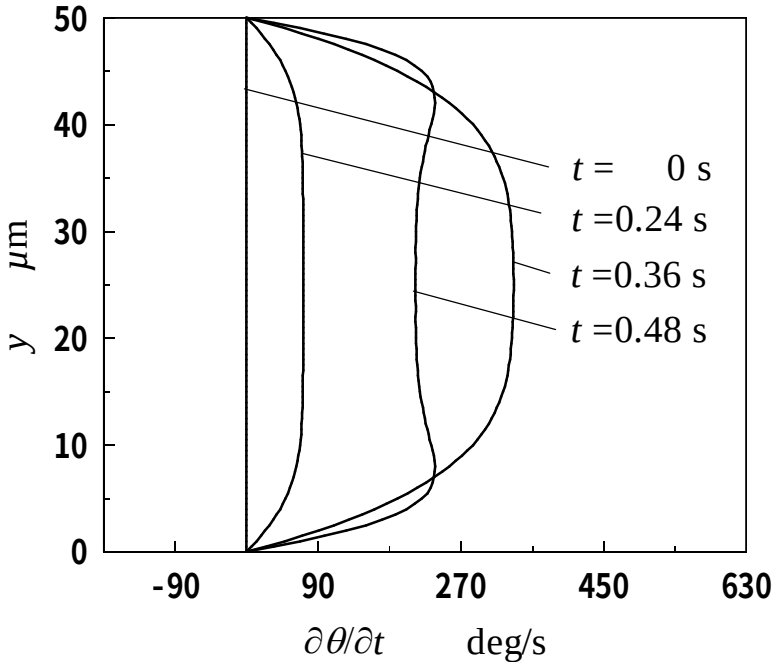

(a) Angular velocity profiles of director

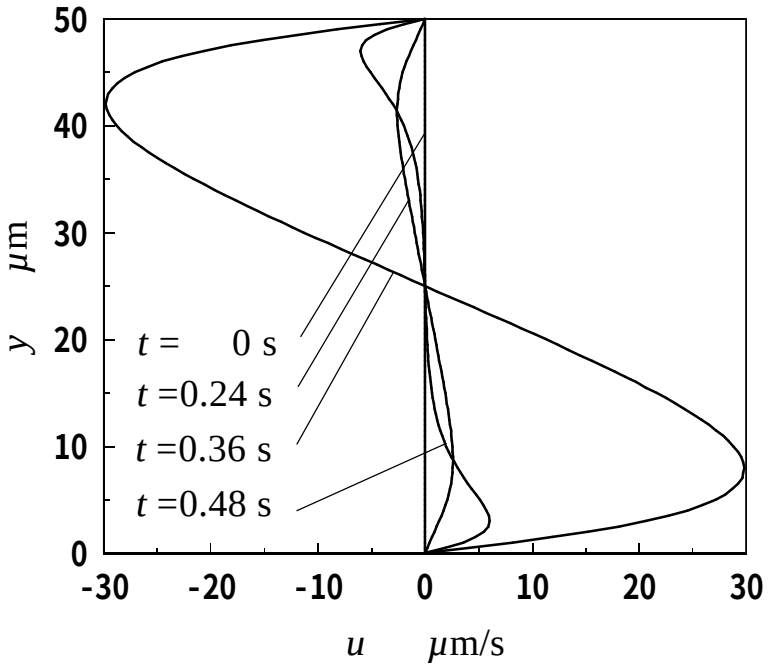

(b) Velocity profiles of x direction

Fig.4-6 Time series of profiles for electric field off→on (twist angle 0 deg)

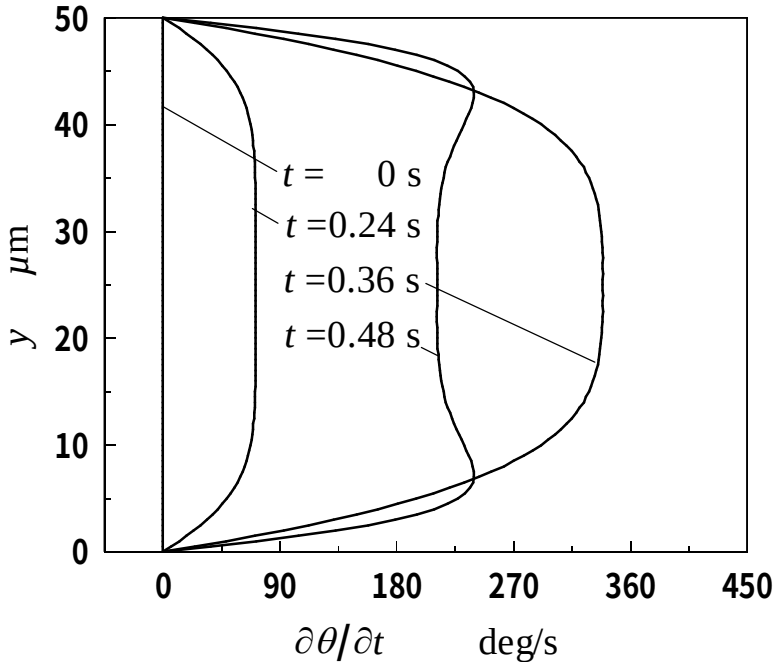

(a) Angular velocity profiles of director

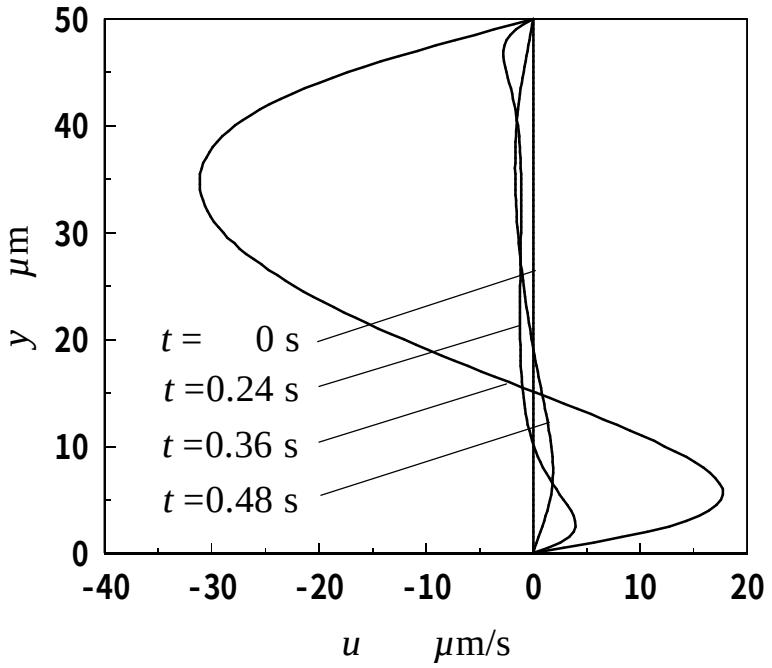

(b) Velocity profiles of x direction

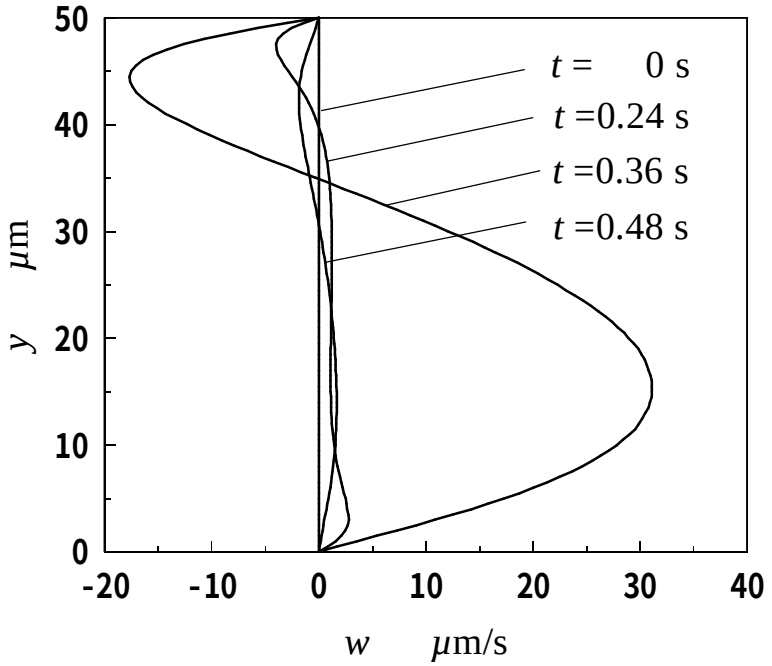

(c) Velocity profiles of z direction

Fig.4-7 Time series of profiles for electric field off→on (twist angle 90 deg)

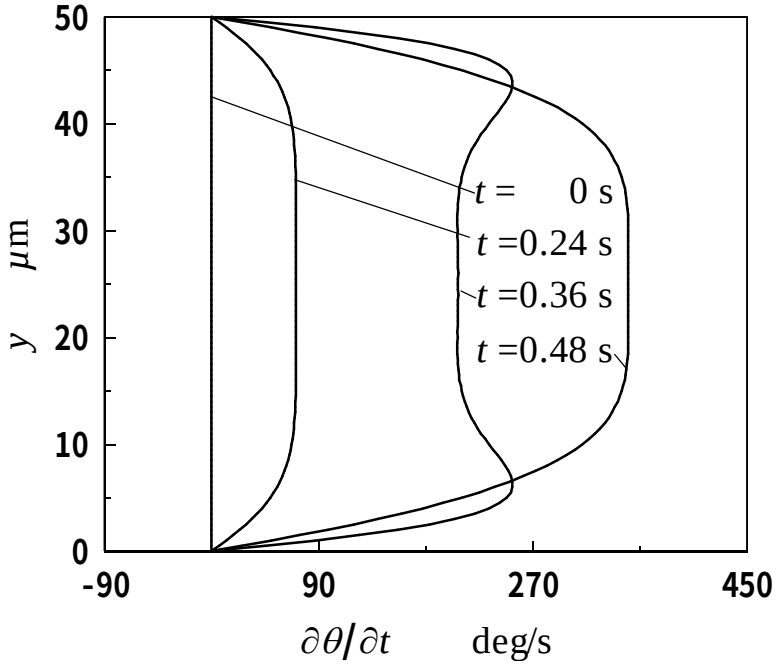

(a) Angular velocity profiles of director

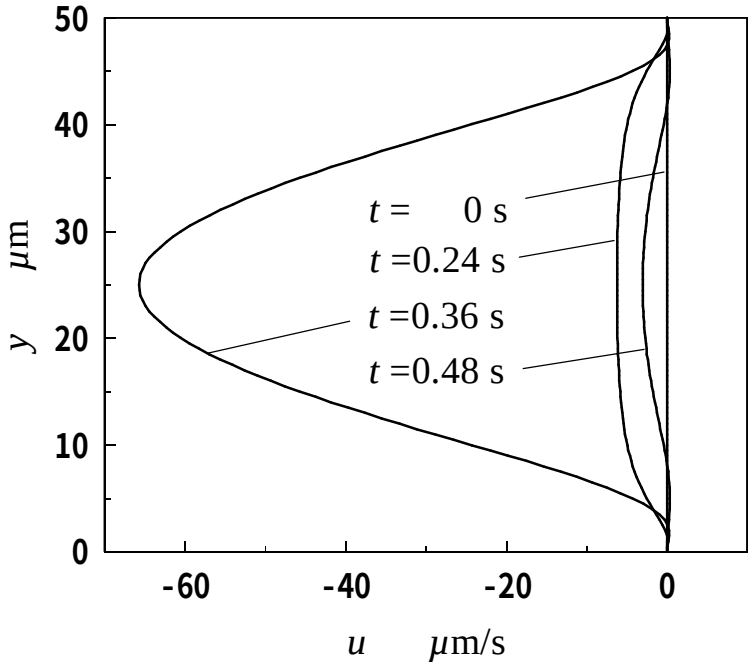

(b) Velocity profiles of x direction

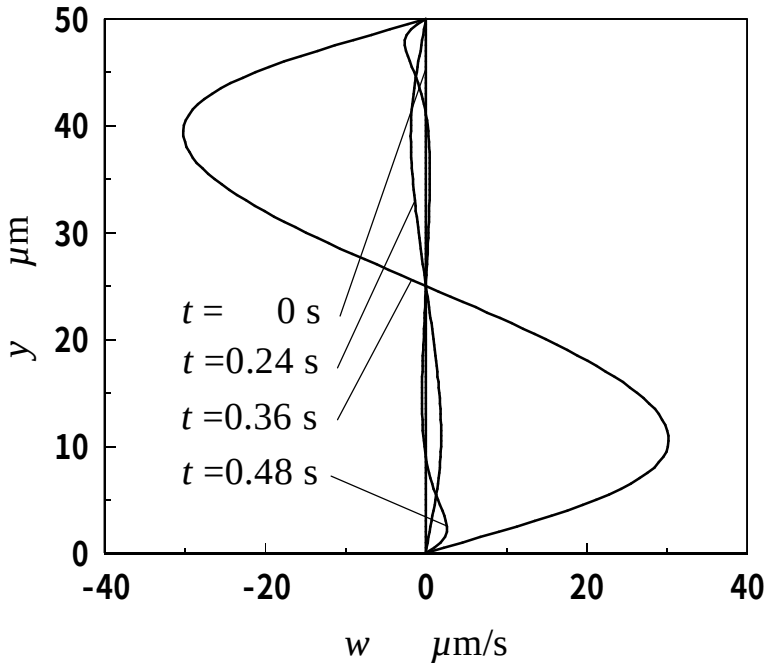

(c) Velocity profiles of z direction

Fig.4-8 Time series of profiles for electric field off→on (twist angle 180 deg)

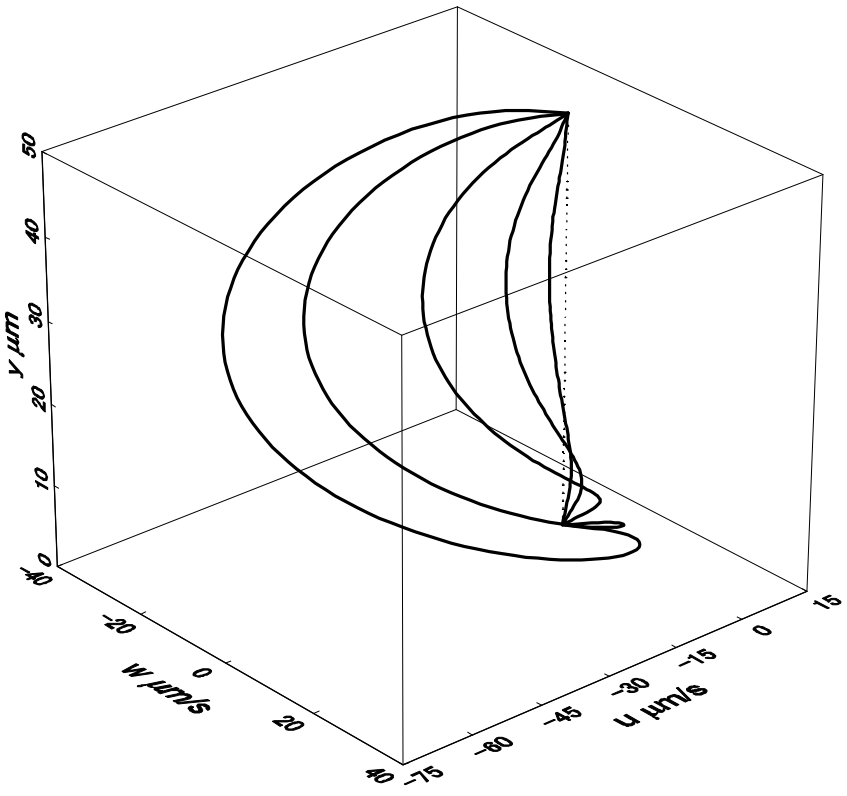

Fig. 4-9 Synthesis velocity of twist angle 180 deg

Mechanism of the occurrence of the flow

Here we make some explanation on the mechanism of the flow induced by the rotate of director with different orientation initial through two examples. Figure 4-10 shows the situation of 0 deg twist angle, in order to make it easy to understand; here we use liquid crystal molecule in stead of the director to explain. Figure (a) is the orientation initial without electric field, the molecules line in order with 0 deg twist angle and 1 deg tilt angle and parallel to each other. After the electric is imposed, show as figure (b), the molecules begin to rotate and at the same time the velocity gradient is generated. Because the plates are fixed, under the influence of the anchoring effect, the molecules near the plates do not rotate, so the velocity gradient is small. The combination of all the velocity gradient forms velocity profile shown in figure (c), and because the velocity at the plates is 0, so the velocity profile of 0 twist angle becomes anti-symmetry S-shape like figure (d). The rotate direction of the molecules can be controlled by the tilt angle, in the figures; the tilt angle is 1 deg, so the rotate direction is counterclockwise.

On the other hand, when the twist angle is 180 deg, showing in figure 4-11, same as figure 4-10, figure (a) is the orientation initial, the change of the twist angle is continuous. After the electric field is imposed, different from 0 deg twist angle, the rotate direction of the molecules is not the same. As showing in the figure (b), tilt angle is 1 deg, so the rotate direction of the lower half molecules is counterclockwise and at the same time the molecules in upper half rotate clockwise, so contrary velocity gradient is induced. On the base of the contrary velocity gradient, the X-direction velocity profile of 180 deg twist angle is one way, and with the situation that the plates are fixed, we get the final velocity profile showing in figure (d)

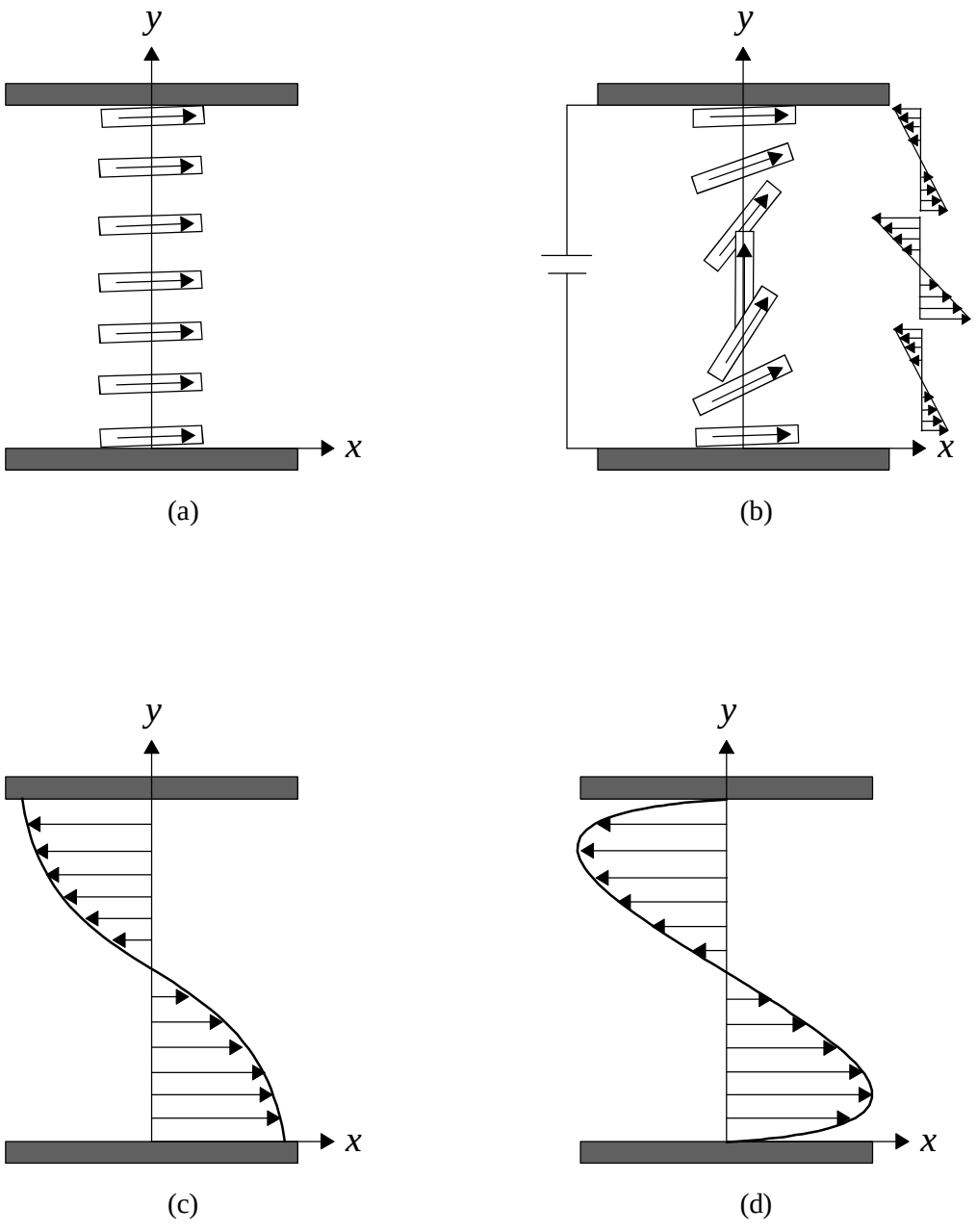

Fig. 4-10 Mechanism of generation of flow for twisted angle of 0 deg

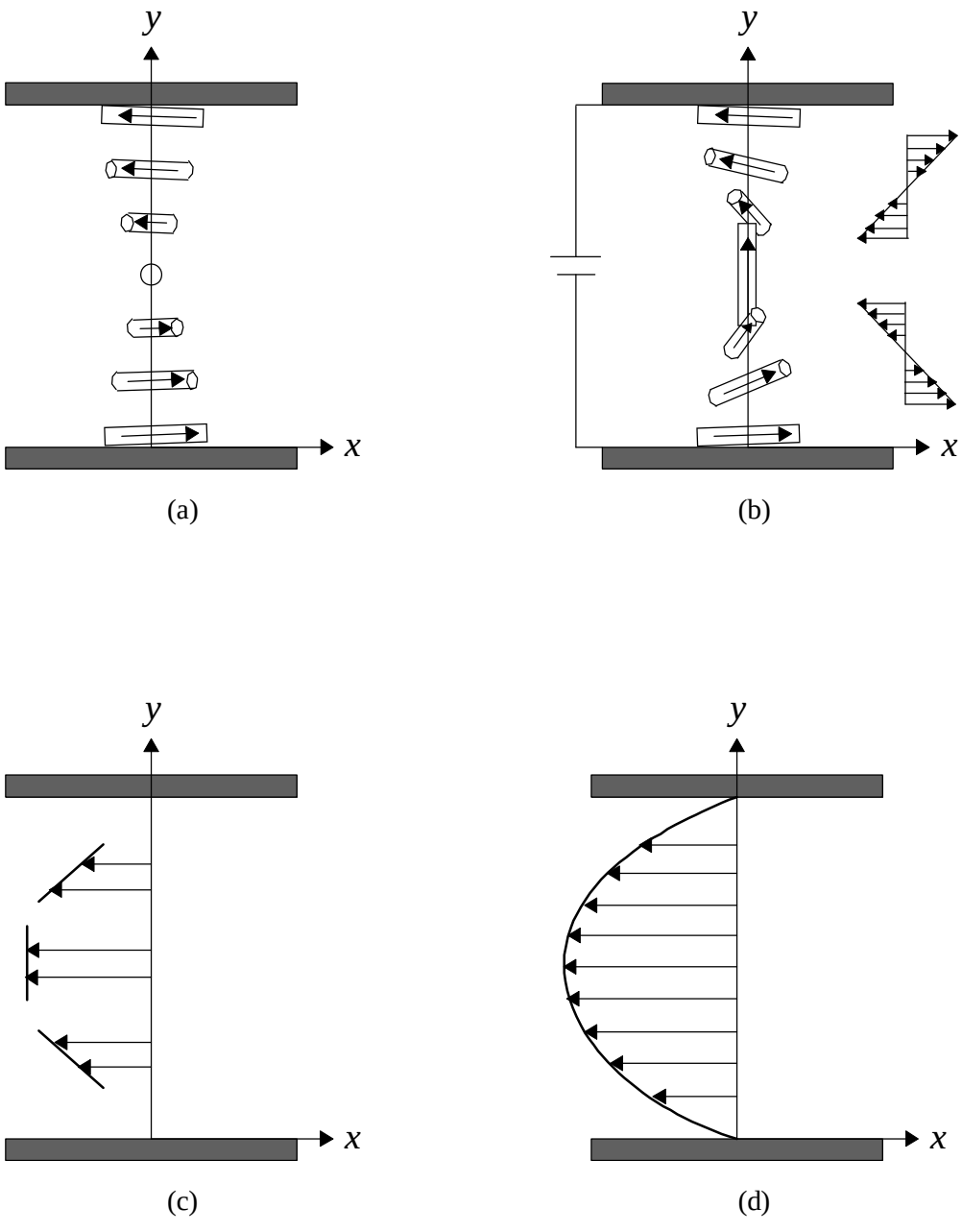

Fig. 4-11 Mechanism of generation of flow for twisted angle of 180 deg

The effect of the applied voltage (Parameter: E = 10V, H = 50μm, θ = 1°)

(1) Twist angle φ = 0°

In this part, we want to find out all the parameters that affect the shape of the velocity profile, above we discussed the twist angle and reach a conclusion that the change of the twist angle will affect the velocity profile. Now it is turn to the applied voltage, figure 4-12 shows the effect of the applied voltage on the shape of the profile, here we divide the process into two parts, the magnitude of the velocity changes from start to maximum and from maximum to cessation. From the figure we can see that the shape of the velocity profile is the same as the applied voltage of 5V, anti-symmetry S-shape and along with the change of time, the anti-symmetry is always kept, the different point is the time when the velocity reaches the maximum magnitude, instead of the 0.36 s of 5V, in the case of 10V, it changes to 0.09s.

(2) Twist angle φ = 180°

In the case of 180 deg twist angle, here we only give the profiles of X-direction, same as above the process of electric field off→on is divided into two parts showing in figure 4-13. From the figure we can easily find that in spite of the maximum reaching time, there are no differences from the results of applied voltage of 5V. Until now we can say that the applied voltage have no effect on the shape of the velocity profiles.

We also have check on the other parameters including the gap of two plates and the tilt angle, same as the voltage; they also have no effect on the profile, so here we omit the figures.

Summary

From the discussion above we can give conclusion that among the computation parameters only the twist angle can give effect on the shape of velocity profiles, so in the discussion of the effect of the symbol parameters below the twist angle is always deal with parameter.

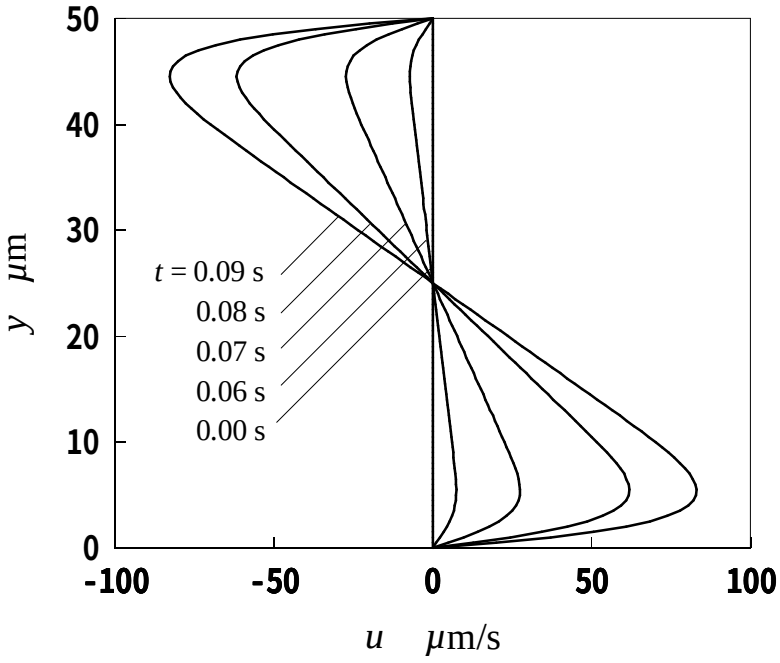

(a) From start to maximum

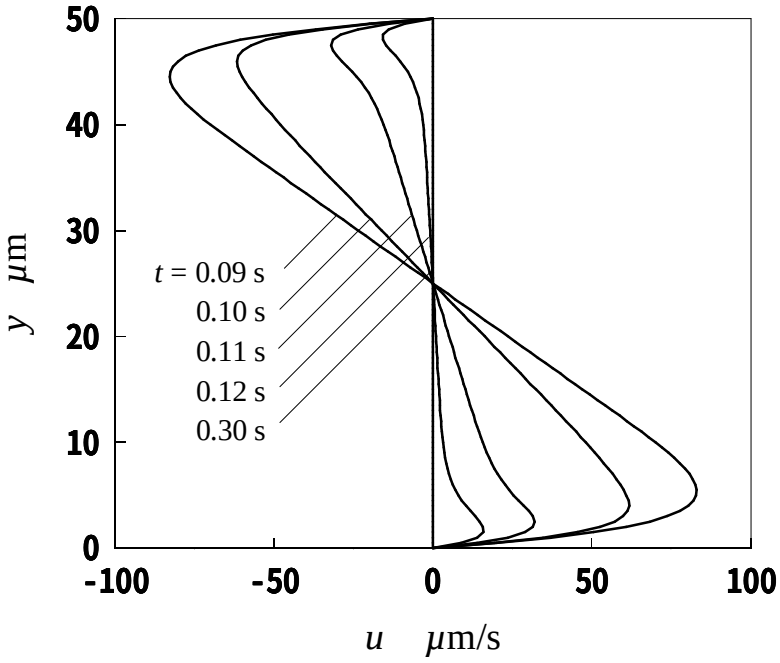

(b) From maximum to cessation

Fig. 4-12 Change in velocity profile with time (twist angle = 0 deg)

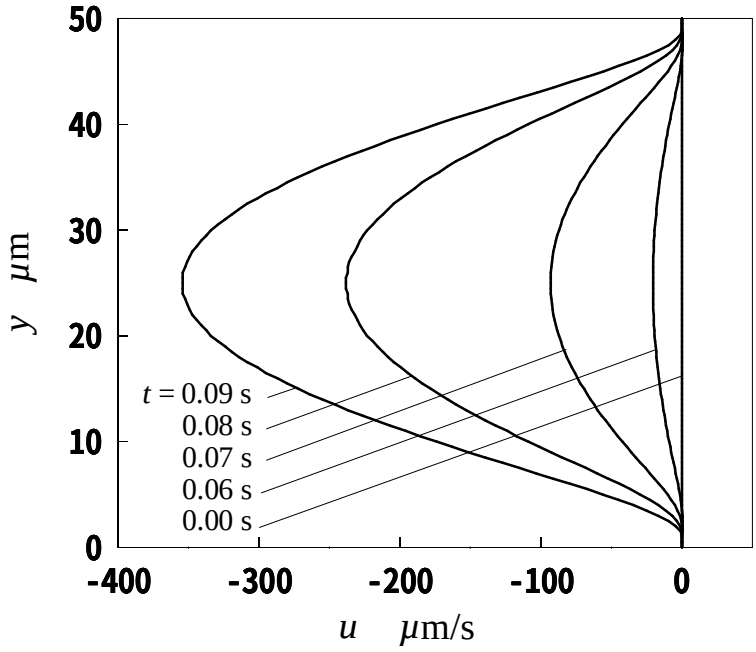

(a) From start to maximum

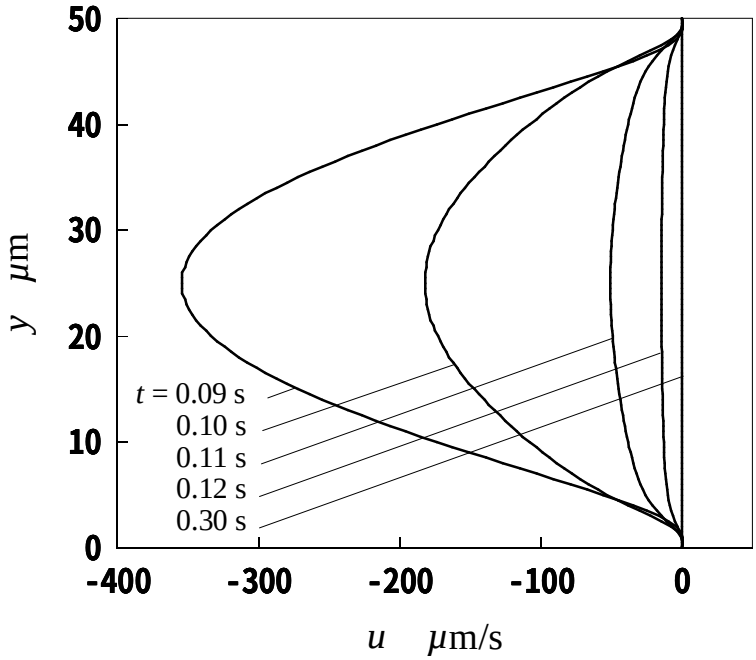

(b) From maximum to cessation

Fig. 4-13 Change in velocity profile with time (twist angle = 180 deg)

2. The effect of symbol parameters

Profiles of different quantities

Figure 4-14 shows velocity profiles of different twist angle from 0 deg to 180 deg, (a) is X-direction and (b) is Z-direction. Same as figures above, we take X-axis as the maximum velocity and Y-axis as position coordinate. As shown in (a), along with the increasing of the twist angle, the anti-symmetry is in stead by asymmetry, until 180 deg, the profile becomes to symmetric and the magnitude shows maximum value: about 65μm/s. On the other hand, the profiles of Z-direction are contrary, when the twist angle is 0 deg, there is no director component at Z-direction, it can be said that in this case the velocity profile is symmetric. Along with the increasing of the twist angle, it become to be asymmetric and when the twist angle reach 180 deg, on the contrary, the velocity profile become anti-symmetric same as the X-direction of 0 deg twist angle, the magnitude is also same of about 30μm/s.

Figure 4-15 gives the orientation profiles of different twist angle from 0 deg to 180 deg when the velocity reaches maximum. We can see that the rotate angle increases along with the increasing of the twist angle, and because the anchoring effect is small in the middle of the gap, the maximum of the angle shows at the middle, the value is about 60 deg.

Time change of typical quantities

We summarize time change of typical quantities such as stress *T*, velocity *U*, flow rate *Q* and rotate angle Θ in figure 4-16. Representative parameters such as voltage 5V, gap 50μm, tilt angle 1 deg is used, and the quantities are the total value of X-direction and Z-direction, for example, *T* is the value of $\sqrt{\tau_{yx}^2 + \tau_{yz}^2}$. From the figures we can see that as soon as the imposition of the electric field, the director begins to rotate, but because the rotate velocity is small at first, so the velocity is not induced immediately, after about 0.2 s, velocity increases rapidly and reach maximum at 0.36 s and then decreases with same gradient, at 0.5 s all the process is over and the rotate angle of that time is about 60 degree. The change processes of the stress (here is the stress on the upper plate) and the flow rate is same as the velocity: increase from 0.2 s, reach peak value at 0.36 s and decrease to 0.

In the figure (a) and (d), the effect of the twist angle is small; the maximum of the

stress appears when the twist angle is 0 deg. On the other hand, in figure (b) and (c), we can easily see that the quantities increase with increasing of twist angle.

Applied voltage *E* (gap 50μm, tilt angle 1 deg)

The effect of the applied voltage is shown in figures from 4-17 to 4-20, for the parameters except for the voltage, the representative value is used. Figure 4-17 shows the effect of the voltage on the stress and the response time (expressed by the time the stress reaches maximum). Along with increasing of the applied voltage, we can see the tendency of increasing in magnitude of stress and decreasing in the response time, the maximum value of the stress is about 1.2 Pa when the voltage is 10 V and the response time is about 0.1 s. The effect of the twist angle is not so large, and in the case of 0 deg twist angle, the stress can get the maximum, this is can be seen from the profile, the value of gradient of the profile is most large when the twist angle is 0 deg.

Figure 4-18 gives the effect on the velocity and the response time, it can be seen easily that the change tendency of the velocity is same as the stress, increases with the applied voltage and the response time is also same. The different point is the effect of the twist angle, compare to the case of stress, the velocity increase by a wide margin when the twist angle changes from 0 deg to 180 deg, the value is about 60 μm/s with 0 deg twist angle and 350 μm/s with 180 deg twist angle. We can see that the flow rate shows the same change tendency with the velocity from figure 4-19. At last let we see the effect on the rotate angle range of the director showing in figure 4-20, the range is about from 20 deg to 90 degree and along with the increasing of the voltage the range become wide a little.

Gap of the two plates *H*

The effect of the gap is shown in figures from 4-21 to 4-24, for the parameters except for the gap, the representative value is used. Figure 4-21 shows the effect of the gap on the stress and the response time. Along with increasing of the gap, we can see the tendency of decreasing in magnitude of stress and increasing in the response time, the maximum value of the stress is about 6 Pa when the gap is 10μm and the response time is about 0.01 s. It is also can be seen that there is a large gap in the value of the stress between the gap of 10μm and 20μm, the decreasing of the gap from 20μm can make an exponential increasing in stress, and it is a predominant point for the micro-actuator. The effect of the twist angle is not so large, and in the case of 0 deg twist angle, the stress can get the maximum.

Figure 4-22 gives the effect on the velocity and the response time, it can be seen easily that the change tendency of the velocity is same as the stress, decreases with the gap and the response time is also same. The different point is the effect of the twist angle, compare to the case of stress, the velocity increase by a wide margin when the twist angle changes from 0 deg to 180 deg, the value is about 150 μm/s with 0 deg twist angle and 320 μm/s with 180 deg twist angle when the gap is 10μm. The effect on the flow rate is showing in the figure 4-23, when the twist angle is 0 deg, the profile is antisymmetic, so the total flow rate is 0. It also can be seen that the gap has not any effect on the flow rate while the twist angle has, from the profiles showed above, along with the change of the twist angle, the profiles changes from anti-symmetric to asymmetric then to symmetric, so the total flow rate increases with the increasing of the twist angle. The value is 500μm^2/s of 60 deg and reaches to 1700μm^2/s when the twist angle reaches 180 deg. At last let we see the effect on the rotate angle range of the director showing in figure 4-24, the range is about from 15 deg to 90 degree except the gap of 10μm, and along with the increasing of the voltage the range become wide a little. The results above is get with a steady voltage of 5V, so when the gap is changed, the electric strength is also changed, in order to find exact effect of the gap, we do another computation with steady electric strength (0.1V/μm) and the results is showing in figure 4-25. From the figure we can see that with same strength the quantities change little with the increasing of the gap, and the tendency of the change is contrary to the one showing in figure 4-22 and 4-23. In addition, the response time when the gap is 10μm is very long, this is because with this gap, in order to keep the electric strength as same as others, the applied voltage must to be set as 1V, this value is very near to the Freedericksz transition critical voltage value of 0.745V, so the rotate velocity of the director is very small.

Tilt angle θ

The effect of the tilt angle is shown in figures from 4-26 to 4-28, for the parameters except for the tilt angle, the representative value is used. Figure 4-26 shows the effect of the tilt angle on the stress and the response time. We can see that the change of the tilt angle does not induce any change on the stress and for the response, there is little effect, with the increasing of the tilt angle the response becomes better. From figure 4-27 and 4-28 we can get the conclusion that the change of the tilt angle has little influence on the velocity and flow rate.

An example of small gaps

In the section of the effect of gap, we can see that when the gap is less than 20μm, the quantities including the stress, velocity and flow rate change exponential with the decreasing of the gap, and the response also becomes better. Here we will give an example of small gaps from 5μm to 20μm to see how excellent of the characteristic. Figure 4-29 shows the transient behaviors for small gap, the representative value of other parameters except gap is used. Because the twist angle is 0 deg, flow rate is 0, here we only give the figures of stress, velocity and rotate angle. From the figures we can see when the gap is 5μm, the maximum of the stress can reach 23Pa, and in addition, the response time is only about 0.004s, the velocity also shows good characteristic when the gap is decreasing to 5μm. Now in the field of liquid crystal display, it is very common that the gap is a few microns. Certainly, it is very difficult to make the liquid crystal cell when the gap is very small, from the computation results we can easily see that there is certain connection between the small gap and the high performance of the actuator.

An example of large twist angle

Figure 4-30 shows the results of velocity profiles with different twist angle, different from figures above, this time the twist angle selected is very large and with an interval of 90 deg which is more common to the cell used in the field of real liquid crystal display. With different director field (mainly decided by the twist angle), the resistance exposed on the molecules when they rotate is very different.

Figure 4-31 shows the variation of maximum magnitude of the velocity vector with twist angle. The horizontal axel shows twist angles, the perpendicular axel is the time velocity reaches the maximum and the magnitude of the velocity vector. It is found that at first the velocity increases with the increasing of the twist angle to maximum when twist angle is 450 deg, the maximum is about 120μm/s, almost 4 times of the one when the twist angle is 0 deg. while the time do not change so much. That is means that the response is not affected by the twist angle much. From the results we can say when the twist angle is 450 deg; the orientation state is suitable for the molecules of liquid crystal to rotate to turn electric to kinetic energy.

Figure 4-32 shows the variance of the flow rate with twist angle, the perpendicular axel is flow rate direction and magnitude. It is easily known that flow rate is just like velocity in magnitude, increases with the increasing of twist angle, the difference is that flow rate reaches maximum at twist angle of 360 instead of the 450 deg of the velocity, because the flow rate depends on not only the magnitude of the velocity but also the

symmetry property of the velocity profiles. As shown in Fig. 4, the time when the flow rate reaches maximum is almost same as the velocity, so here we omit the figure that shows response ability of flow rate with twist angle, it is easily predicted that it is same as the one of the velocity.

The direction of the flow rate changes linearly with the twist angle, and with a increasing rate of 1/2 of the twist angle, that is to say along with the increasing of the twist angle from 0 deg to 540 deg, the flow direction increases from 90 deg to 360 deg with a fixed increasing rate.

Figure 4-33 shows the variance of the shear stress exposed on the upper plate with the twist angle. The perpendicular axel is the stress direction and magnitude of the stress vector. As shown in Fig.3 the gradient of the velocity profile at the upper plate decreases with the twist angle, so the magnitude of shear stress vector decreases with the increasing of the twist angle. The maximum value appears at the point of twist angle 0 deg, and the magnitude is nearly 0.24 Pa. The change tendency of the direction of the shear stress is same as the flow rate, changes linearly but with a start angle of 180 instead of 90 of the velocity. The response ability is the same as flow rate.

Summary

By discussing the effect of parameter such as twist angle, applied voltage and gap on the induced backflow, conclusions following are achieved.

1. The direction of the backflow depends only on the twist angle.
2. The magnitudes of physical quantities depend on the twist angle, the applied voltage and the gap of the two plates. Among the parameters, the effect of the gap is most important; when the gap is set to be very small the stress and the velocity can get exponential change with the decreasing of the gap.
3. The response time depends only on the applied voltage.

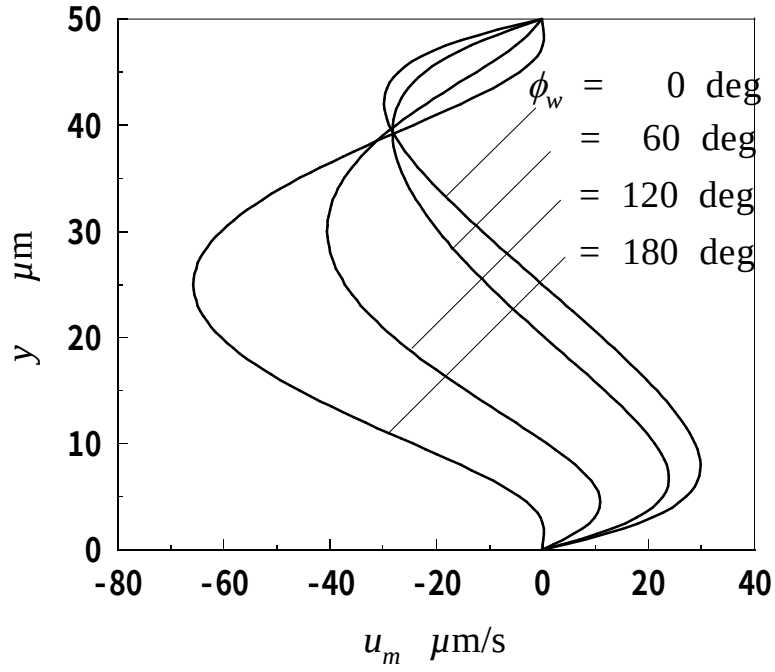

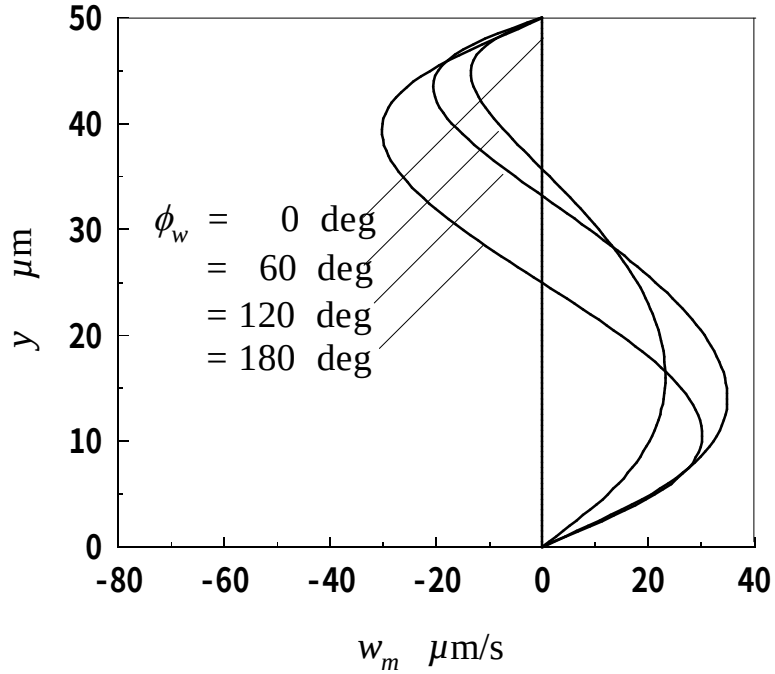

Fig. 4-14 Velocity profiles

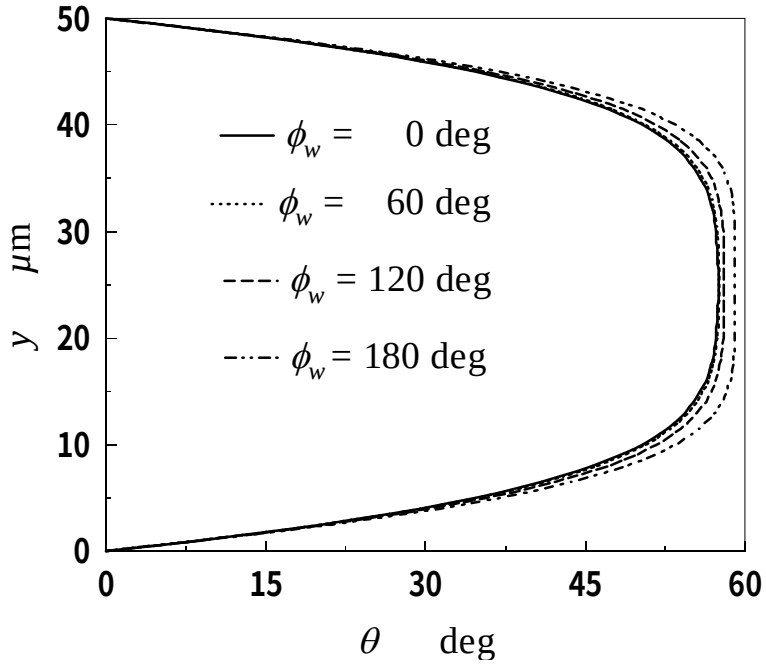

Fig. 4-15 Orientation profile

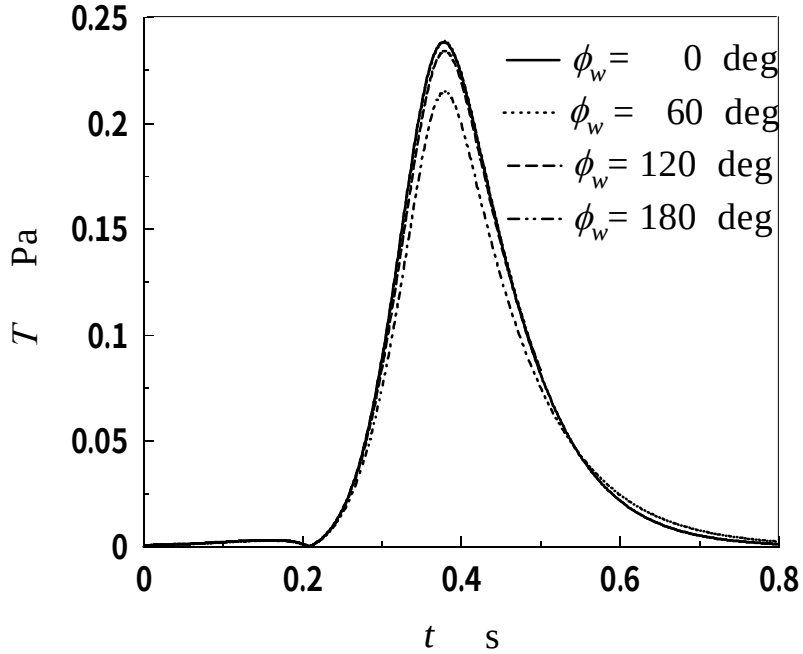

(a) Change of stress impact on the upper plate with time

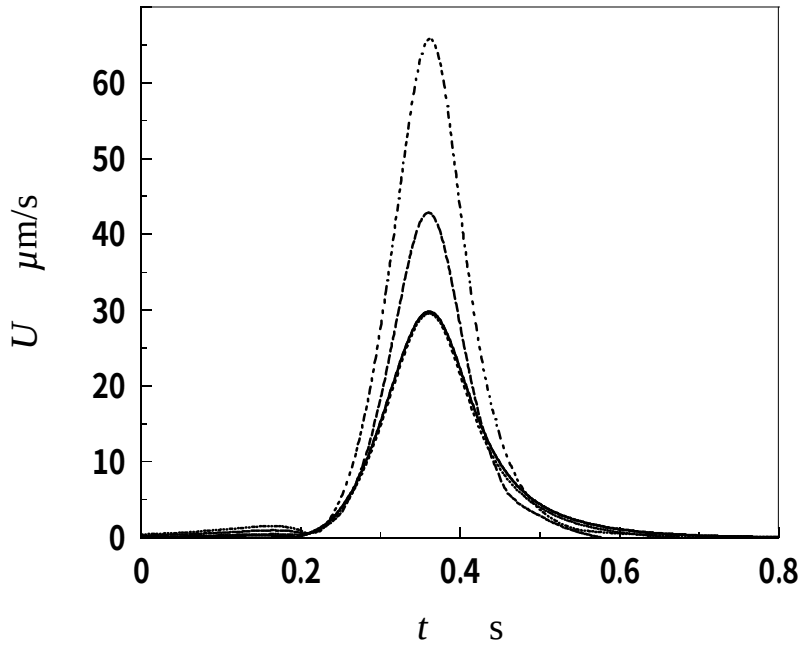

(b) Change of flow velocity with time

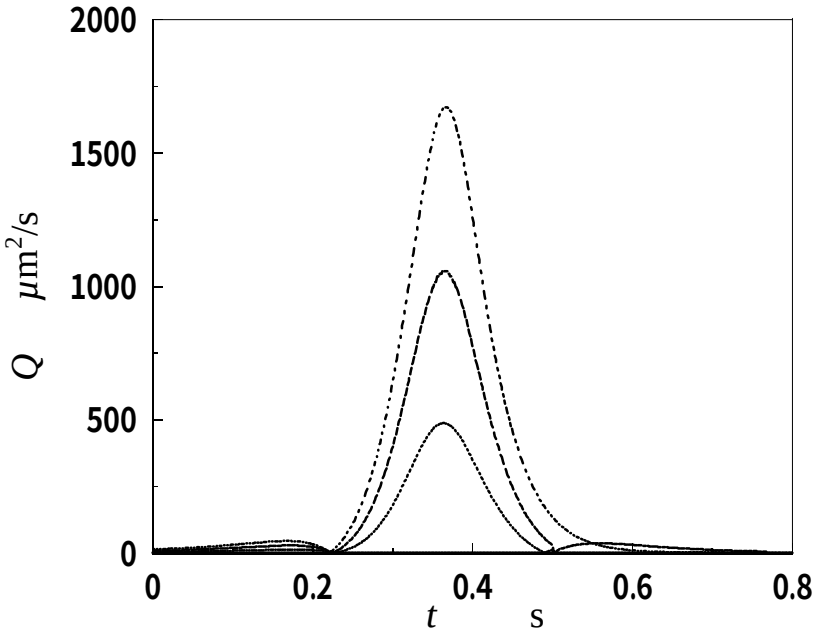

(c) Change of flow rate with time

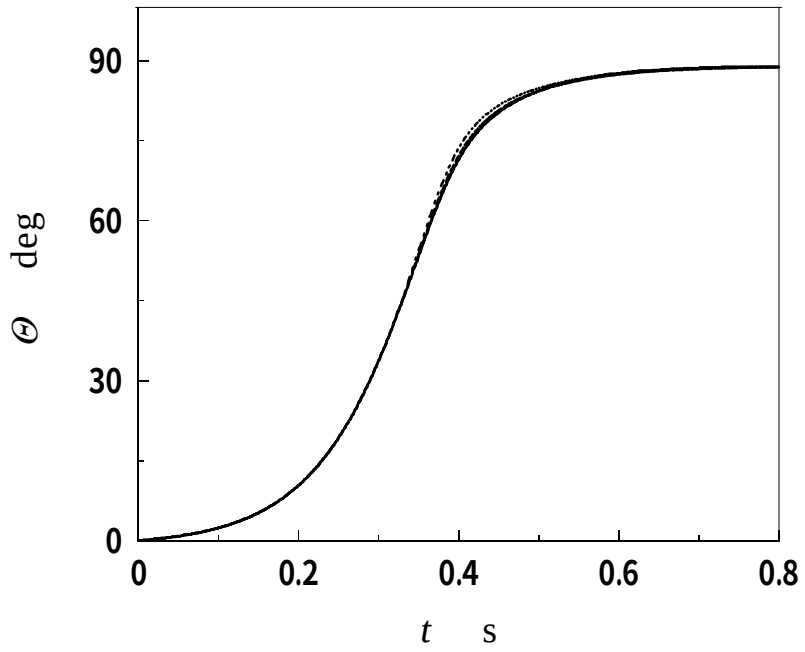

(d) Change of orientation angle with time

Fig. 4-16 Transient behaviors of typical quantities

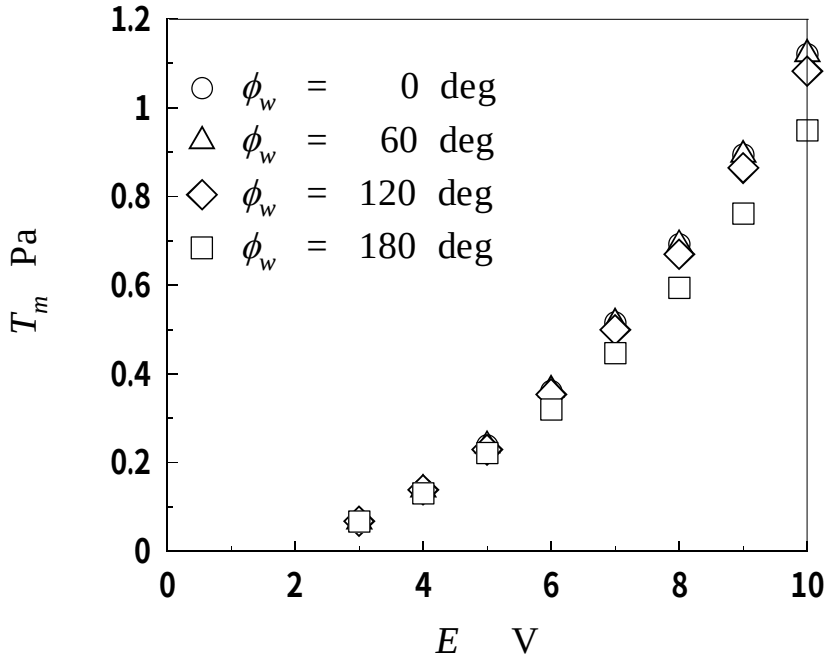

(a) Influence on the stress magnitude

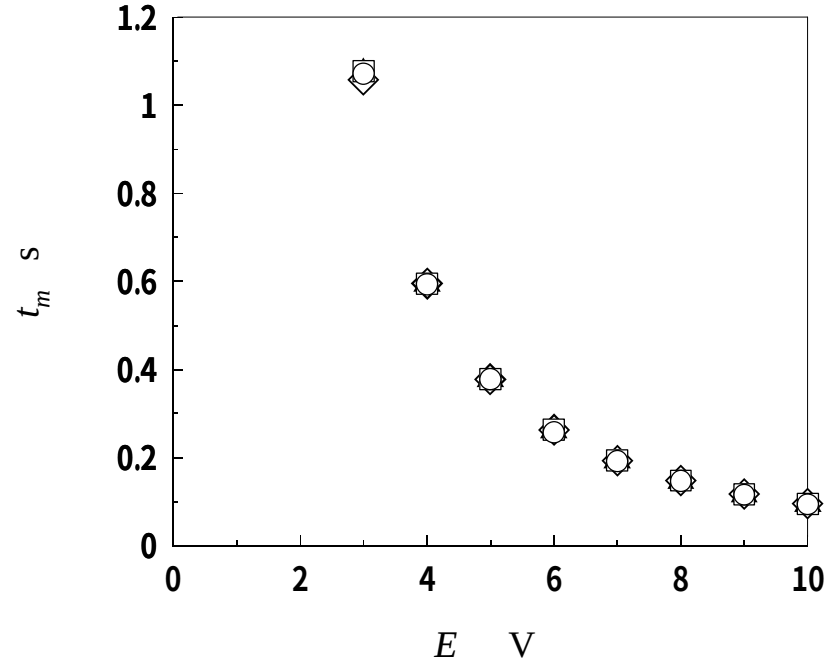

(b) Influence on the time to reach to maximum

Fig. 4-17 Effect of applied voltage on the stress

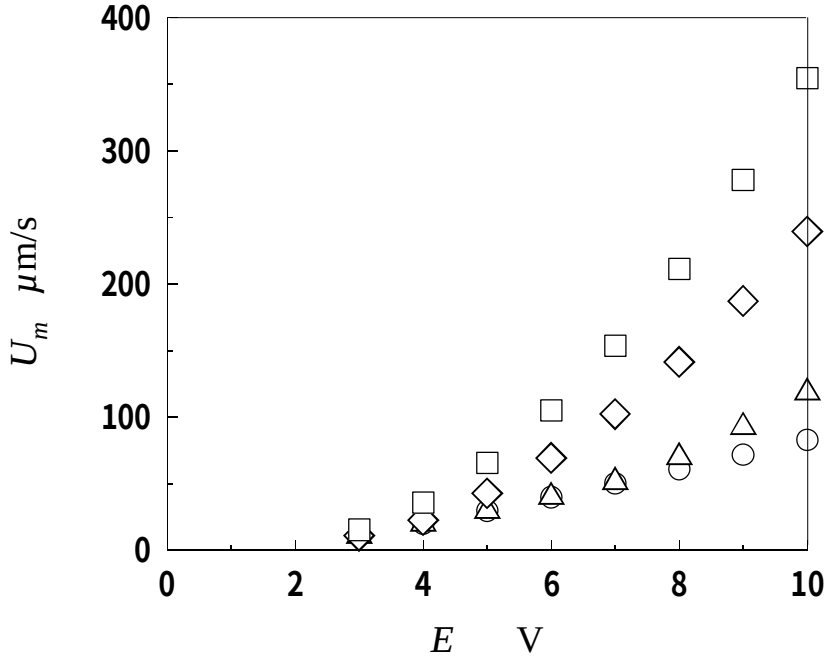

(a) Influence on the velocity magnitude

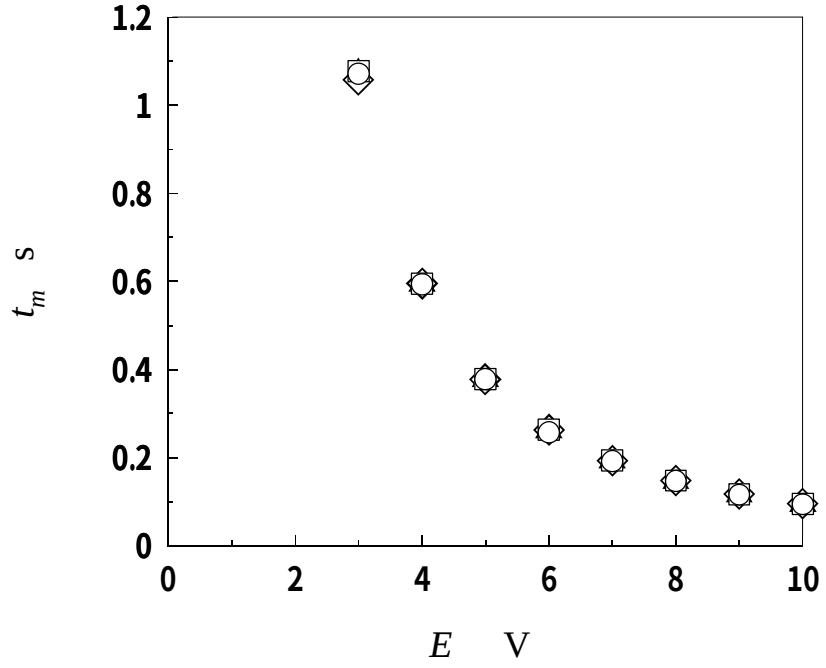

(b) Influence on the time to reach to maximum

Fig. 4-18 Effect of applied voltage on the velocity

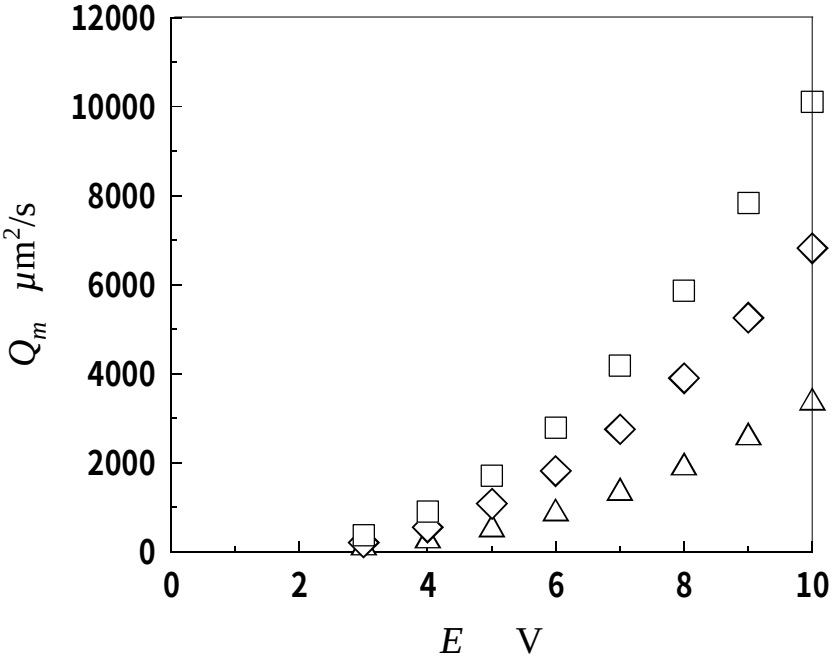

Fig. 4-19 Effect of applied voltage on the flow rate

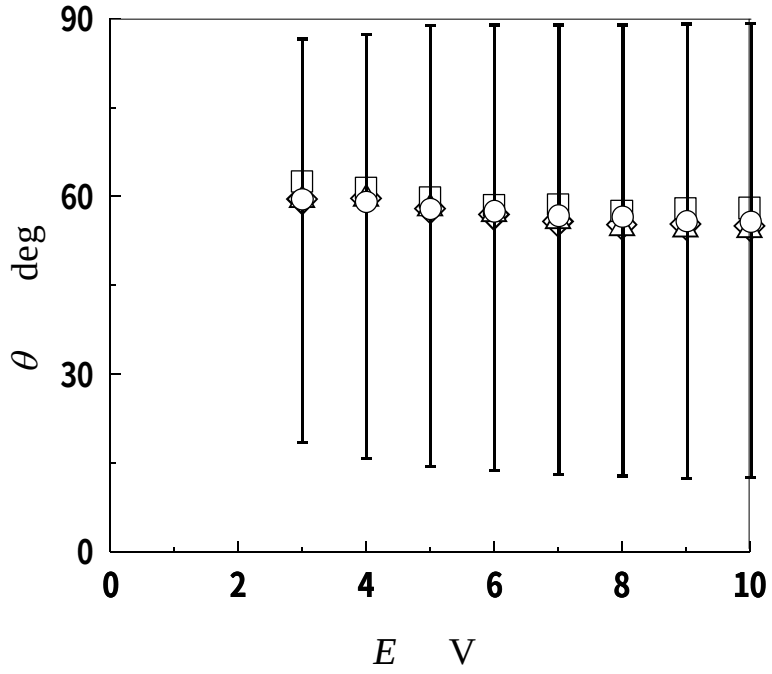

Fig. 4-20 Effect of the applied voltage on the rotate angle

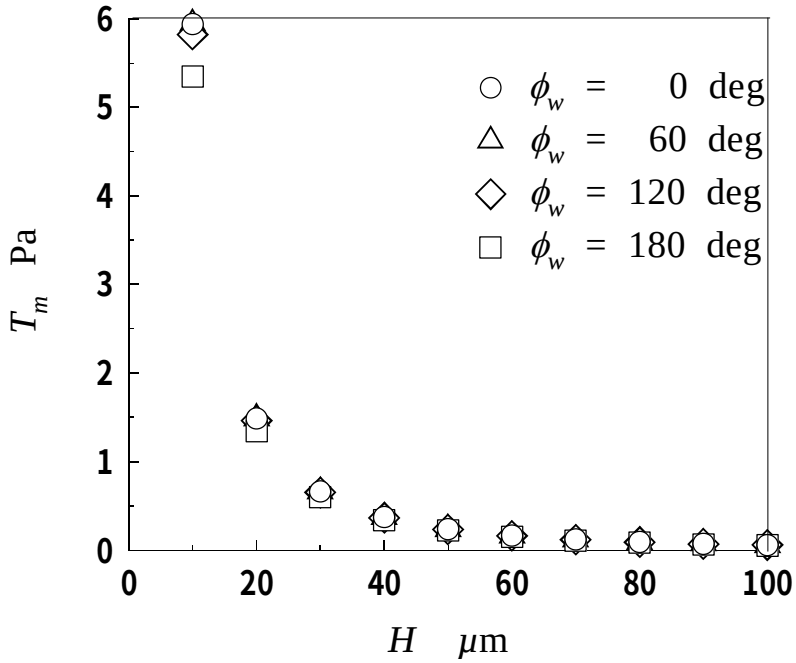

(a) Influence on the stress magnitude

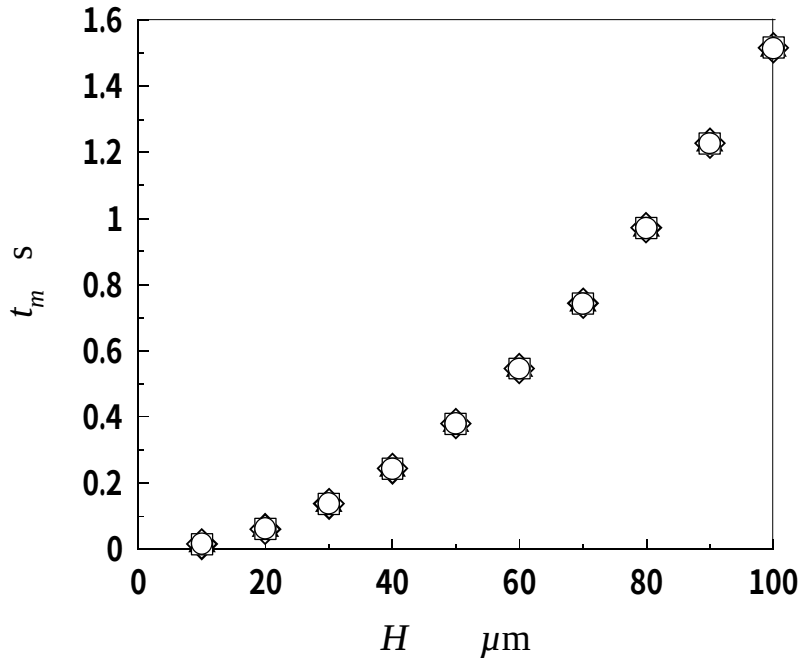

(b) Influence on the time to reach to maximum

Fig. 4-21 Effect of gap between the two plates

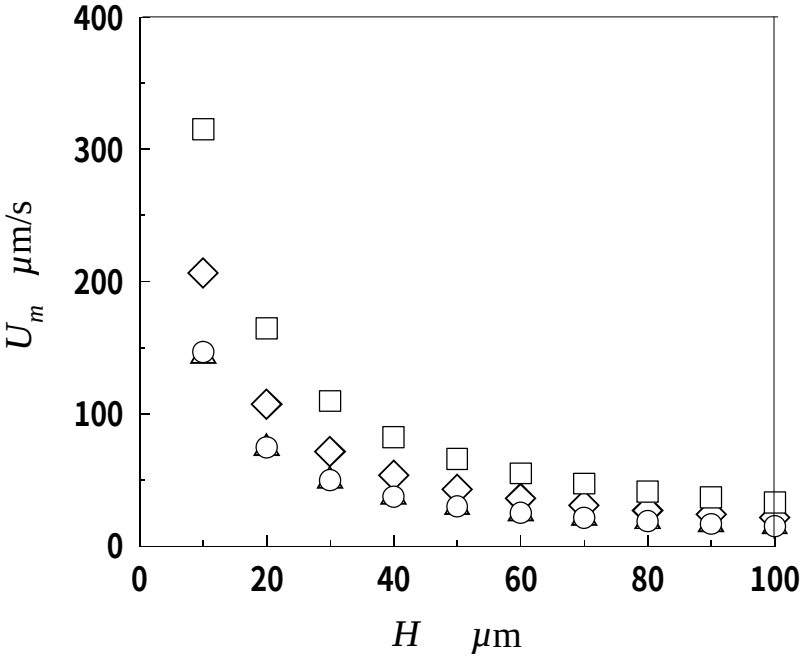

(a) Influence on the velocity magnitude

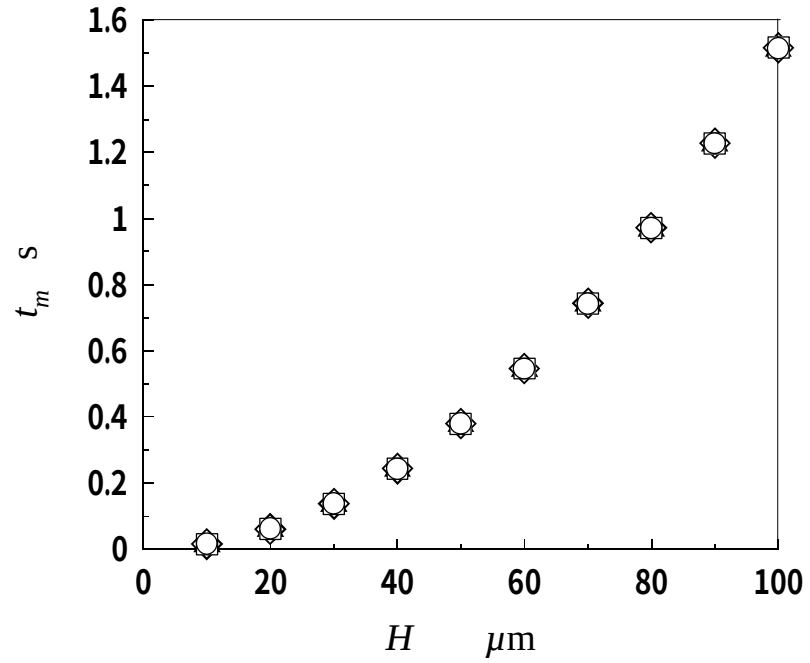

(b) Influence on the time to reach to maximum

Fig. 4-22 Effect of gap between the plates

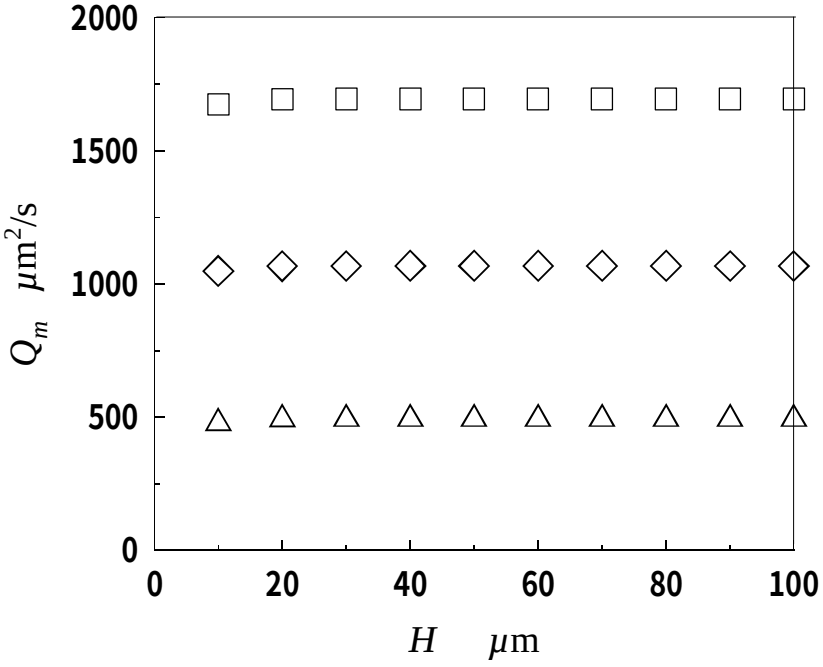

Fig. 4-23 Effect of the gap on the flow rate

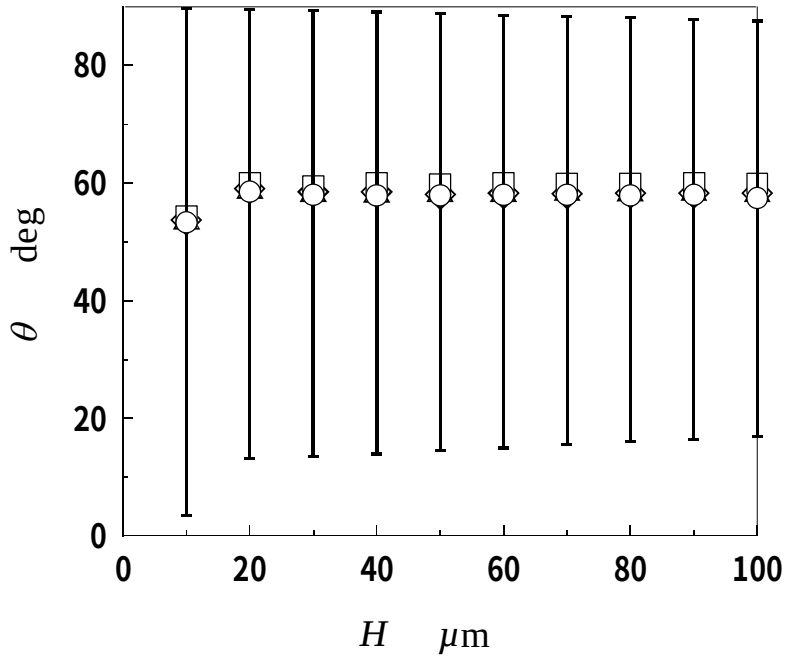

Fig. 4-24 Effect of the gap on the rotate angle

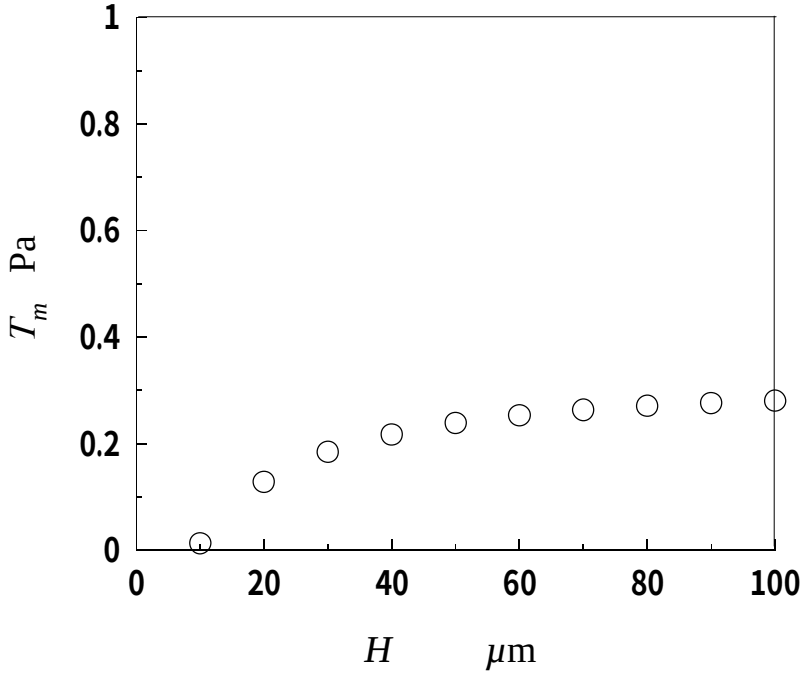

(a) Influence on the stress magnitude

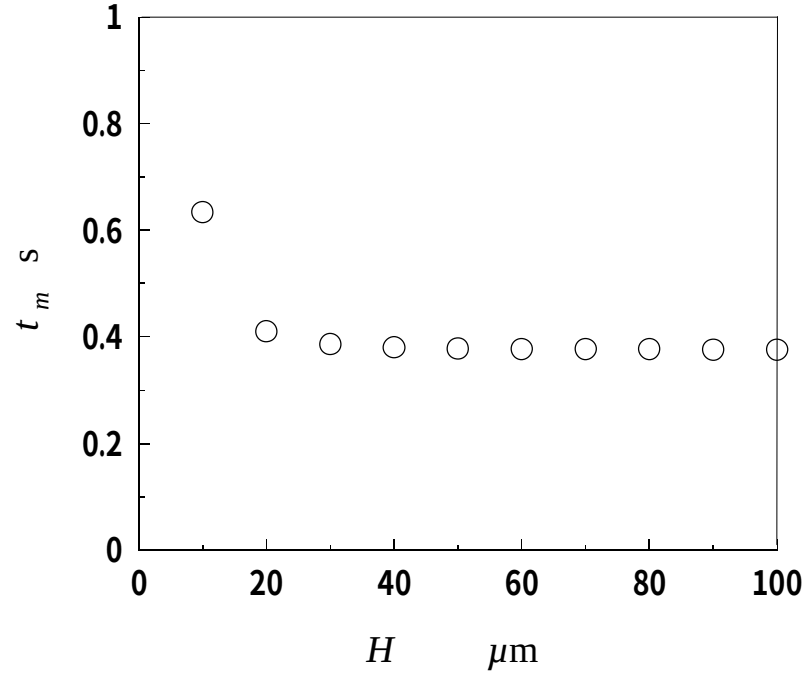

(b) Influence on the maximum reach time

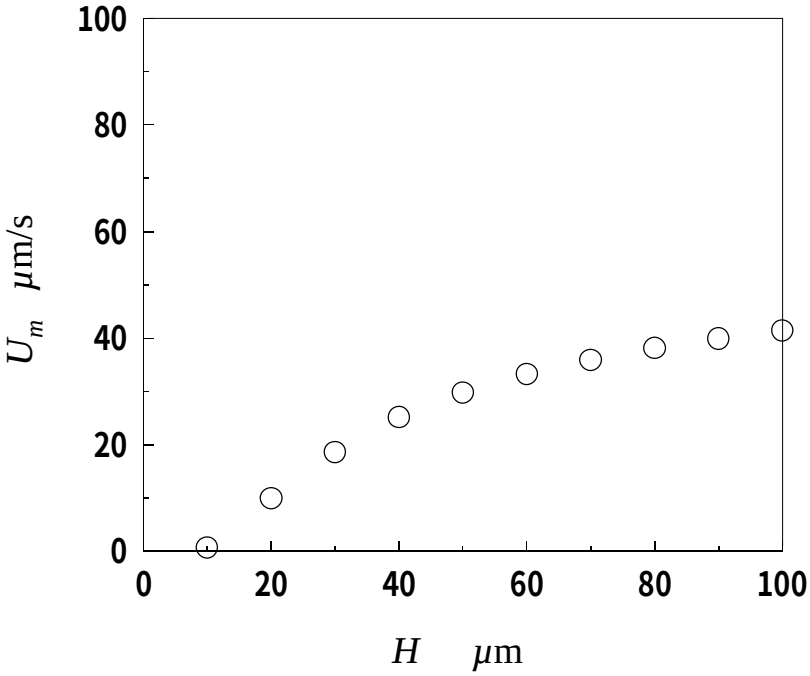

(c) Influence on the velocity magnitude

Fig. 4-25 Effect of gap with constant electric field

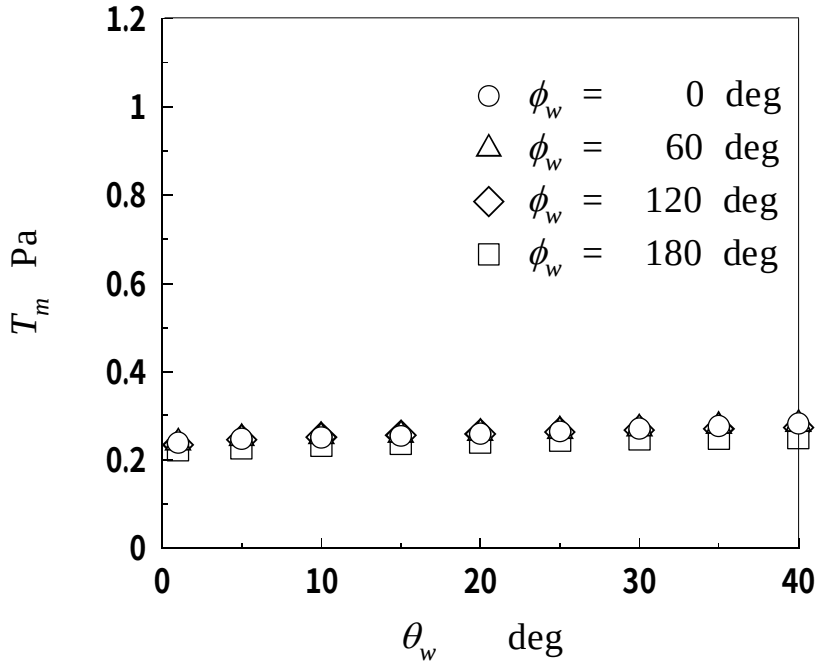

(a) Influence of the stress magnitude

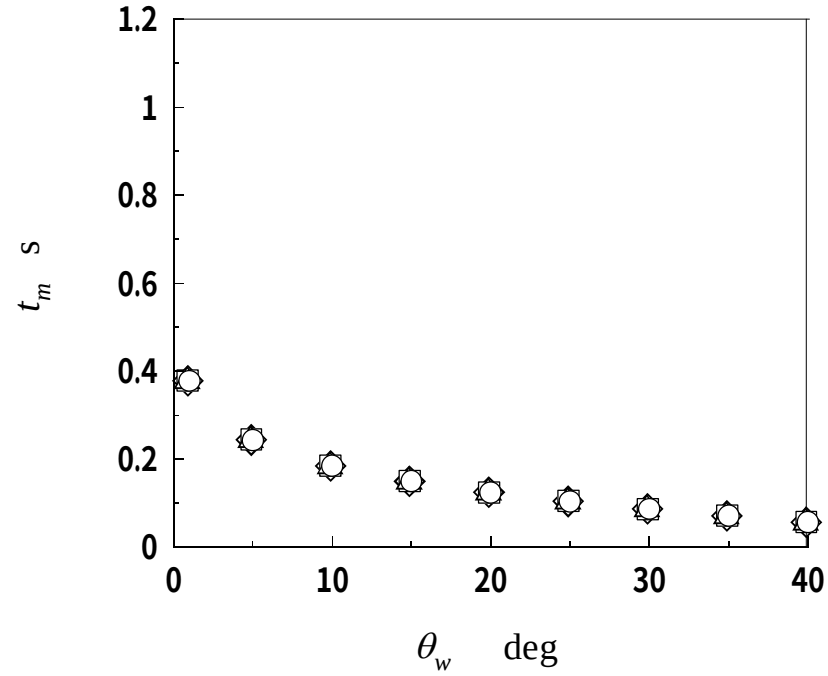

(b) Influence on the time to reach to maximum

Fig. 4-26 Effect of tilt angle

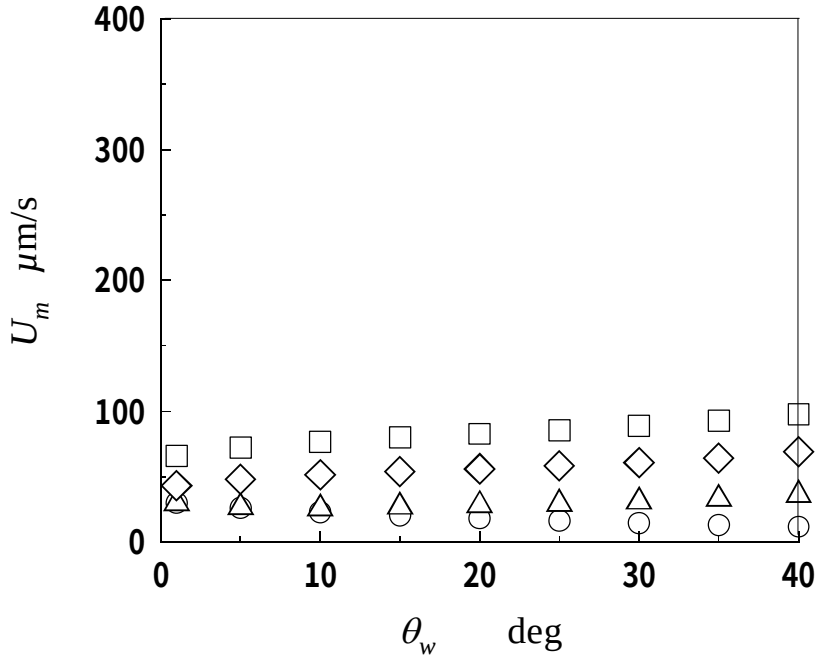

(a) Influence on the velocity magnitude

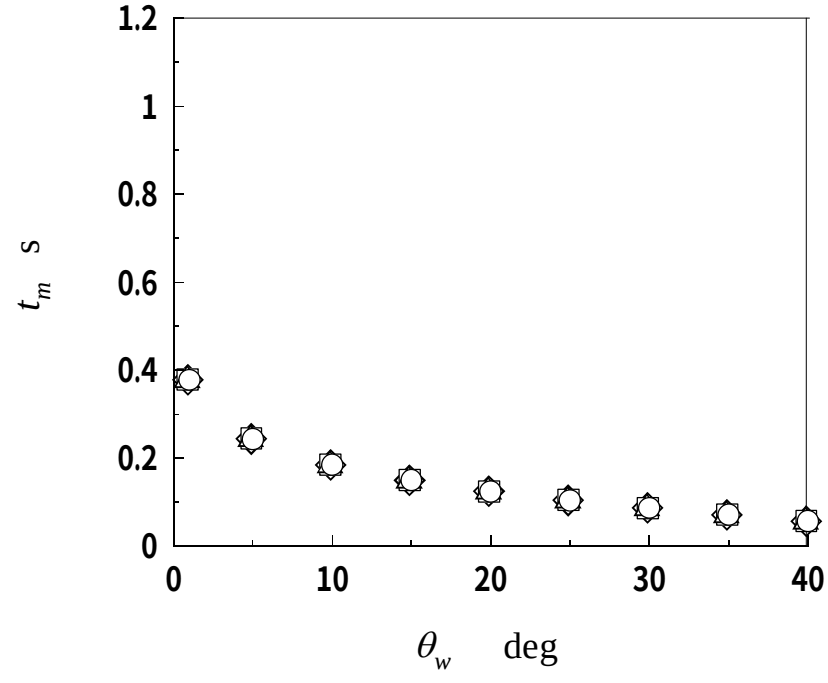

(b) Influence on the time to reach to maximum

Fig. 4-27 Effect of tilt angle

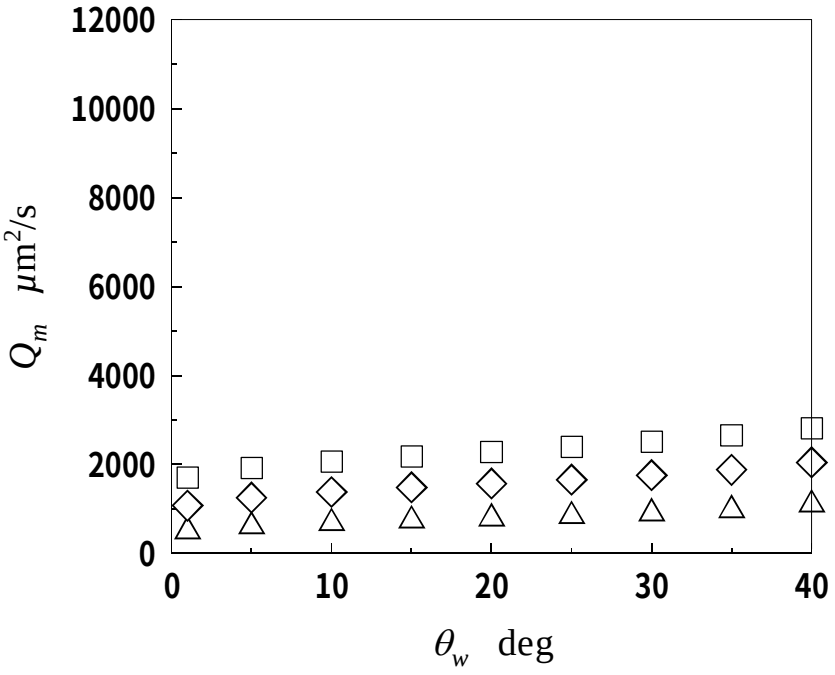

Fig. 4-28 Effect of the tilt angle on the flow rate

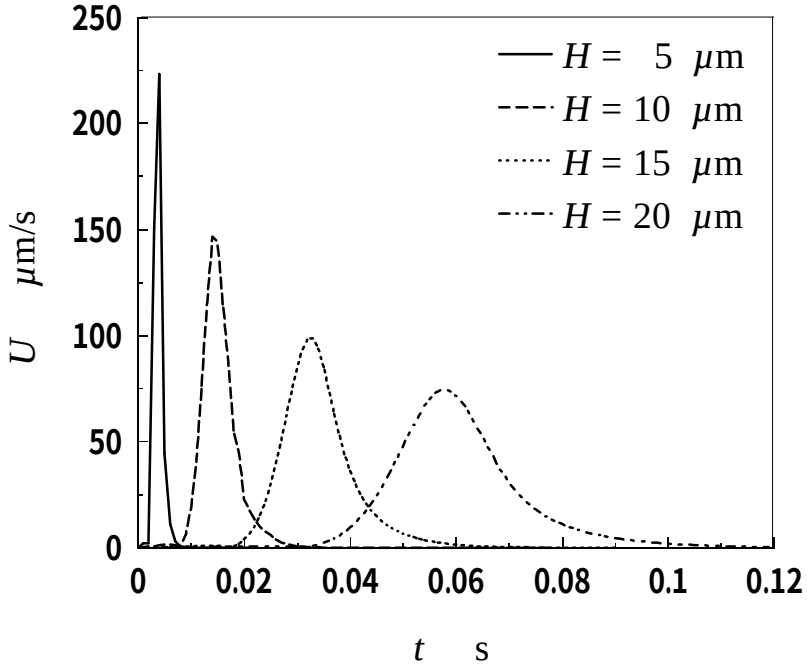

(a) Change of velocity magnitude with time

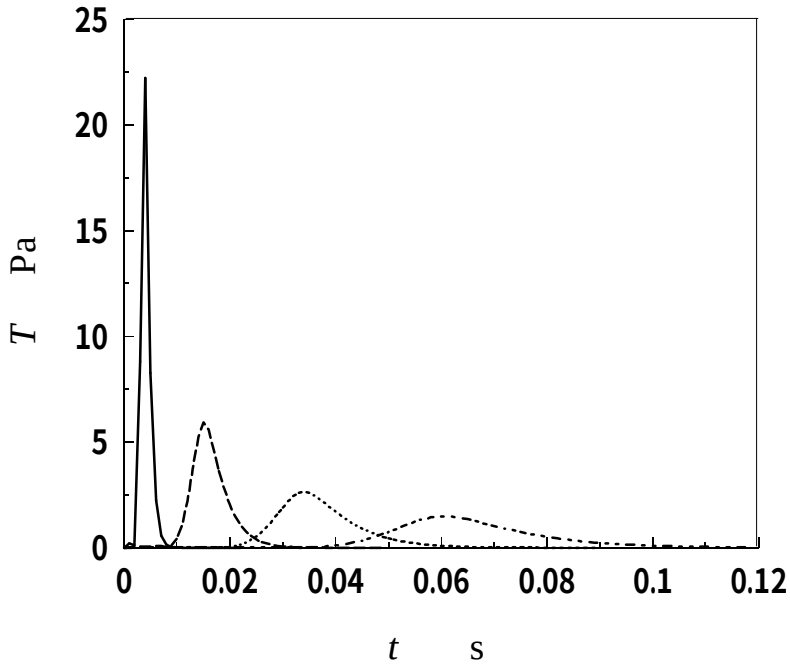

(b) Change of the stress magnitude with time

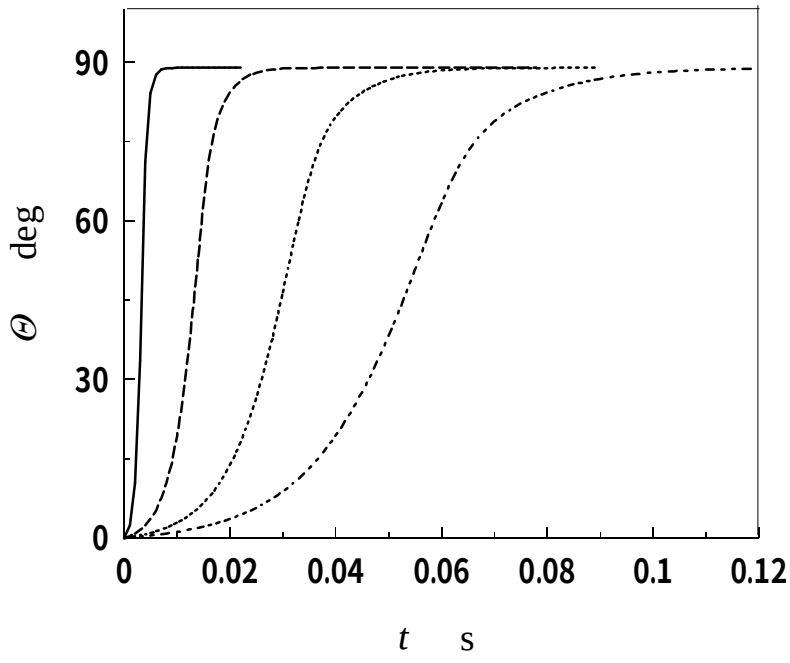

(c) Change of the rotate angle with time

Fig. 4-29 Transient behaviors for small gaps

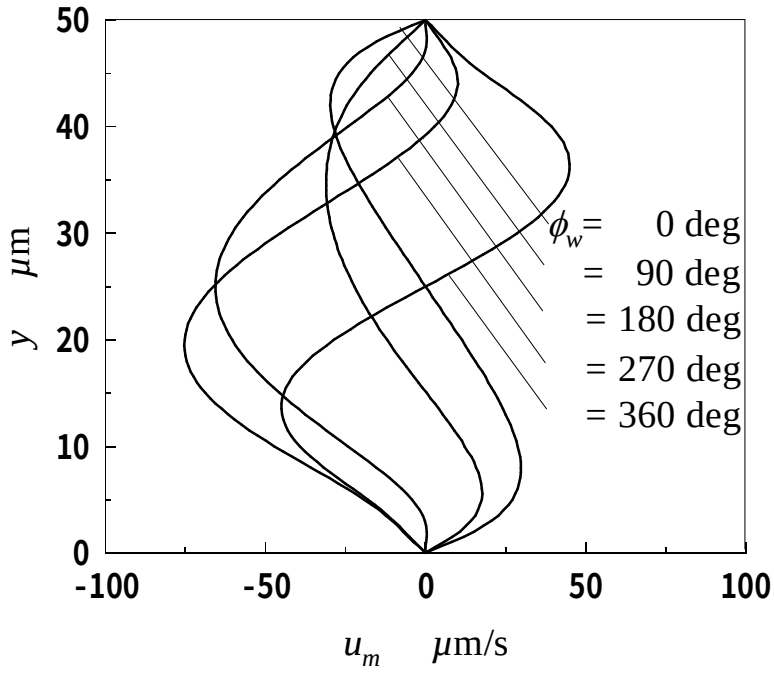

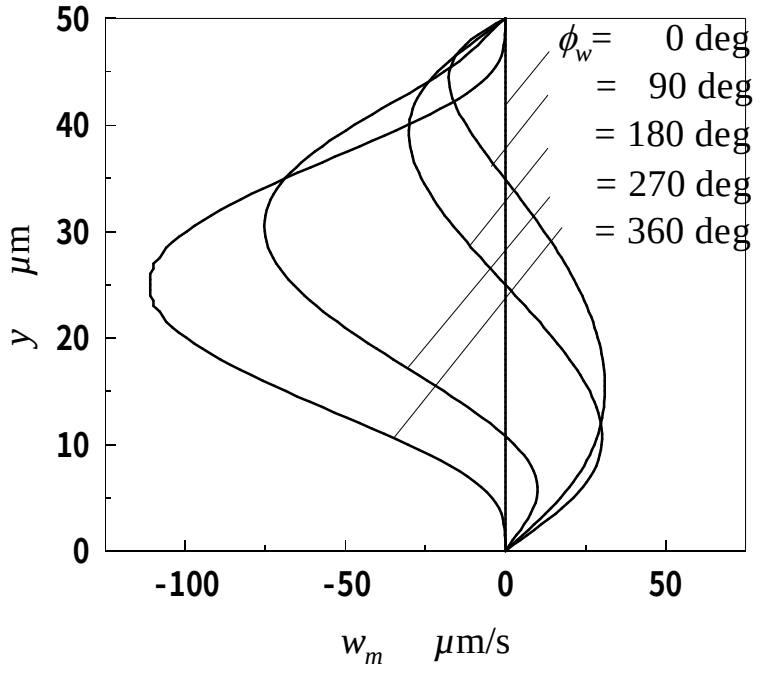

Fig. 4-30 Velocity profiles

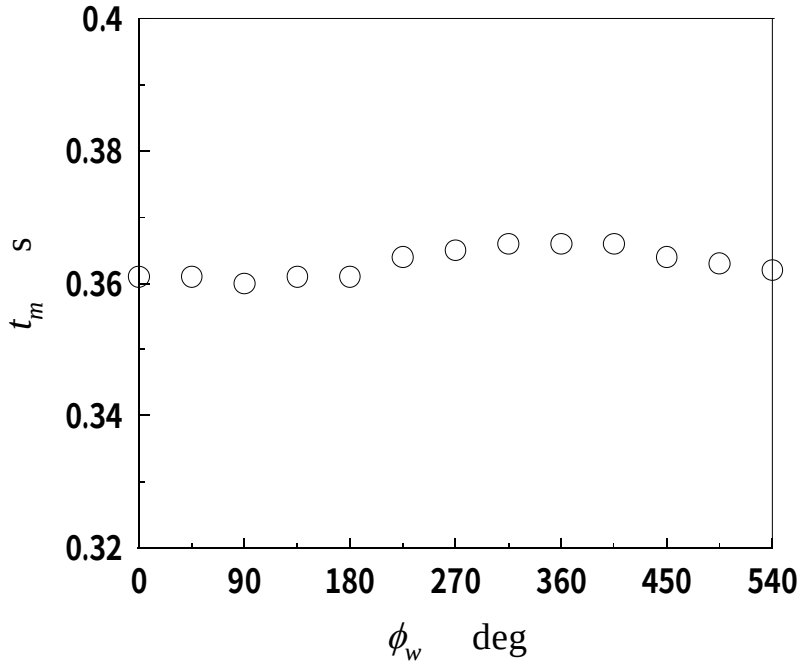

(a) Influence on the maximum reach time

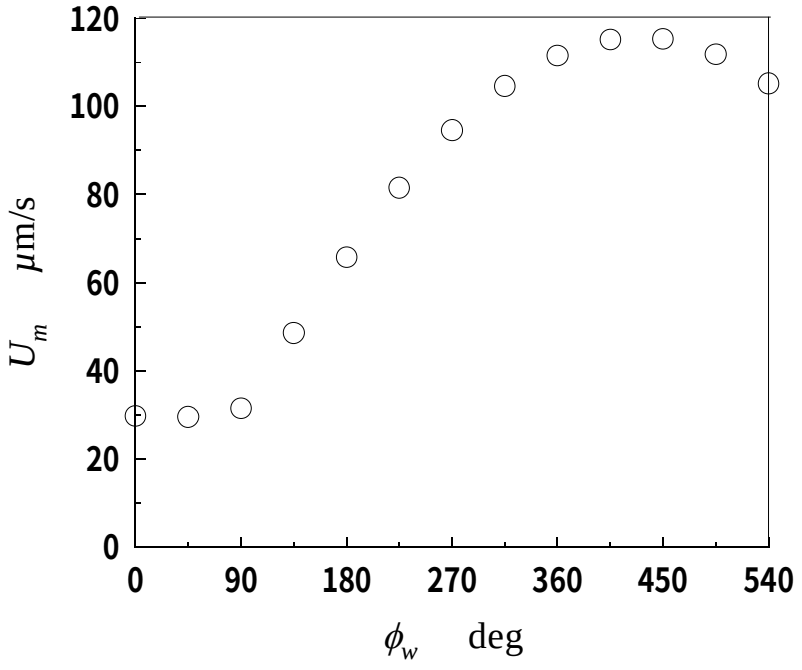

(b) Influence on the velocity magnitude

Fig. 4-31 Effect of the twist angle on the velocity

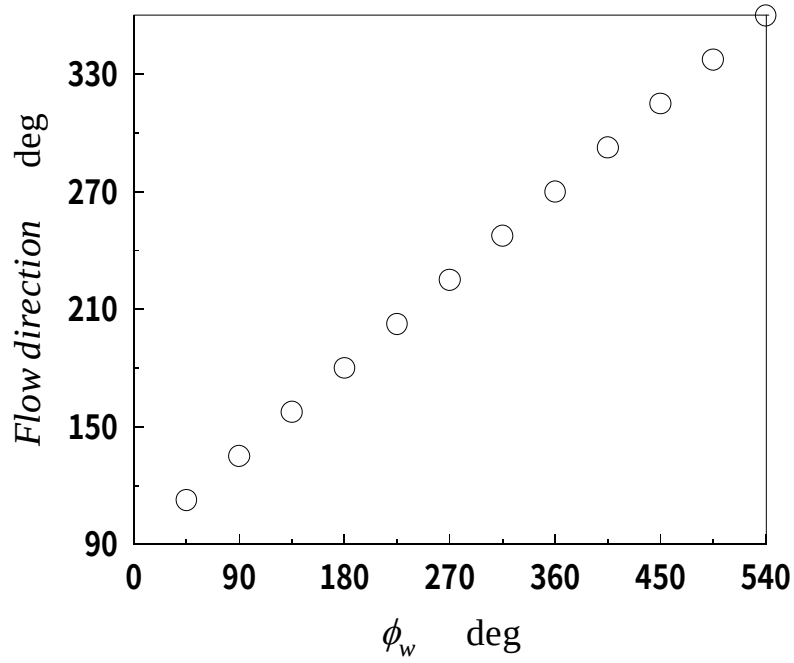

(a) Influence on the flow rate direction

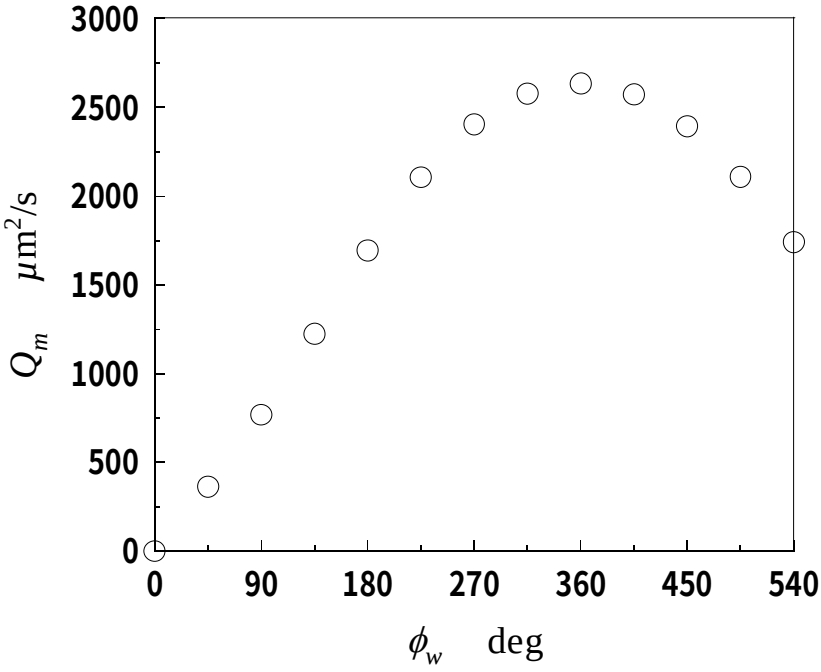

(b) Influence on the flow rate magnitude

Fig. 4-32 Effect of the twist angle on the flow rate

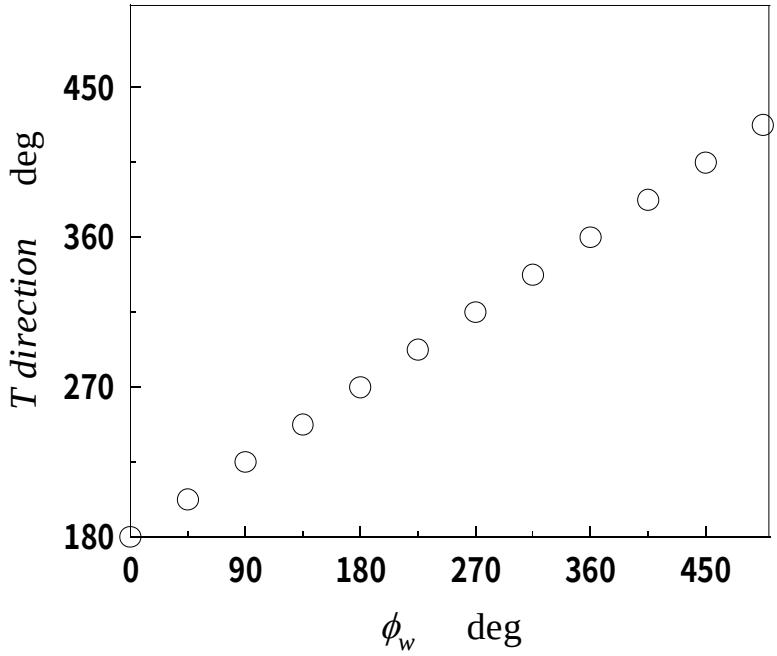

(a) Influence on the stress direction

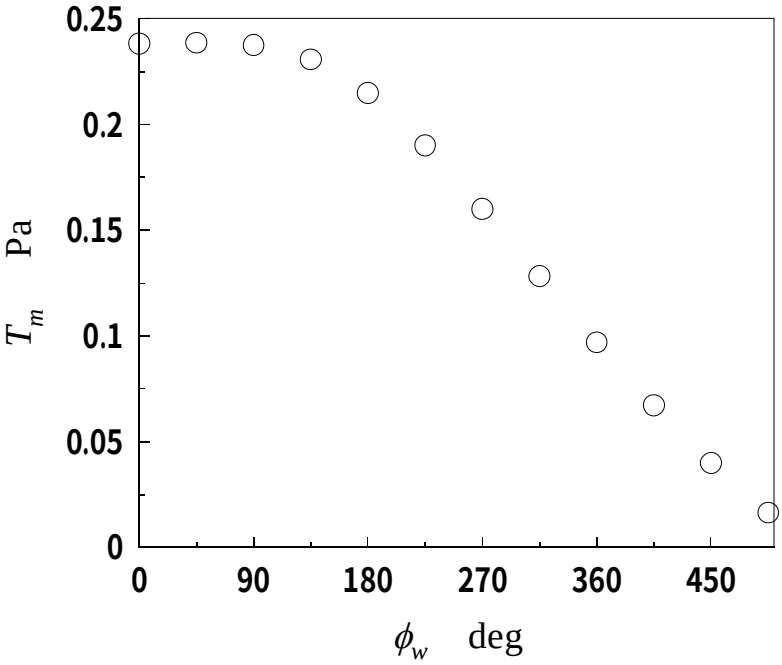

(b) Influence on the stress magnitude

Fig. 4-33 Effect of the twist angle on the stress

Electric field from on to off

In order to develop micro-actuator with liquid crystal, it is necessary to produce continuous flow by imposition of the electric field, but as the discussion above, if we use the DC power supply, the director of the rod-like liquid crystal molecules will rotate from 0 deg to 90 deg firstly, then stop because the direction of the director has come to the steady state that same with the direction of the electric field, so rotation will stop, and no flow has be induced any more. Here in order to induce flow continuously, some operation which can put the director back to initiall state is necessary, the easiest scheme is using AC power supply, so it is necessary to find out the action of the molecule when the electric field is cut off. In this section we sill make some discussion about this.

Before this computation, preparation was done, turn on the electric field and wait one second to let the director reach the steady state with electric field on, then cut off the electric field, begin to do simulation.

Figure 4-34 shows the time series of profiles for electric field on → off in the case of 0 deg twist angle. Different from the case of electric field off → on, from the moment the electric is cut off, because of the anchoring effect, the director near the plates begins to rotate to steady state without electric field, at the same time anti-symmetric S-shape velocity profile is induced, under the flow, the director in the middle of the two plates rotates to the diverse direction from the one near the plates. Along with time, the induced velocity evanishes and inverse rotation to of the director in the middle will stop and then begin to rotate to the same direction with the director near the plates, but because the angular velocity is very small, at that time, no flow is induced. The maximum value is same as the process of electric field of off → on, about 30μm/s. Figure 4-35 gives the change process of 90 deg twist angle, just like the one of 0 deg, just after the cut off of the electric field, the director near the plates begins to rotate firstly, at the same time, both in X-direction and Z-direction, asymmetric profile velocity is induced. After about 0.2 s, both the angular velocity of the director and the induced velocity vanish to deg/s and 10μm/s respectively. The maximum is also same as the process of electric field of off → on. Figure 4-36 shows the time series of 180 deg twist angle; from the angular velocity profiles we can see the directors of upper part and lower part rotate to different direction, and just like the process of off → on, in the X-direction symmetric velocity profile is induced, and the flow direction is also adverse to the off → on process. Near the plates there is no director component in the Z-direction, so there is no velocity is induced.

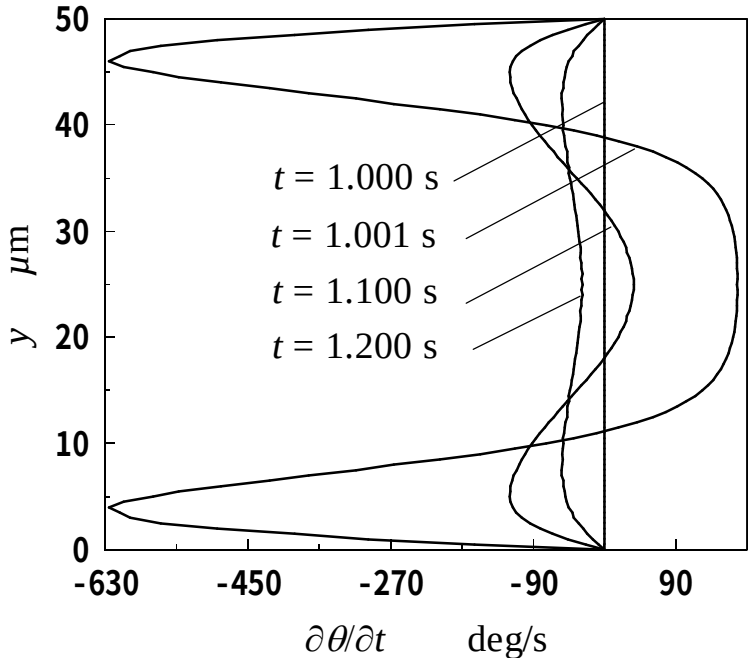

(a) Angular velocity profiles of director

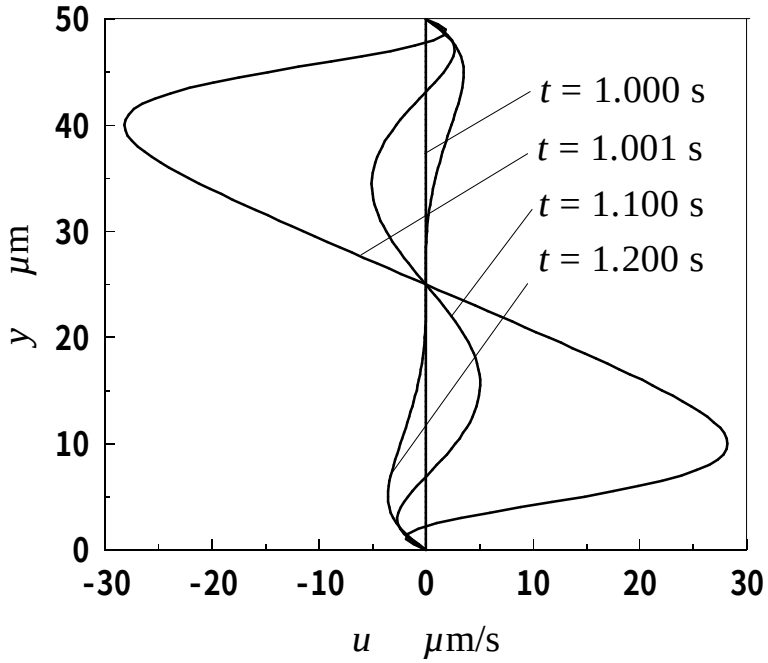

(b) Velocity profiles of x direction

Fig. 4-34 Time series of profiles for electric field on→off (twist angle 0 deg)

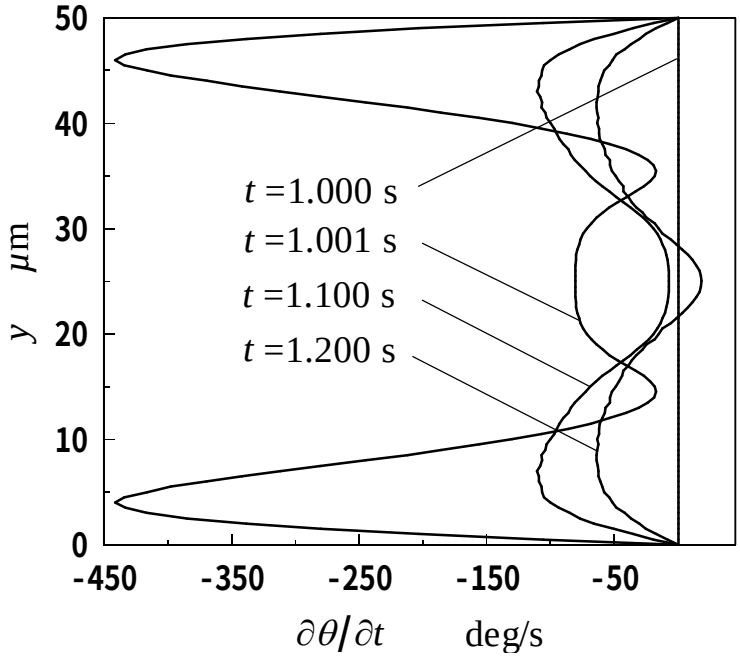

(a) Angular velocity profiles of director

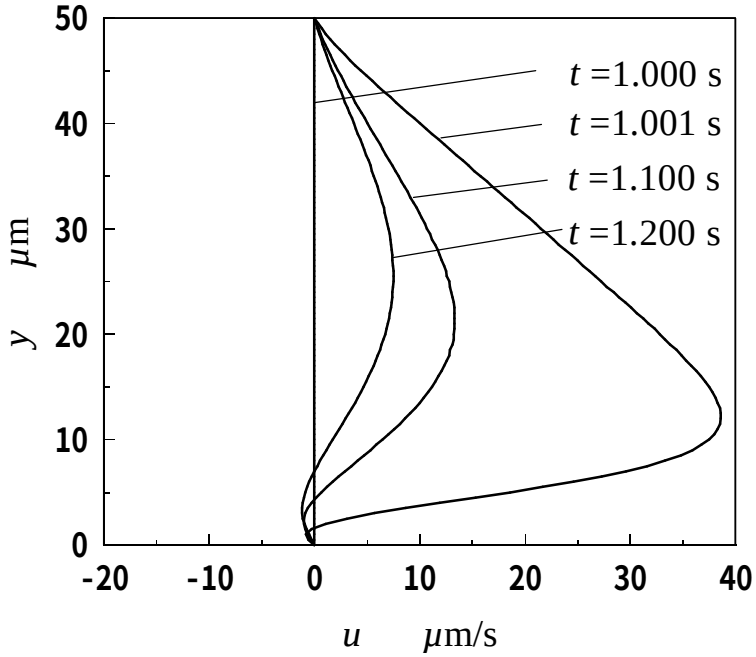

(b) Velocity profiles of X direction

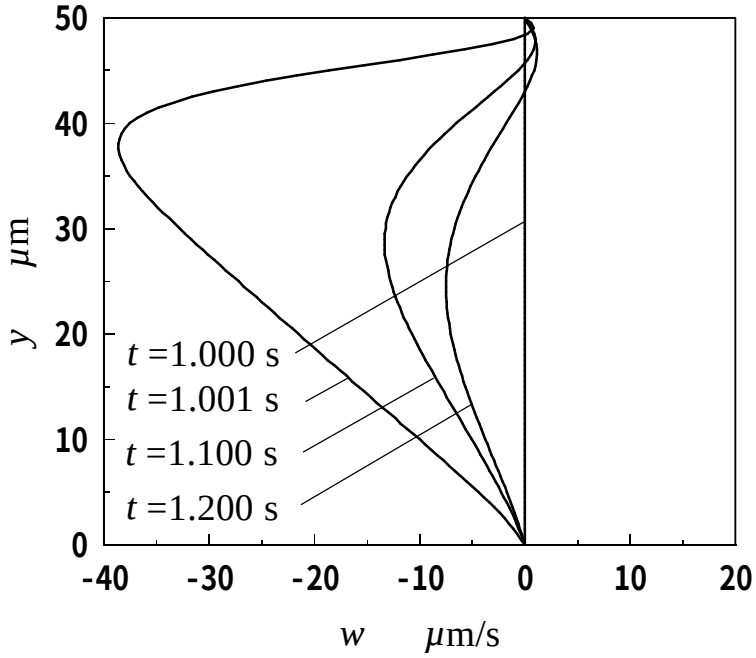

(c) Velocity profiles of Z direction

Fig. 4-35 Time series of profiles for electric field on →off

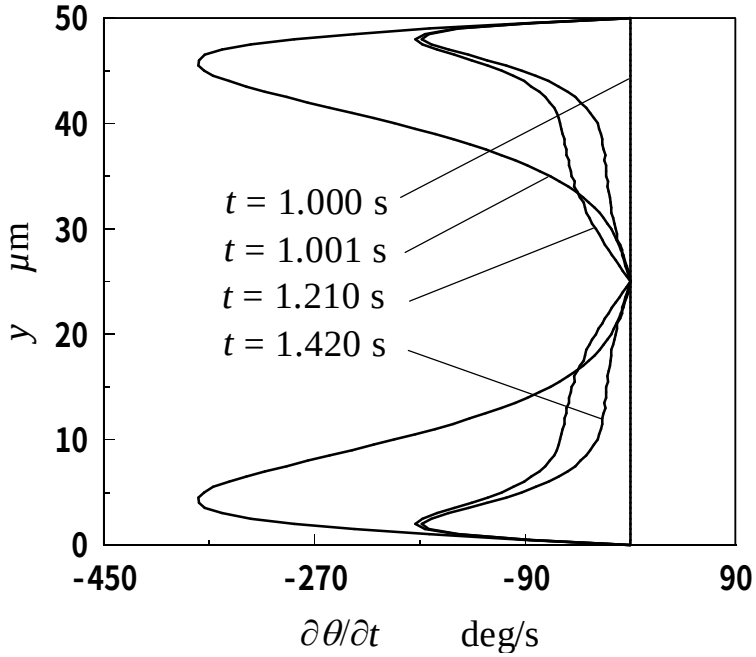

(a) Angular velocity profiles of direction

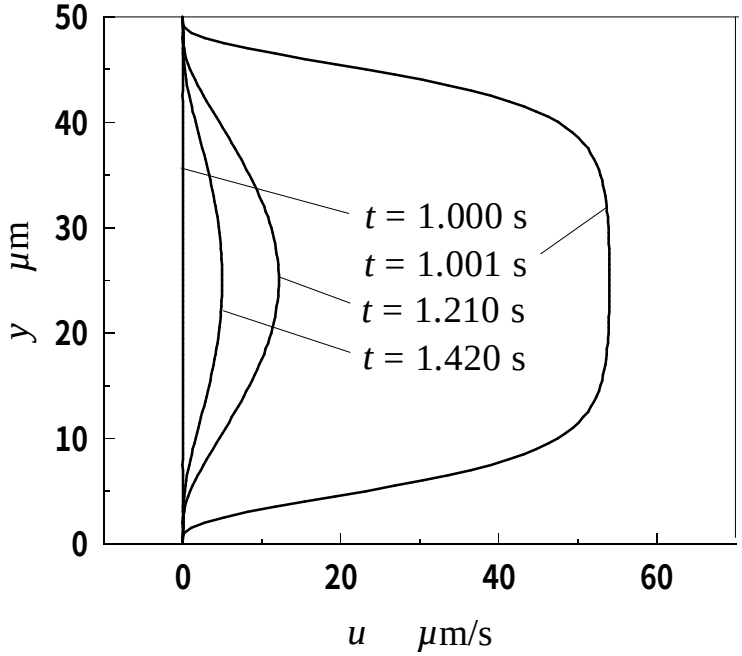

(b) Velocity profiles of X direction

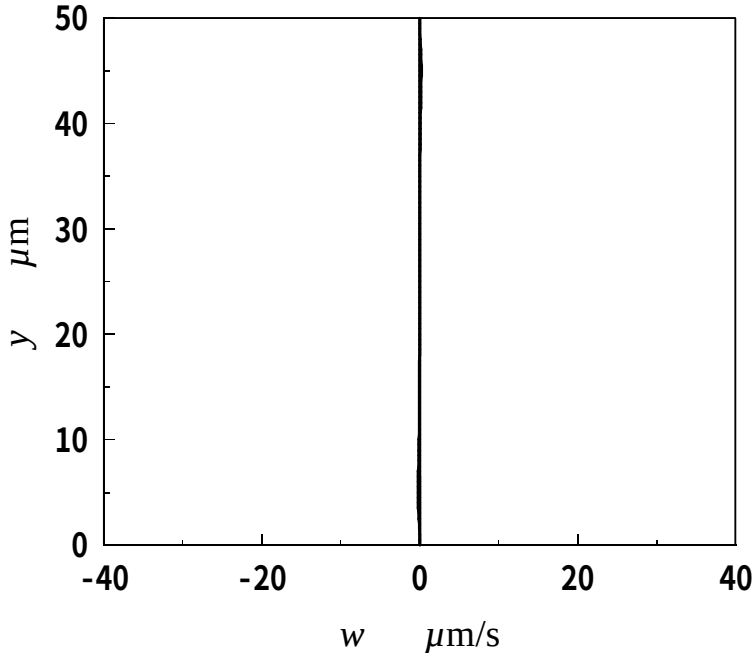

(c) Velocity profiles of Z direction

Fig. 4-36 Time series of profiles for electric field on→off

Compare with the experimental results

Compare of the simulation and experiment results is shown in figure 4-37, we can see that the simulation result is in agreement with the experimental result.

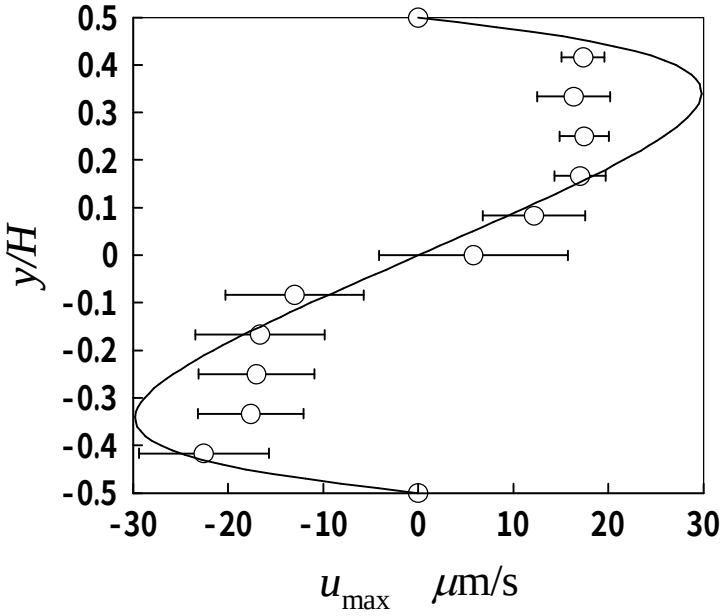

(a) Twist angle = 0 deg

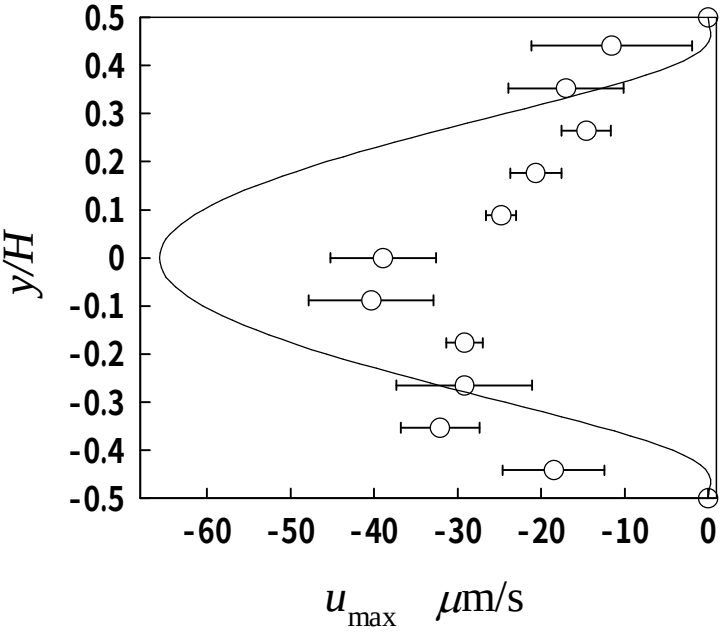

(b) Twist angle = 180 deg (X-direction)

Fig. 4-37 Contrast with the experiment results

4.4.2 In the case of the upper plate being free

The simplest way to take the force out of the liquid crystal is through the bounding plates. As a next step, the upper plate is set to be free, as shown in figure 4-38

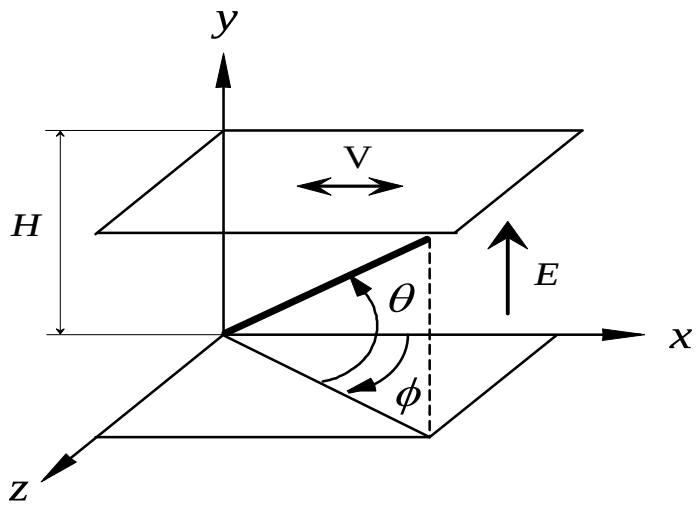

Fig. 4-38 Computation field

Effect of the twist angle

Figure 4-39 shows the velocity profiles in case the upper plate is free, because the elastic resistance becomes smaller, the induced velocity becomes larger, about 4 times to the one that upper plate is fixed in both X-direction and Z-direction, and the induced backflow is strongly affected by the twist angle on its direction and magnitude.

From the figure 4-40 of transient behaviors of typical quantities, the change process of the velocity is same as the fix one: begins to arise after 0.2 s time interval, and reaches peak at about 0.36 s, the total process will over about 0.5 s. Different point is the value of the peak and the effect of the twist angle, in the case of fix plate, the maximum of the velocity is about 60μm/s with 180 deg twist angle, but in the case of free upper plate, the maximum become 270μm/s with 0 deg twist angle. Figure 4-41 shows the effect of the twist angle, we can see along with the increasing of the twist angle the velocity and moved distance decrease, and the moved direction changes linearly with a start angle of 180 deg.

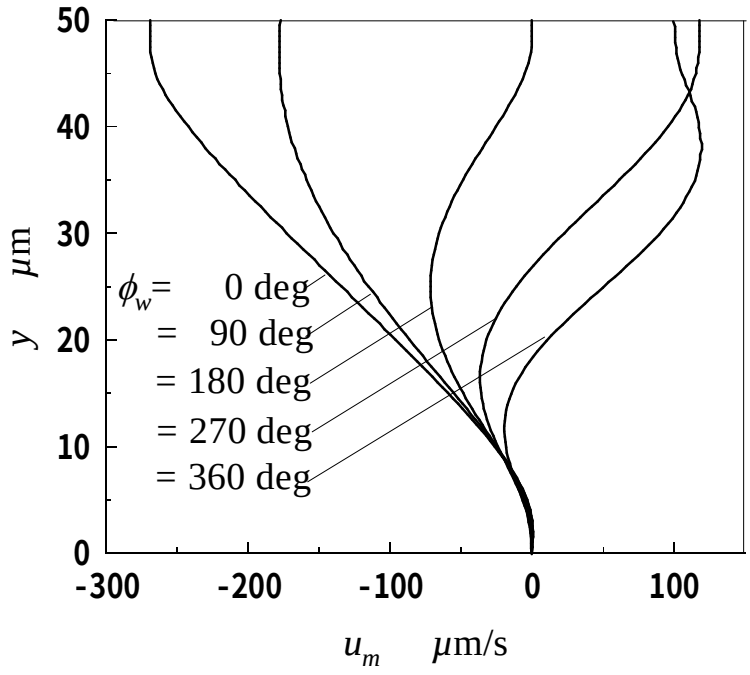

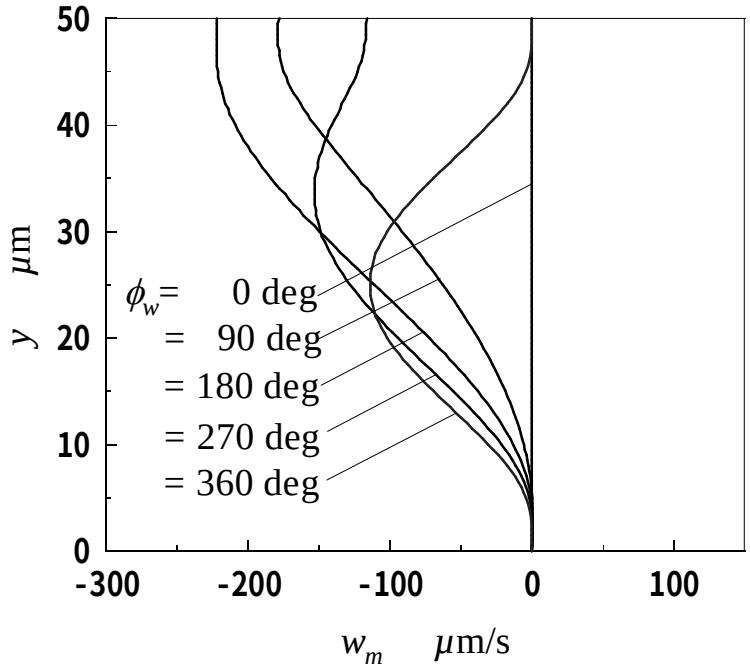

Fig. 4-39 Velocity profiles

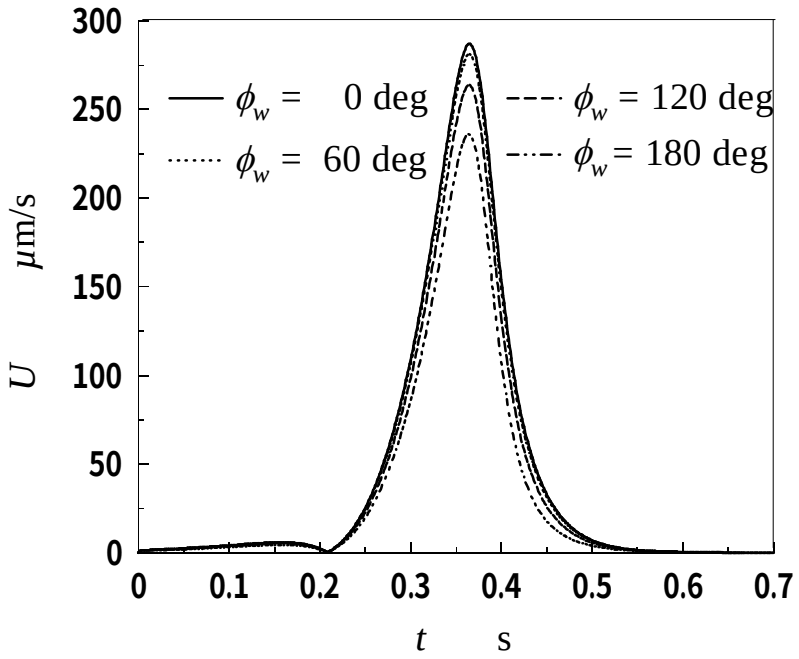

(a) Change of the velocities with time

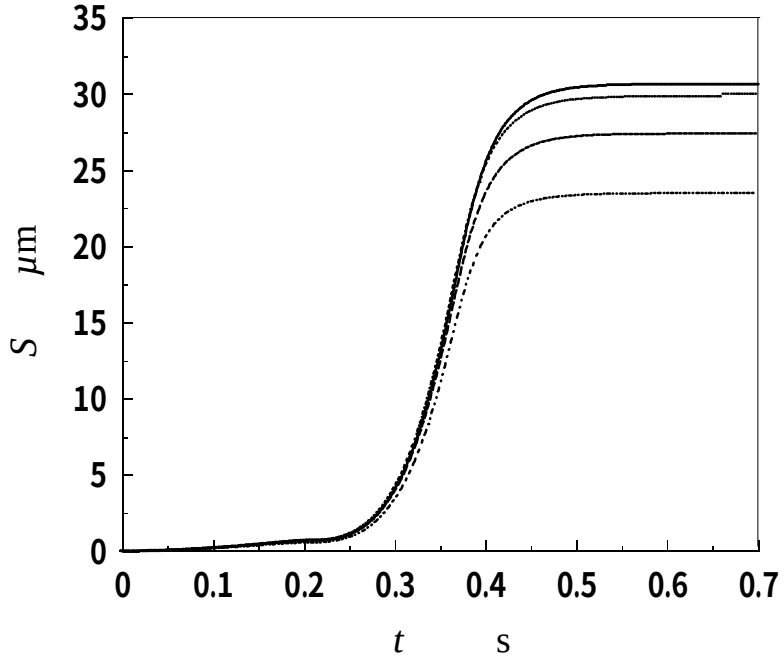

(b) Change of the moved distances of upper plate with time

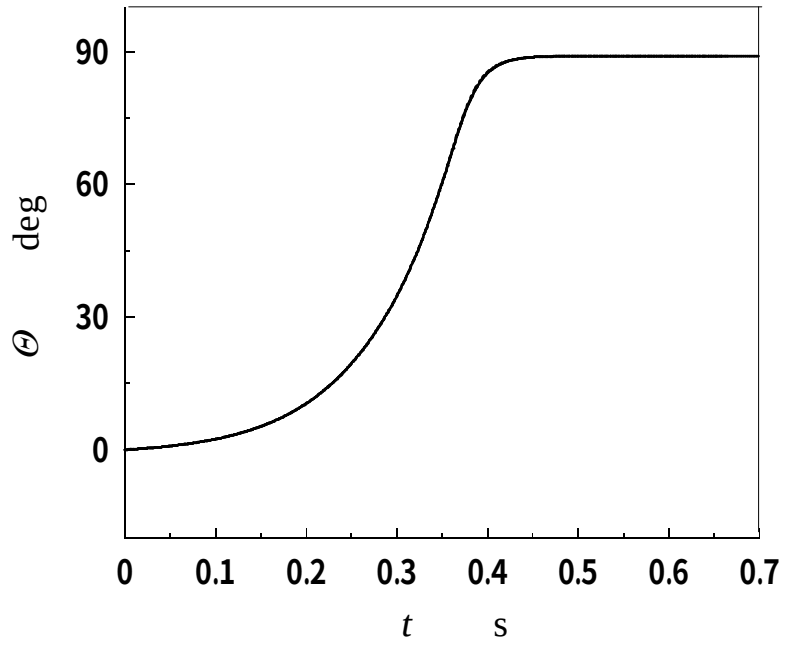

(c) Change of the rotate angles

Fig. 4-40 Transient behaviors of typical quantities

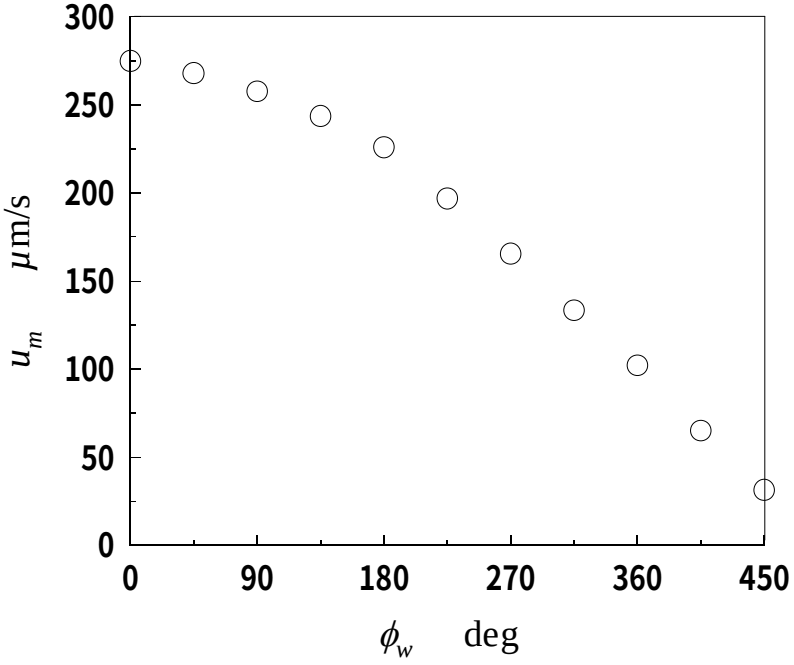

(a) Influence on the velocity magnitude

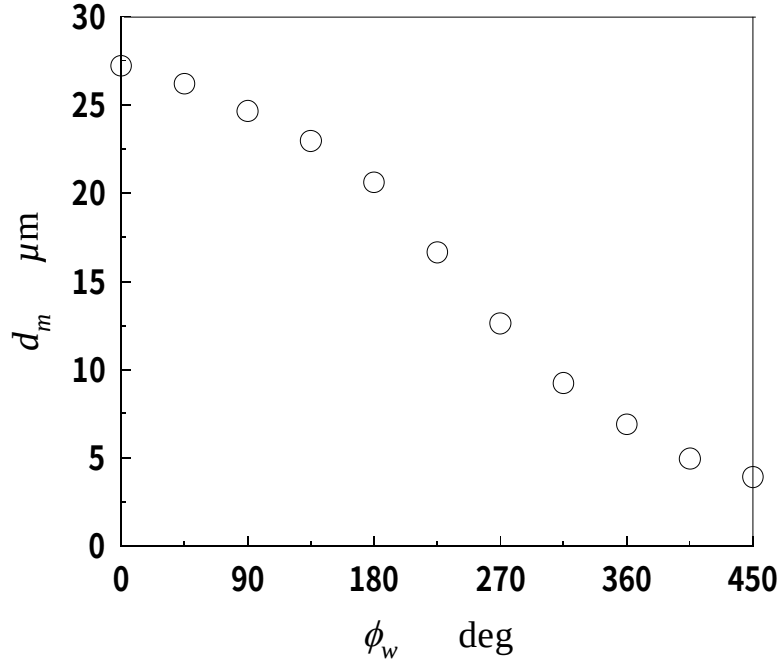

(b) Influence on the moved distance

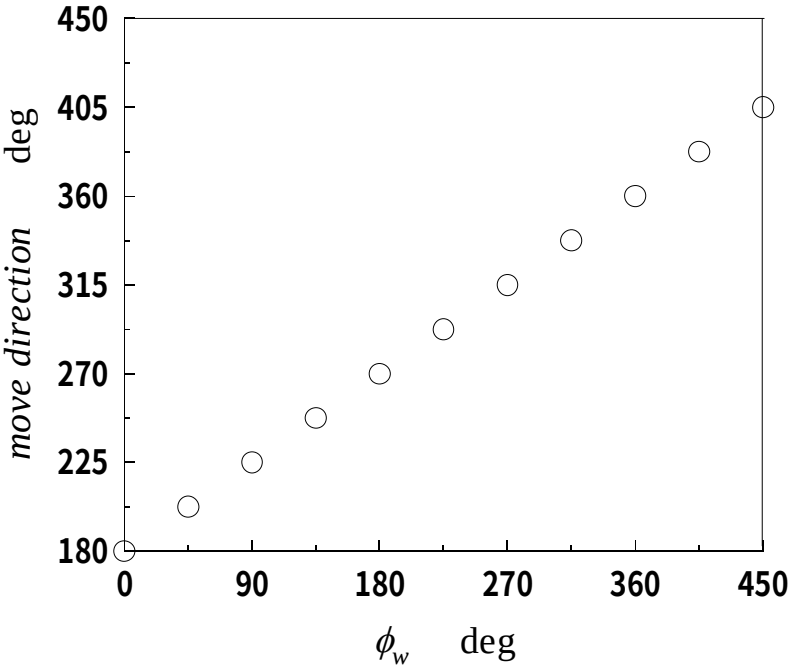

(c) Influence on the moved direction

Fig. 4-41 Effect of the twist angle

Applied voltage *E* (gap 50μm, tilt angle 1 deg)

The effect of the applied voltage is shown in figure 4-42, for the parameters except for the voltage, the representative value is used. Figure (a) shows the effect of the voltage on the velocity. Along with increasing of the applied voltage, we can see the tendency of increasing in magnitude of velocity .The effect of the twist angle is not so large, and in the case of 0 deg twist angle, the velocity can get the maximum, this is can be seen from the discussion in the case of fix plate, the stress shows maximum in case of 0 deg twist angle.

Figure (b) gives the effect on the moved distance of the upper plate and (c) gives the response time, it can be seen easily that the change tendency of the distance is same as the velocity, increases with the increasing of applied voltage while the response time decreases.

Gap of the two plates *H*

The effect of the gap is shown in figures from (a) to (c) of figure 4-43, for the parameters except for the gap, the representative value is used. From the figure we can see along with the increasing of the gap, the velocity of the upper plate decreases, but the moved distance increases. The cause is in the response time, from figure (c), it is can be easy to know that the moved time changes to be longer with the gap becoming bigger, so the moved distance of course take a tendency of increasing. In figure 4-43, when the gap is changed, in the case of fixed applied voltage, the electric field strength is changed, in order to find the real effect of the gap, in figure 4-44, we give the results of steady electric field strength. This time, the velocity and the moved distance of the upper plate show same change tendency that is increasing with the increasing of the gap, and except the gap of 10 μm, the response time does not show much change along with the change of the gap.

Tilt angle θ

The effect of the tilt angle is shown in figures 4-45, for the parameters except for the tilt angle, the representative value is used. We can see that the change of the tilt angle has little effect on the velocity and moved distance. But from figure (c), we can make the conclusion that the change of the tilt angle can make change on the rotate angle, along with the increasing of the tilt angle, the angle at which the velocity of the upper plate reach the maximum decrease, with a change of 40 tilt angle, the rotate angle changes from 70 deg to about 63 deg.

Effect of the mass per volume

Figure 4-46 gives the effect of the mass per volume; it can be know that when the mass per volume changes from 0.5 to 1kg/m^2, there is not any change on the velocity, moved distance and response time.

An example of small gaps

In the section of the effect of gap, we can see that when the gap is less than 20μm, the quantities including the stress, velocity and flow rate change exponential with the decreasing of the gap, and the response also becomes better. Here we will give an example of small gaps from 5μm to 20μm to see how excellent of the characteristic. Figure 4-47 shows the transient behaviors for small gap, the representative value of other parameters except gap is used. From the figures we can see when the gap is 5μm, the maximum of the velocity can reach 2200μm/s, and in addition, the response time is only about 0.004s that is same with the fixed upper plate, the moved distance also shows good characteristic when the gap is decreasing to 5μm.

Summary

By discussing the effect of parameter such as twist angle, applied voltage and gap on the velocity and moved distance of the upper plate, conclusions following can be achieved.

1. The direction of the upper plate depends only on the twist angle.
2. The magnitudes of physical quantities depend on the twist angle, the applied voltage and the gap of the two plates. Among the parameters, the effect of the gap is most important; when the gap is set to be very small the stress and the velocity can get exponential change with the decreasing of the gap.
3. The response time depends only on the applied voltage.
4. If the backflow is used to drive particle dispersed in the liquid crystal, we should select the twist angle at about 360 deg.
5. If the backflow is sued to drive the upper plate, we should select the twist angle at about 0 deg.

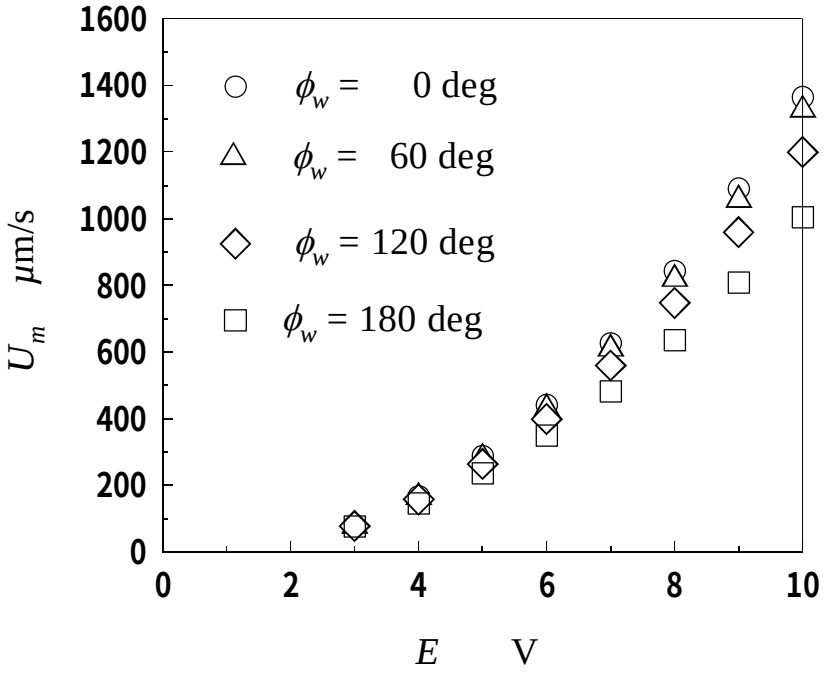

(a) Influence on the velocity magnitude

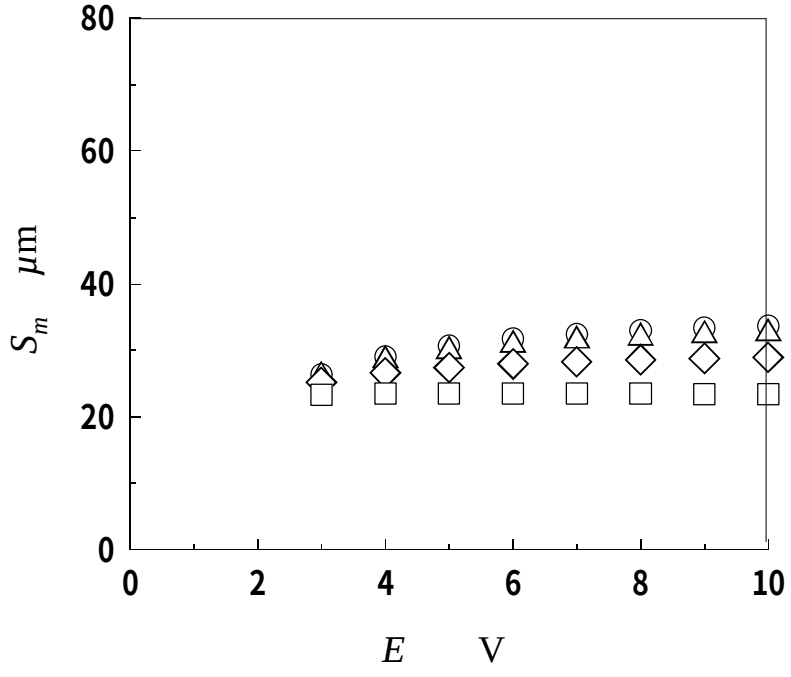

(b) Influence on the moved distance of the upper plate

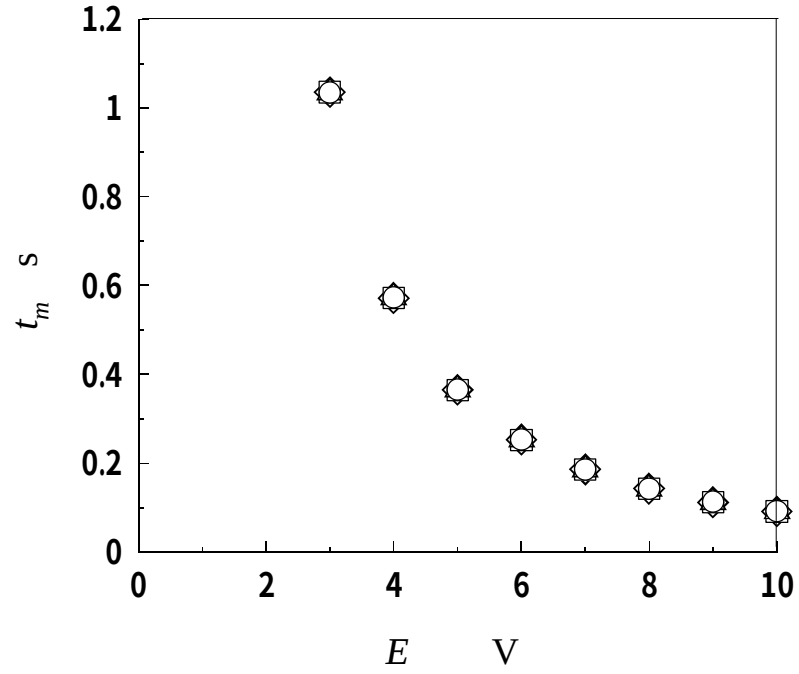

(c) Influence on the maximum reach time

Fig. 4-42 Effect of the applied voltage

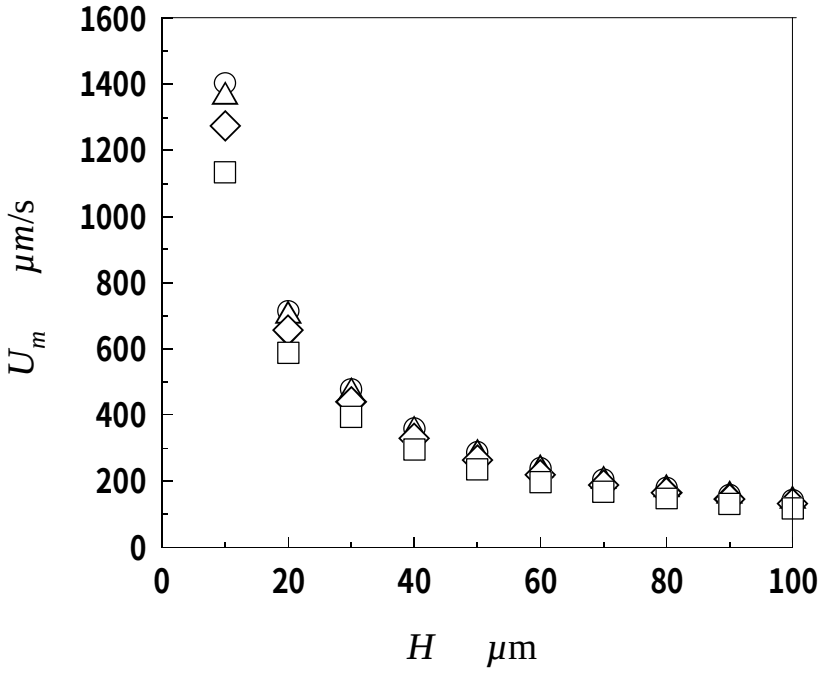

(a) Influence on the velocity magnitude

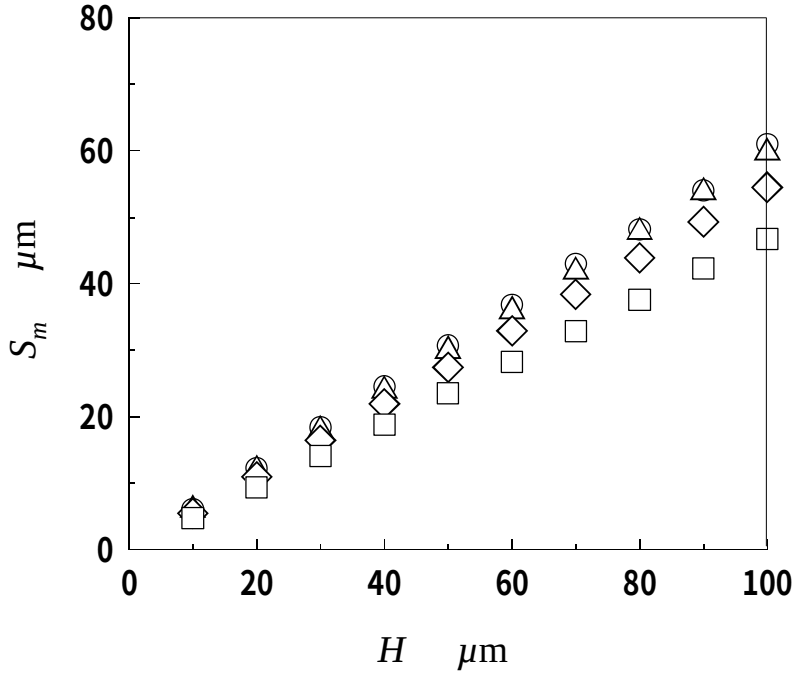

(b) Influence on the moved distance magnitude

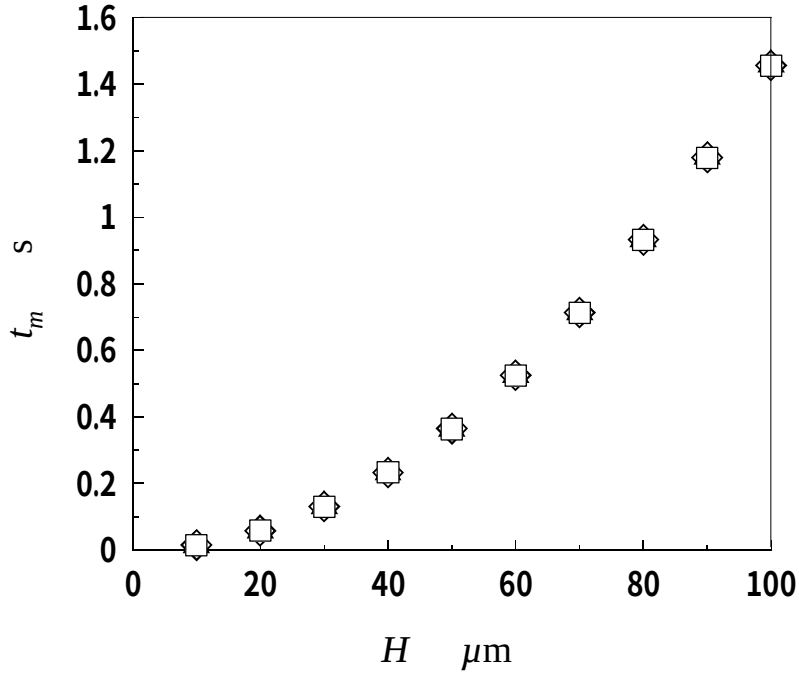

(c) Influence on the maximum reach time

Fig. 4-43 Effect of the gap between the two plates

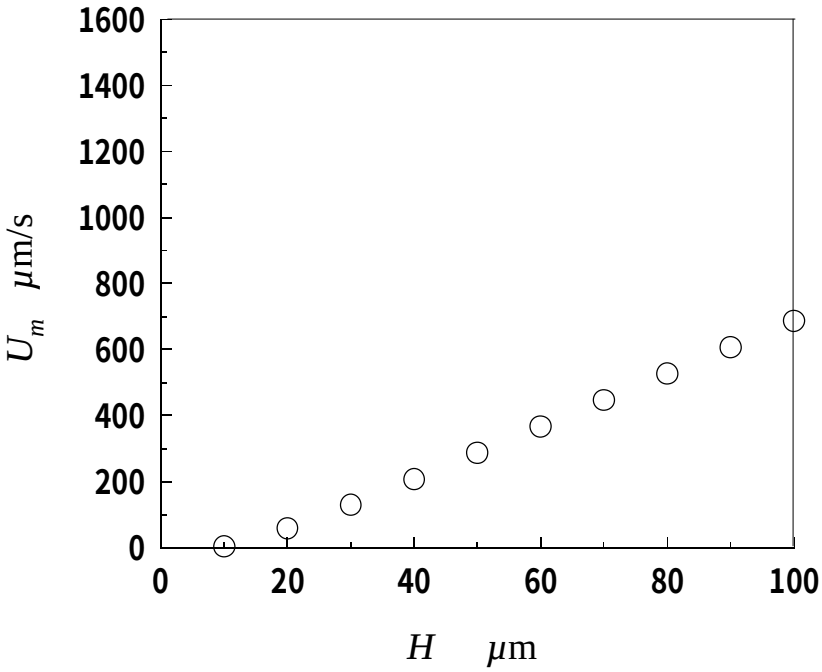

(a) Influence on the velocity magnitude

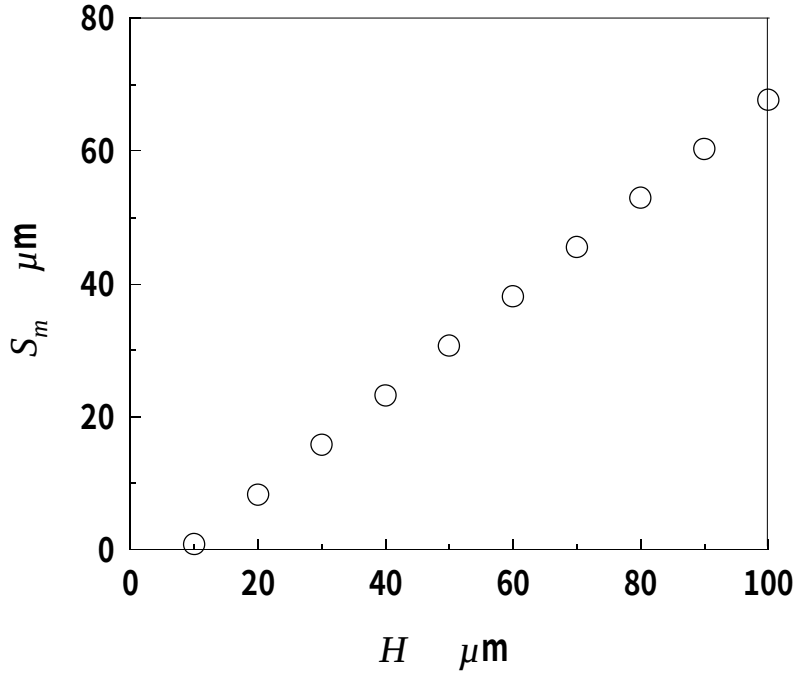

(b) Influence on the moved distance magnitude

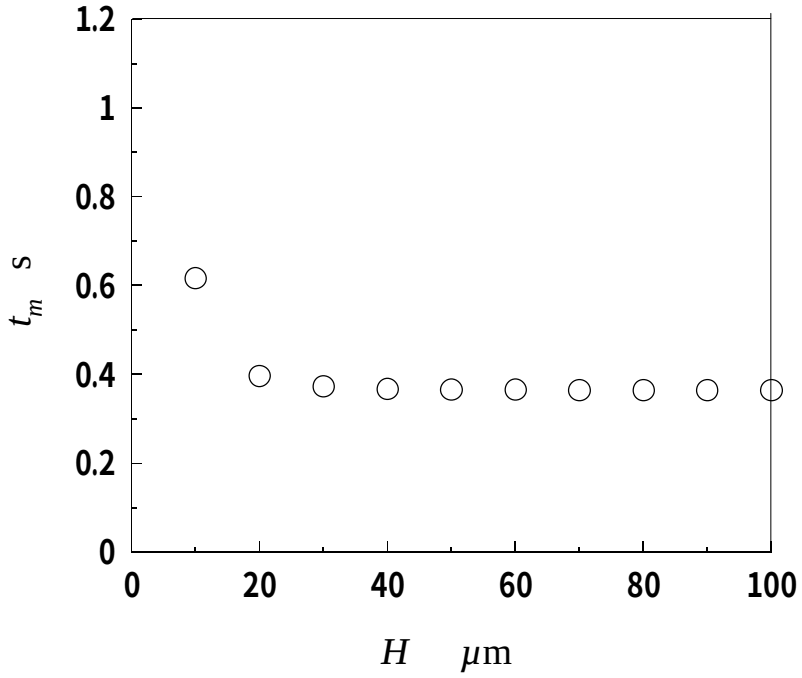

(c) Influence on the maximum reach time

Fig. 4-44 Effect of gap with constant electric field

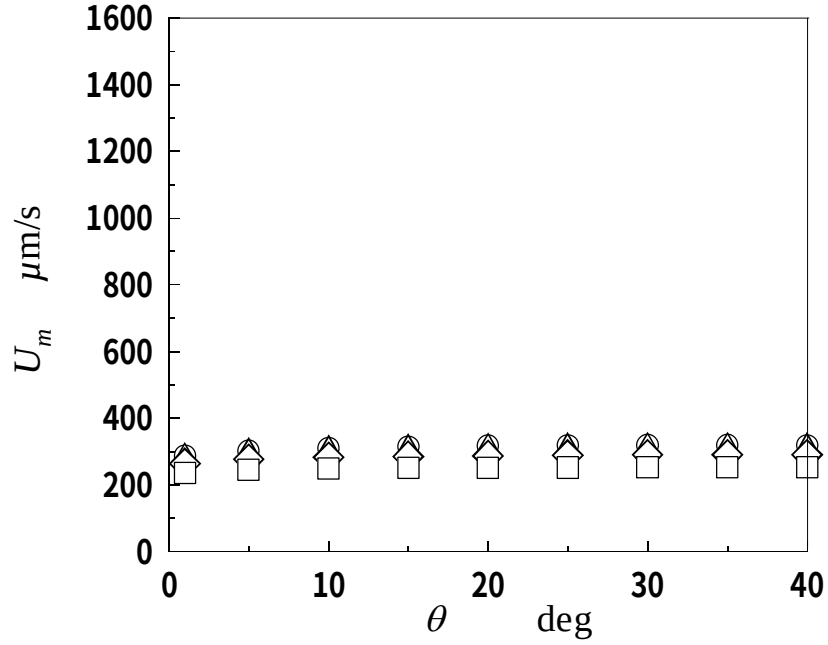

(a) Influence on the velocity magnitude

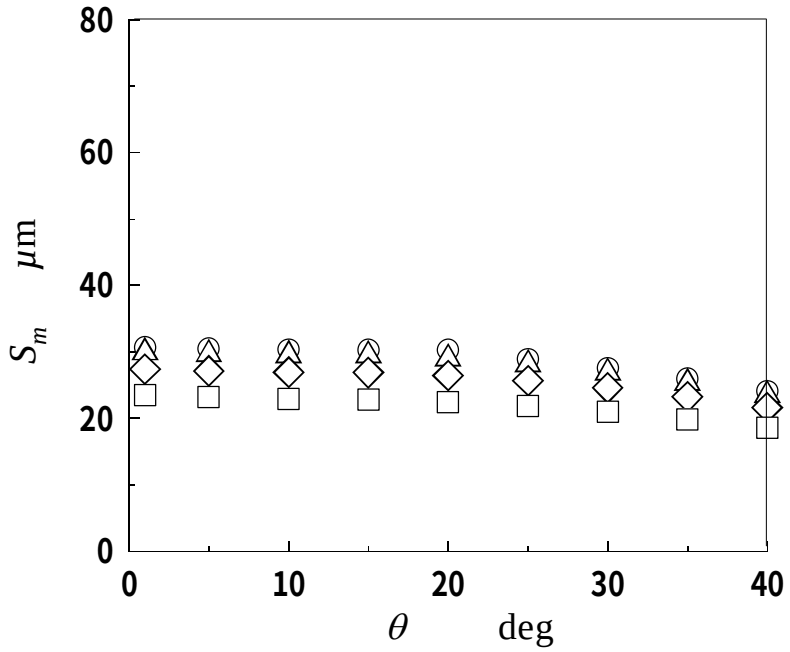

(b) Influence on the moved distance magnitude

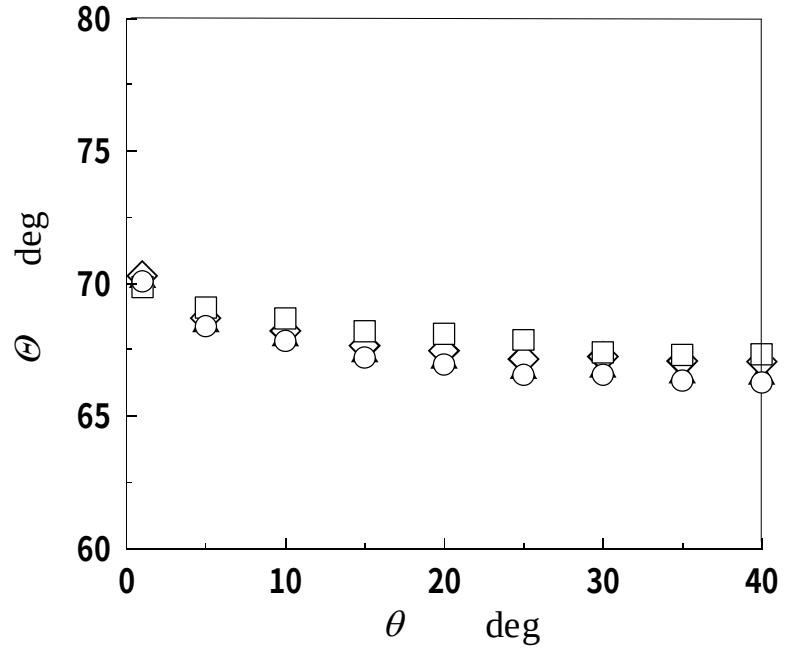

(c) Influence on the rotate angle

Fig. 4-45 Effect of the tilt angle

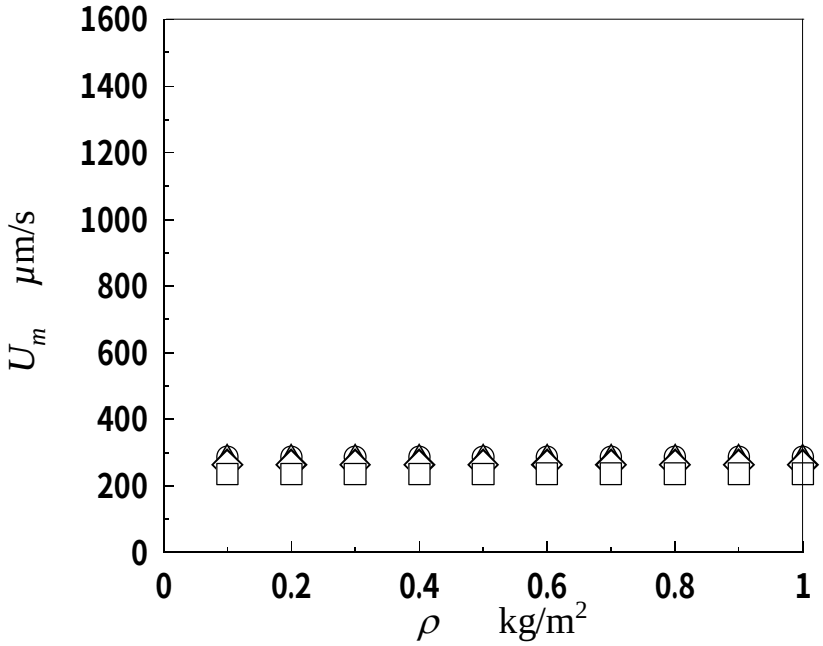

(a) Influence on the velocity magnitude

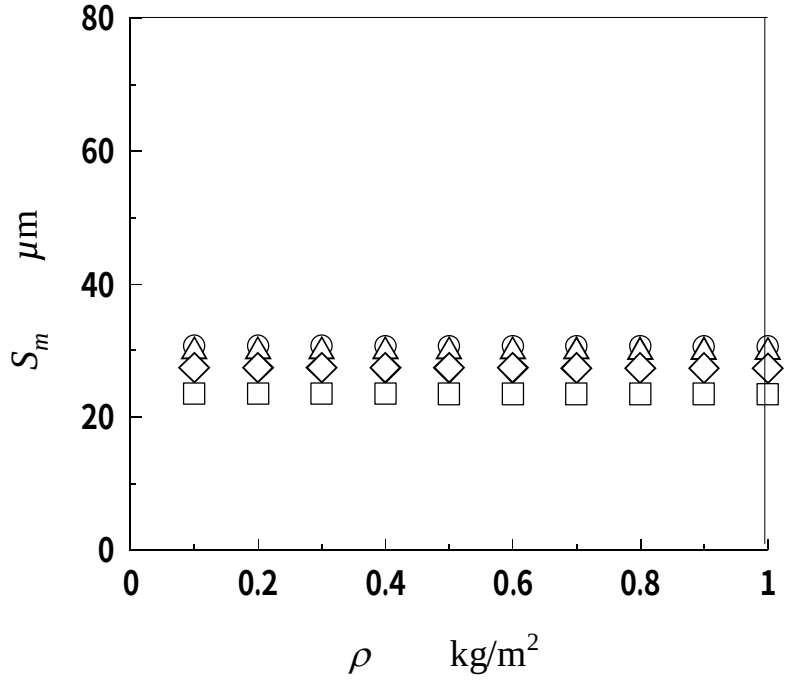

(b) Influence on the moved distance magnitude

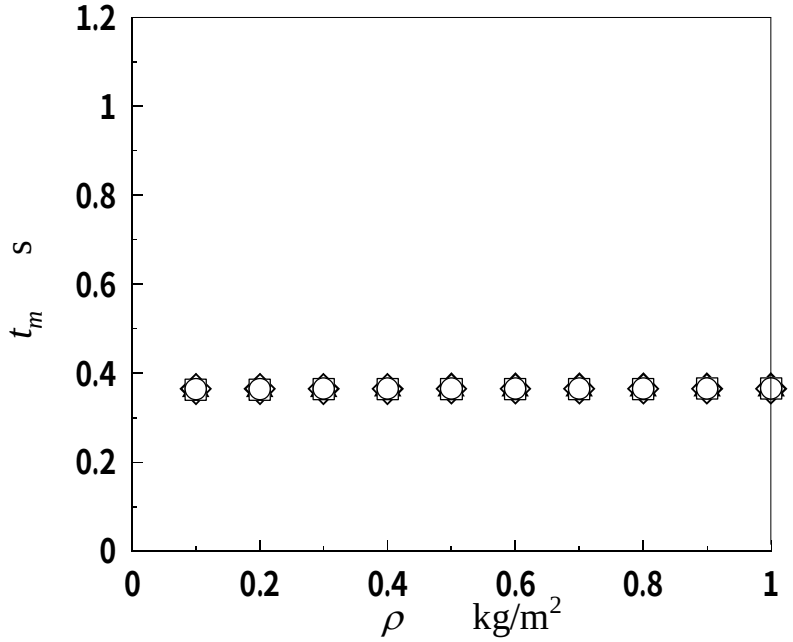

(c) Influence on the maximum reach time

Fig. 4-46 Effect of the unit volume mass

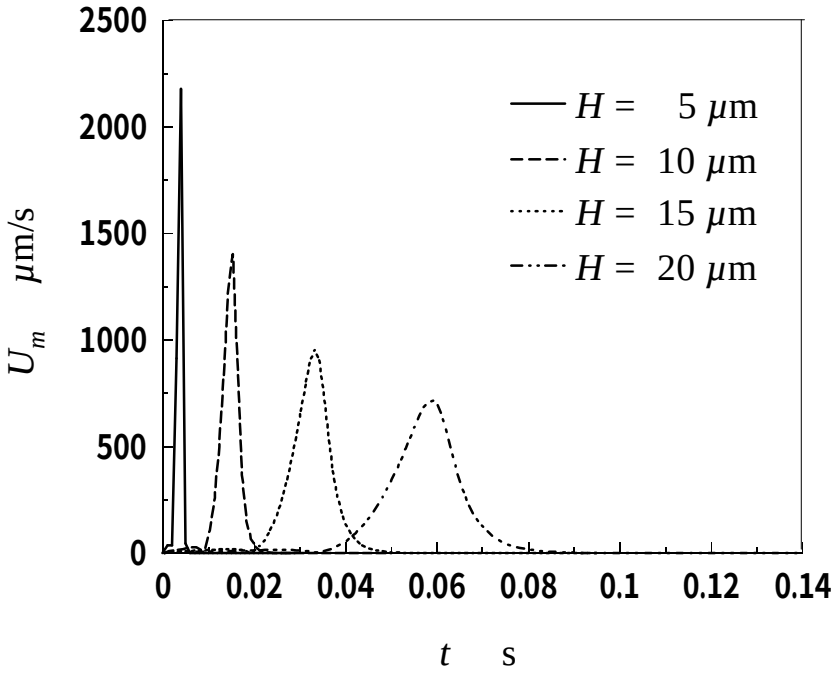

(a) Change of the velocities with time

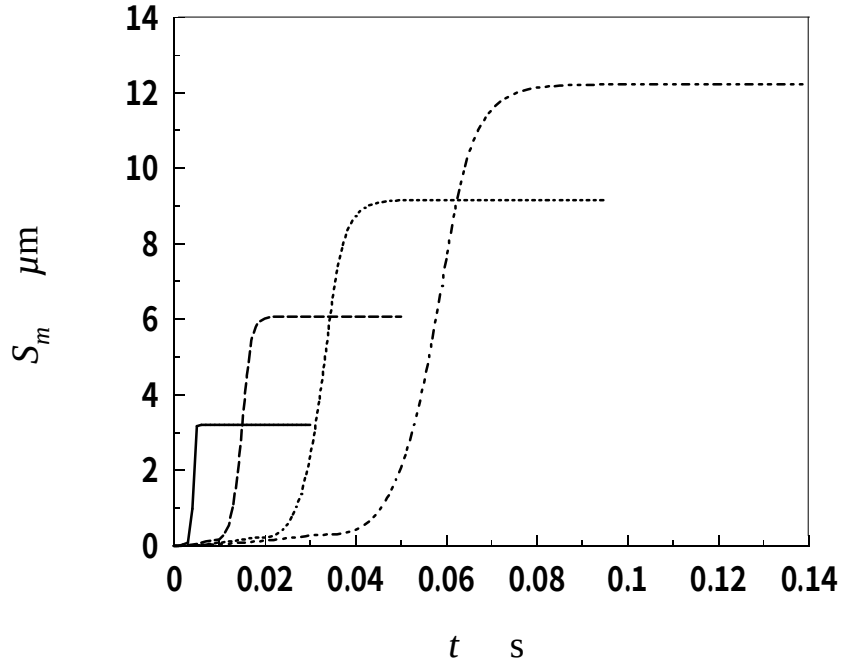

(b) Change of the moved distances with time

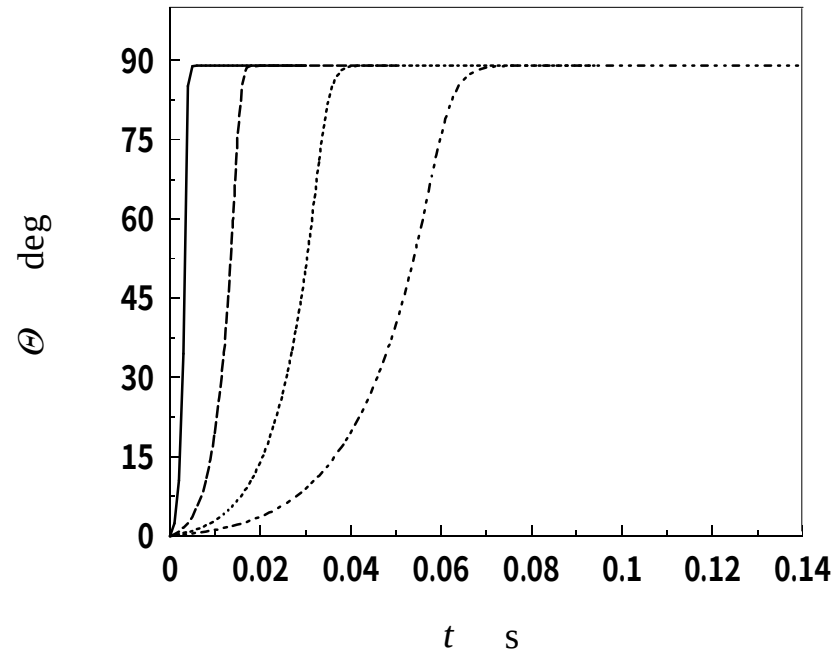

(c) Change of the rotate angle with time

Fig. 4-47 Transient behavior for small gap

Chapter 5: Imposition of the pulse voltage

5.1 Introduction

In order to imply the back flow to the actuator, it is necessary to induce continuous flow firstly, and it is very difficult to realize this aim by using DC electric field, so this chapter we will give some results achieved using AC electric filed. By the results discussed in the chapter 4, we can see that in the case that the upper plate is free, as the orientation parameters, when the twist angle is 0 deg, we can get the most fast of velocity of the upper plate, and the tilt angle does not affect the quantities very much, so in this chapter as the orientation initiall, we select the one of 0 deg twist angle and 1 deg tilt angle.

Coordinate system and expansion of the formulas

On the base of restriction of the orientation initial, we can simplify the coordinate system to figure 5-1, in this case, the upper plate only moves in the X-direction, and the expansion of the governing equation also can be reduced to formulas 5-1 and 5-2.

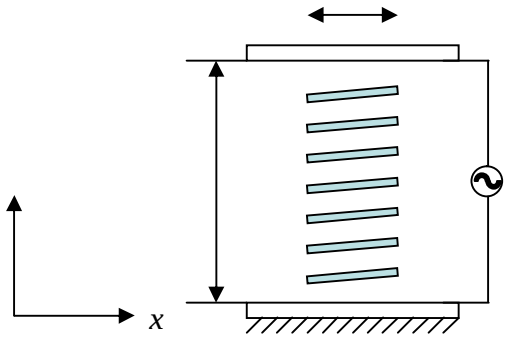

Fig. 5-1 Computation field and coordinate system

$$\rho\frac{\partial u}{\partial t}=\alpha_1\left\{\frac{\partial}{\partial y}\left(n_x^2n_y^2\right)\frac{\partial u}{\partial y}+n_xn_y^2\left(n_x\frac{\partial^2u}{\partial y^2}\right)\right\}+\alpha_2\frac{\partial}{\partial y}\left(n_y\frac{\partial n_x}{\partial t}\right)+\alpha_3\frac{\partial}{\partial y}\left(n_x\frac{\partial n_y}{\partial t}\right)$$
$$+\frac{\alpha_4}{2}\frac{\partial^2u}{\partial y^2}-\frac{\alpha_2-\alpha_5}{2}\left(2n_y\frac{\partial n_y}{\partial y}\frac{\partial u}{\partial y}+n_y^2\frac{\partial^2u}{\partial y^2}\right) \tag{5-1}$$
$$+\frac{\alpha_3+\alpha_6}{2}\left(2n_x\frac{\partial n_x}{\partial y}\frac{\partial u}{\partial y}+n_x^2\frac{\partial^2u}{\partial y^2}\right)$$

$$\gamma_1\frac{\partial n_x}{\partial t}=n_y\left\{2\left(K_3-K_2\right)\frac{\partial n_x}{\partial y}\frac{\partial n_y}{\partial y}-\alpha_2\frac{\partial u}{\partial y}\right\}+\left\{K_2+\left(K_3-K_2\right)n_y^2\right\}\frac{\partial^2n_x}{\partial y^2} \tag{5-2a}$$

$$\gamma_1\frac{\partial n_y}{\partial t}=n_y\Delta\varepsilon E^2-\alpha_3n_x\frac{\partial u}{\partial y}+\left\{K_1+\left(K_3-K_2\right)n_y^2\right\}\frac{\partial^2n_y}{\partial y^2}$$
$$-\left(K_3-K_2\right)n_y\left\{\left(\frac{\partial n_x}{\partial y}\right)^2+\left(\frac{\partial n_y}{\partial y}\right)^2\right\} \tag{5-2b}$$

5.2 Results and discussion

5.2.1 Effect of the frequency and the ratio of duty

Time change of typical quantities

Figure 5-2 shows the time change of the velocity, moved distance of the upper plate and the rotate angle of the director in the middle of the cell, the electric field is AC of 5V with 1Hz frequency and 20% duty. The gap of the two plates is 50 μm. It is easy to see that from the third step of the pulse electric field, the induced flow reaches steady state, the velocity of the plate shows property of oscillation, in the part of the electric filed on, the plate moves to the minus direction of X-axis, and in the part of off, it returns a few, but the distance of moving forward is larger than the one of back, in general, from figure (b), we can see that the plate moves toward the minus direction of X-axis at the same time its oscillation. In the figure (c), we give the rotate angle range of the director in the middle of the cell among the process; it is from 60 deg to 90 deg.

From the discussion in the 4th chapter, we know that if we can control the rotate angle range into 50 – 80 deg, we can get the largest velocity of the upper plate. In this section we will find the most proper frequency and ratio duty.

Figure 5-3 gives the results of using an electric field of 5V with 10 Hz frequency and 20% duty, the gap is same. From figure (a), we can see that at first 1.3 s, the velocity of the plate is 0; this is because the time of electric field on is two short, and so it will take many steps to make the director rotate from 1 deg to about 10 deg from which the rotation of the director can induce backflow. After about 2.5 s, the velocity reaches steady state, just like the result of 1Hz, the plate moves towards the minus direction of X-axis, but the swing of the oscillation becomes smaller and so the plate can move more smoothly. From figure (c), we can see that the rotate angle range becomes smaller, about 85-90 deg. It is not in the range of 50-80 deg, so the velocity shows maximum at about 2 s, in order to control the rotate angle range, which is the base of getting fast velocity, into the range of most proper range, we can adjust the frequency and duty.

Effect of frequency and duty to the moved velocity

In figure 5-4 and 5-5, we summary the effect of the frequency and the duty on the average moved velocity. The scheme to request the average velocity is take moved distance of 5 s after the flow reaches the steady state, and then divide the time. From the figure 5-4 we can see with specific frequency of 1Hz, voltage magnitude of 5V and gap of 50μm, the ratio duty of 5% is the most proper, the one that less than 5% can not induce flow and the one more than 5% will create energy waste. On the other hand, when the ratio duty is fixed as 20%, from figure 5-5 it is easy to see that the frequency of 1 Hz is the most proper one.

Figure 5-6 shows the results using the optimal frequency and ratio duty, it can be see that the rotate angle range is be controlled well into the range of 50 -80 deg, so the velocity towards to minus direction of X-axis is be kept as the largest one of about 250 μm/s and at the same time the velocity returning is be reduced to about 25 μm/s, so the net moved velocity becomes larger.

As same as to control the frequency and ratio duty of the applied voltage, we can also find the optimal cell by controlling the magnitude of the voltage and the size of the cell. As the magnitude of the voltage, we can easily find the rule through the results of the effect of the voltage showed in the 4th chapter. But as the gap, because the existence of the effect of the anchoring condition, it is necessary to discuss it in detail.

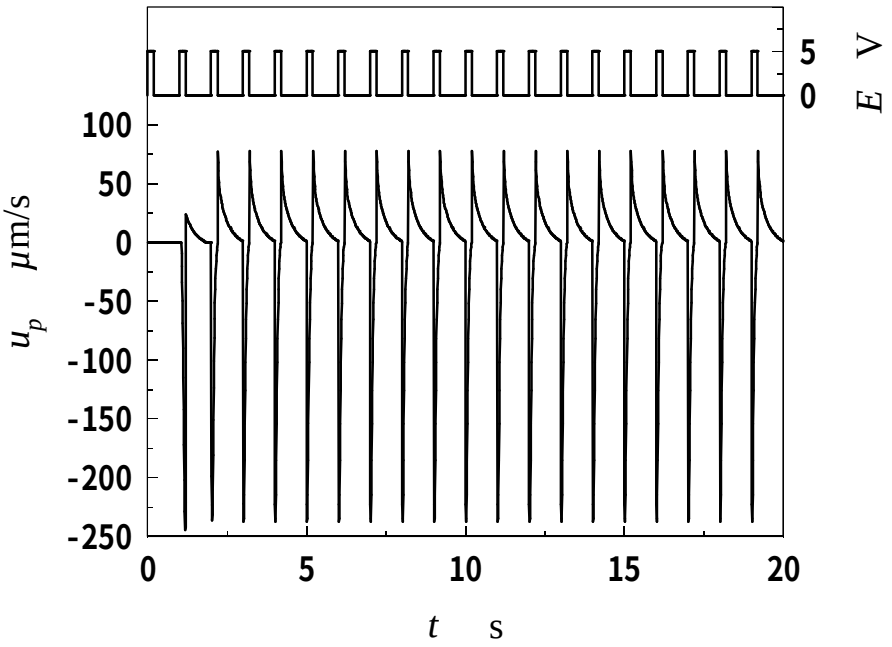

(a) Time change of the velocity

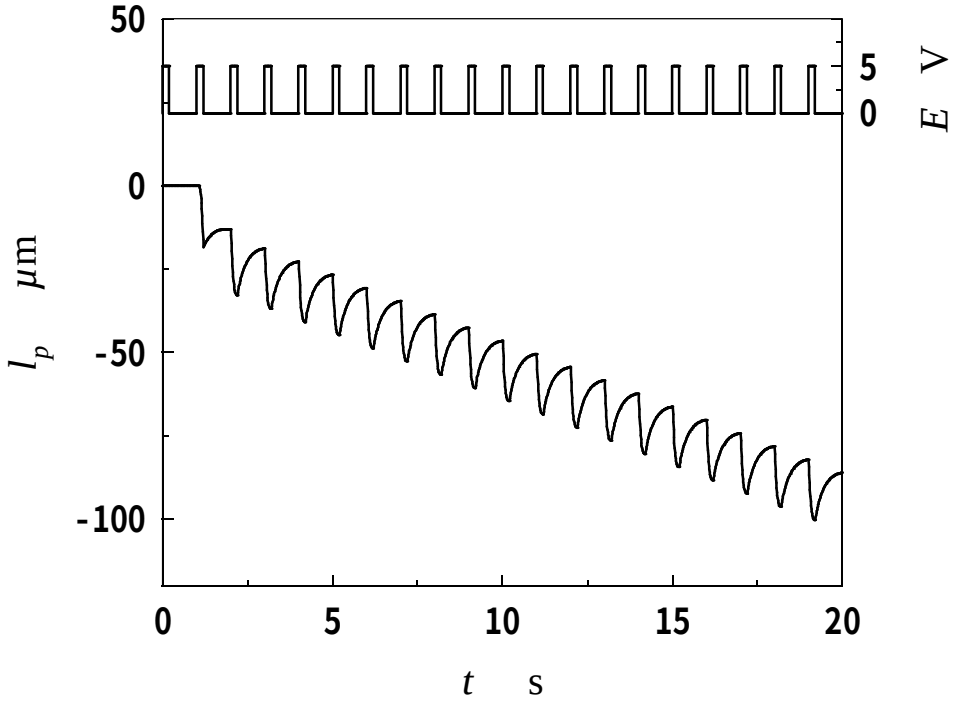

(b) Time change of the moved distance

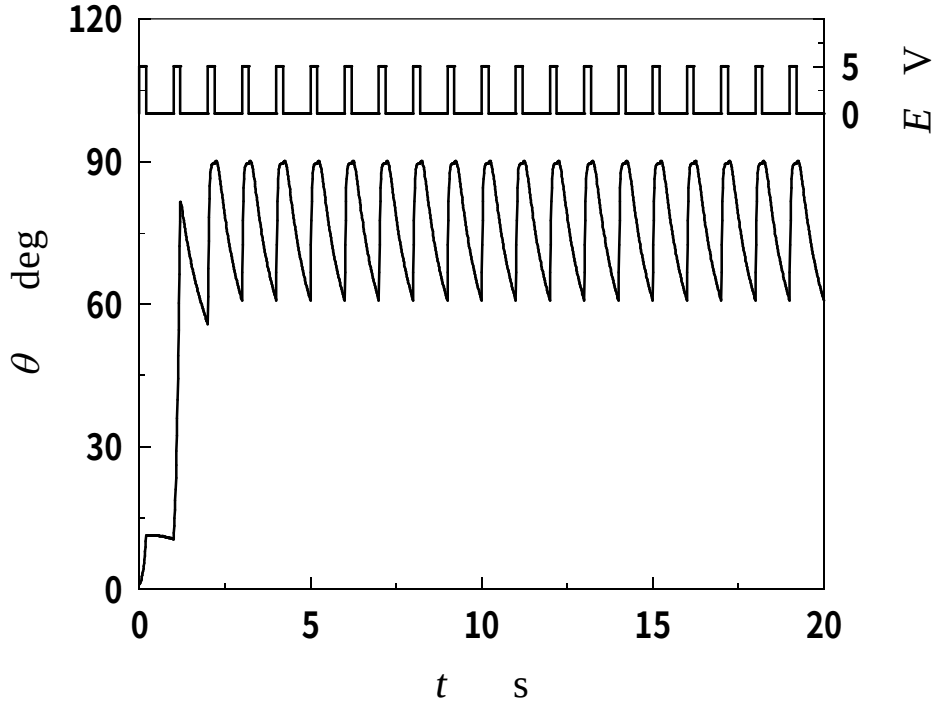

(c) Time change of the angle of the middle

Fig. 5-2 Time change of typical quantities with voltage of f = 1Hz and *Duty* = 0.2

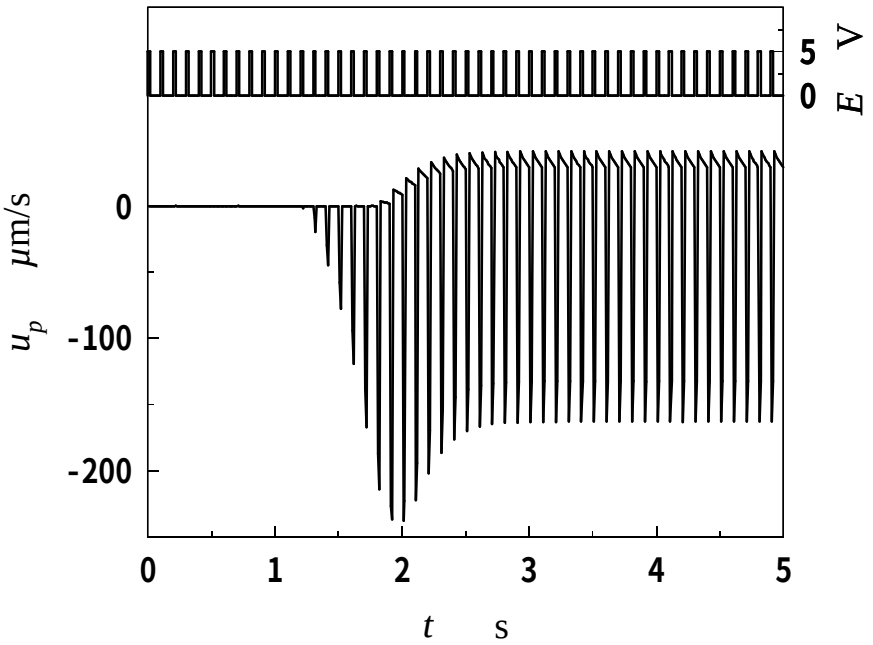

(a) Time change of the velocity

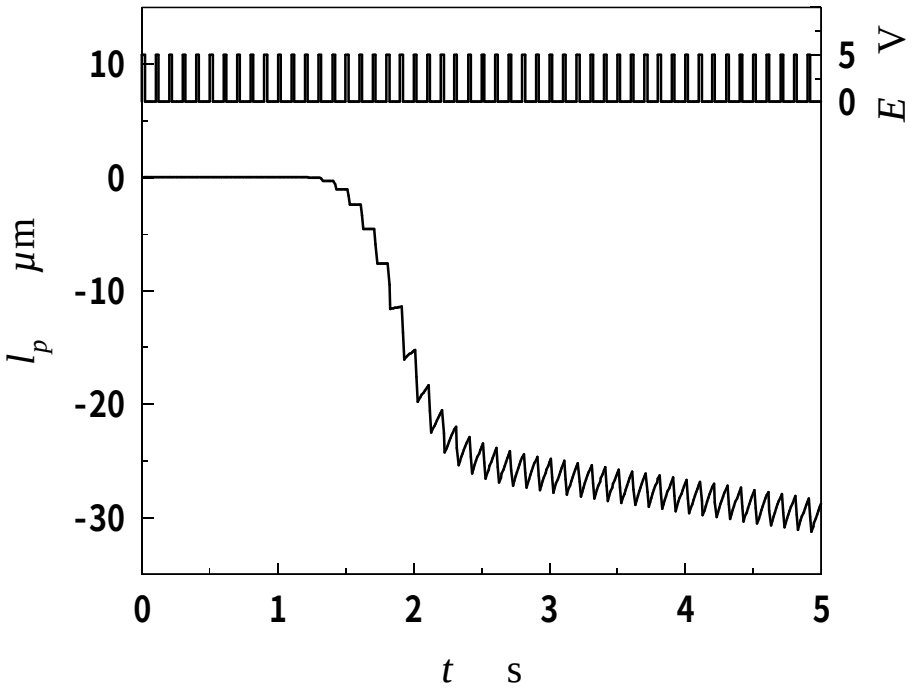

(b) Time change of the moved distance

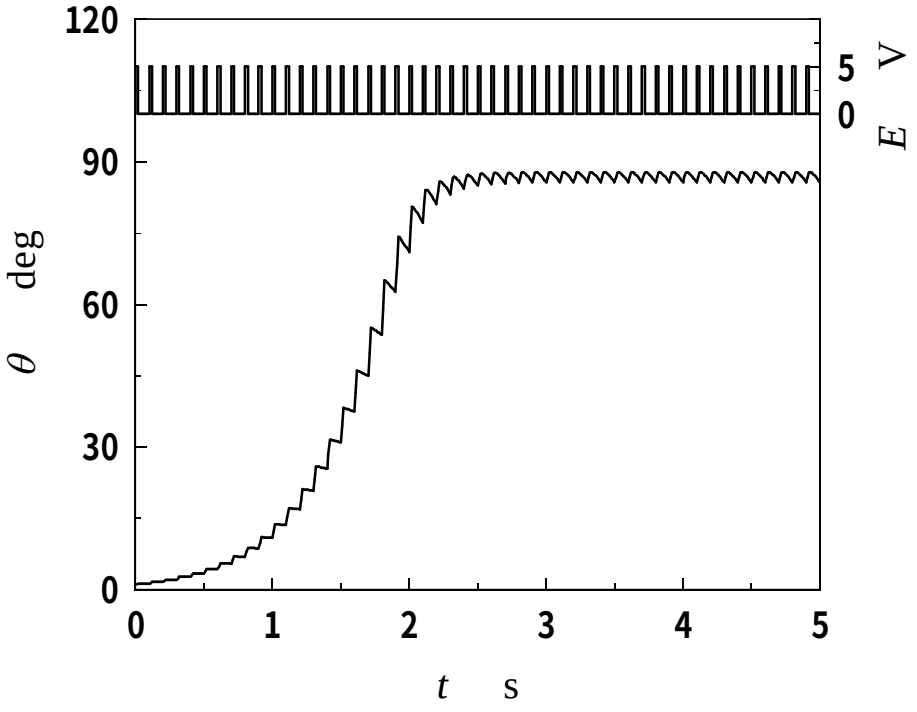

(c) Time change of the angle of the middle

Fig. 5-3 Time change of typical quantities with voltage of f = 10Hz and *Duty* = 0.2

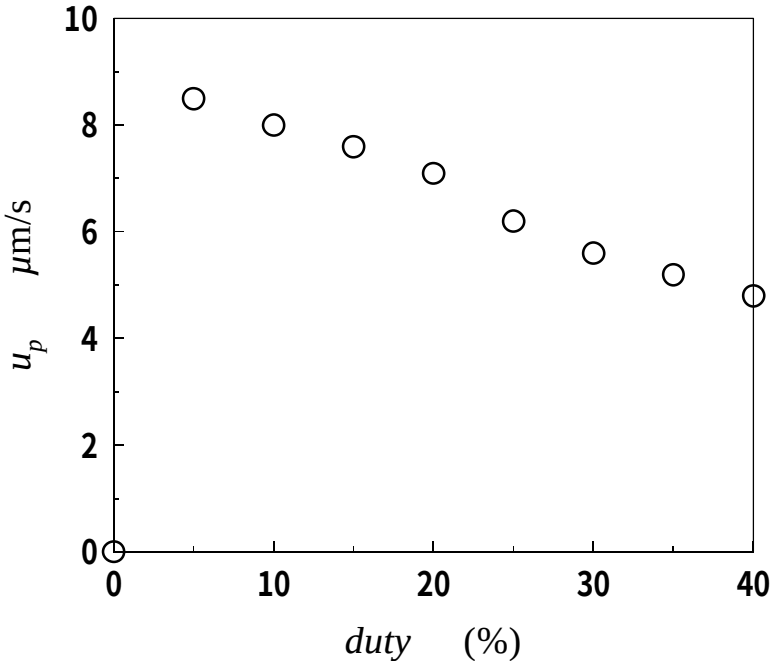

Fig. 5-4 Effect of the duty on the velocity magnitude (*f*=1Hz)

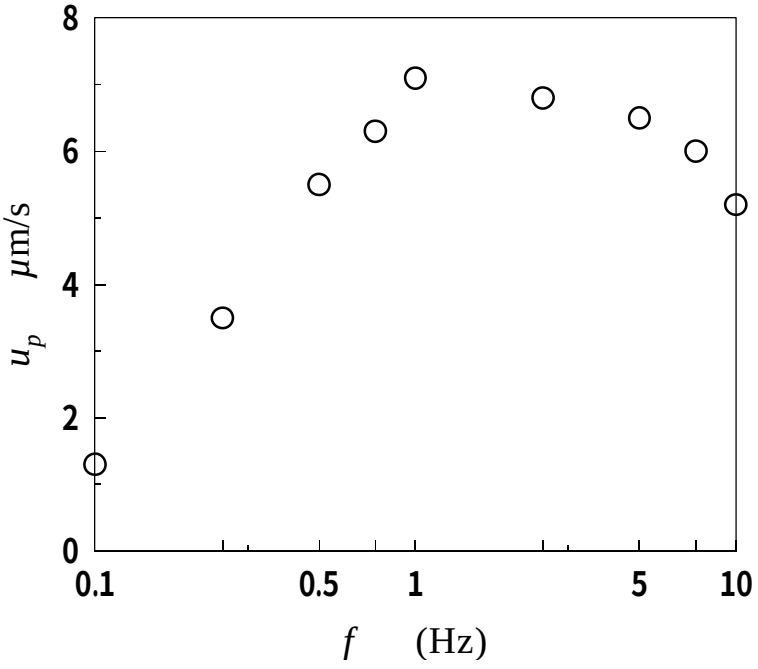

Fig. 5-5 Effect of the frequency on the velocity magnitude (duty=20%)

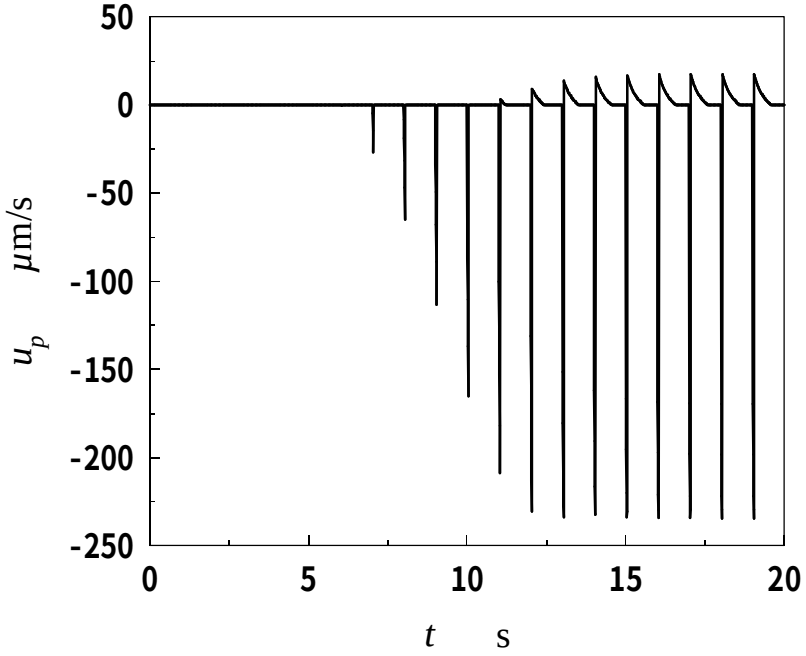

(a) Time change of the velocity

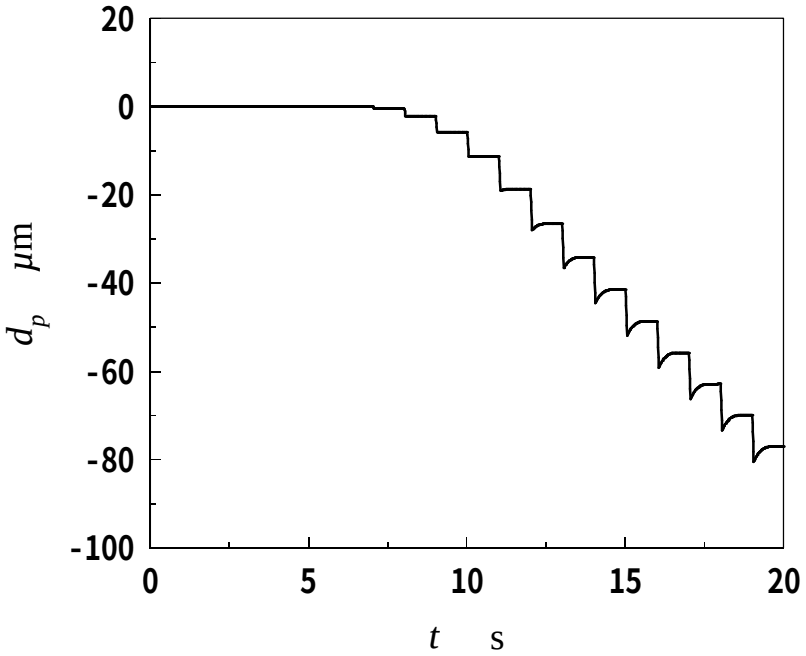

(b) Time change of the moved distance

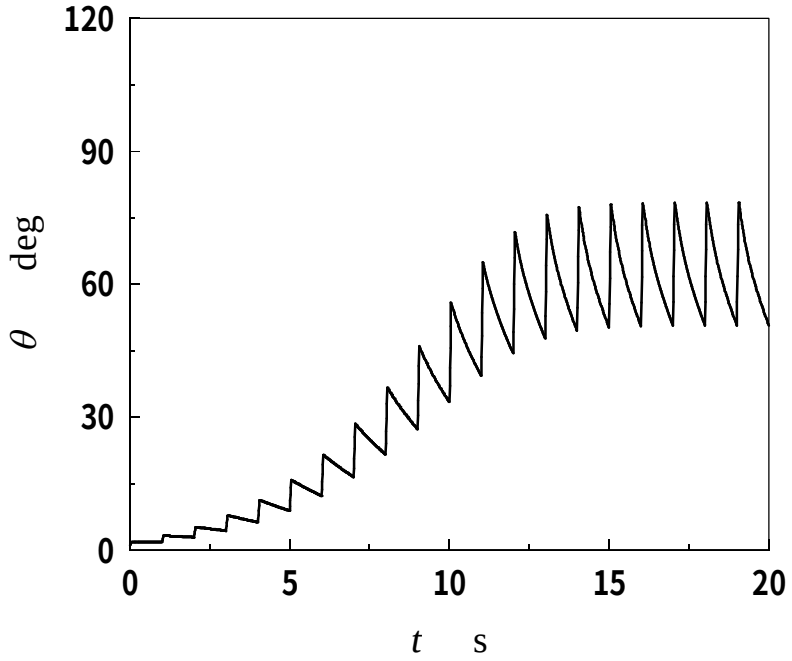

(c) Time change of the angle of the middle

Fig. 5-6 Time change of typical quantities with voltage of f = 1Hz and *Duty* = 0.05

Effect of the gap

From figure 5-7 to 5-12, we give results of time change of the velocity computed with same applied electric filed intensity of 1V/10μm and different gap of 40- 90μm, from the figures we can see, along with the increasing of the gap, from 40 to 60μm, the velocity can keep same and when the gap is larger than 70μm, the maximum of the velocity and the one after the flow reaches steady state becomes different, that is to say that the rotate angle range of the gap larger than 70μm must be over the range of 50-80 deg. Figure 5-13 shows the rotate angle range of the director in the middle of the cell, from this figure we can see that the speculation above is correct. When the gap is small, the effect of the anchoring condition can reach the director in the middle of the cell, so as the electric field is off, under the effect of the anchoring, the director can return to the initial state, so with the same frequency and ratio duty, it is easy for the smaller gap to keep the rotate angle range. But because of the change of the gap will induce the change of strength of the electric field, in order to prove the results above is caused by the change of the gap, we did another simulation which changing the magnitude of the voltage from 4V to 9V to see that change of the velocity and the rotate angle range.

Figure 5-14-5-19 give the results, from the time change of the velocity, we can see although the magnitude of the velocity is not same, but the tendency that the maximum of the velocity is kept all along is same, so we can speculate that the rotate angle ranges of all the figures are almost same and in the range of 50 – 80 deg. From figure 5-20 we can prove the correctness of the speculation.

In the last section we give an example of gap of 50μm, it is less than 60μm, below we will discuss an example of 100μm gap, through this example, we can understand the effect of the gap better. Figure 5-21 give the time change of typical quantities computed using the gap of 100μm, the applied voltage is 10V with frequency of 1 Hz and 20% duty, from the figure, we can see the difference between the maximum velocity and the value in the steady state is very large, so there is a sudden change in the moved distance of the plate. As the change of the rotate angle showing in the figure (c), we can see in the steady stage, the rotate direction of the director in the middle of the cell and the one near the plates is inverse, that is because in large cell, the effect of the anchoring condition can not reach the middle, so after the electric field is cut off, the director will suffer the effect of the velocity profile, when the twist angle is 0 deg, the profile is anti-symmetric S-shape, but the director near the plate will suffer the effect of the anchoring condition, that is rotating to return to the initial state, so the director in the middle will rotate to the diverse direction from the one near the plate. It is obviously that the rotate angle range is out of the range of 50- 80 deg.

Figure 5-22 shows the computation results of cell same as figure 5-21, but this time the frequency of the implied voltage changes to 10 Hz, we can see generally it is same as the figure 5-21except that the rotate range of the director becomes smaller and the moving of the plate becomes smoother.

Summery

From the discussion above, we can get conclusions below:

1. The flow induced by implying AC voltage is affected by the frequency, ratio duty and the magnitude of the voltage, the gap of the two plates.

2. When the gap is smaller than 60μm, we can control the rotate range of the director well, and so we can get the fast velocity of the plate, but when it is over than 60μm, the rotate range can not be controlled.

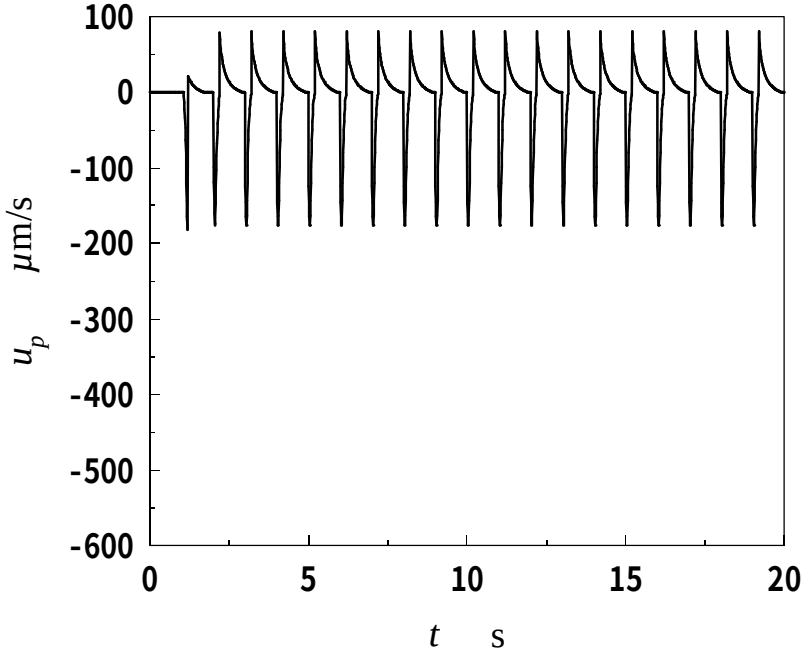

Fig. 5-7 Time change of the velocity with constant electric field (H = 40μm)

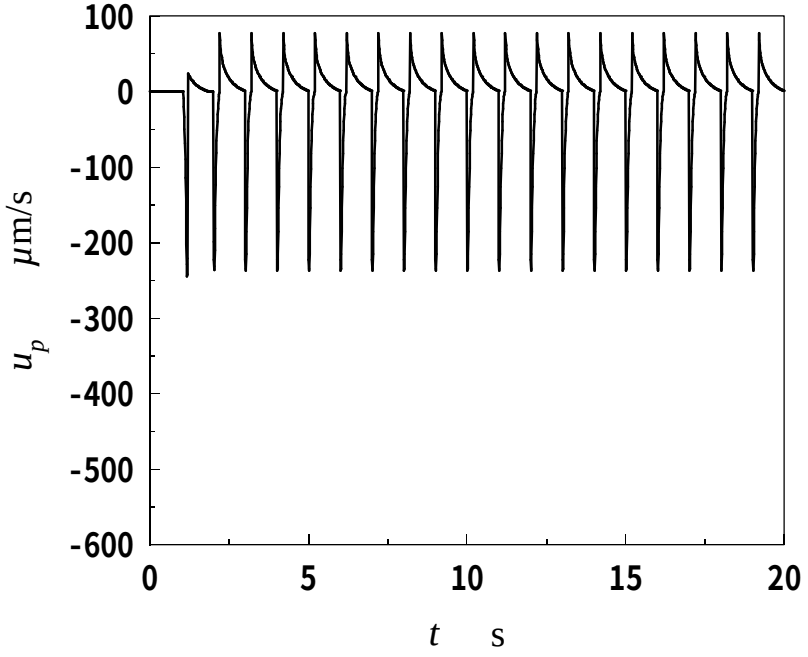

Fig. 5-8 Time change of the velocity with constant electric field (H = 50μm)

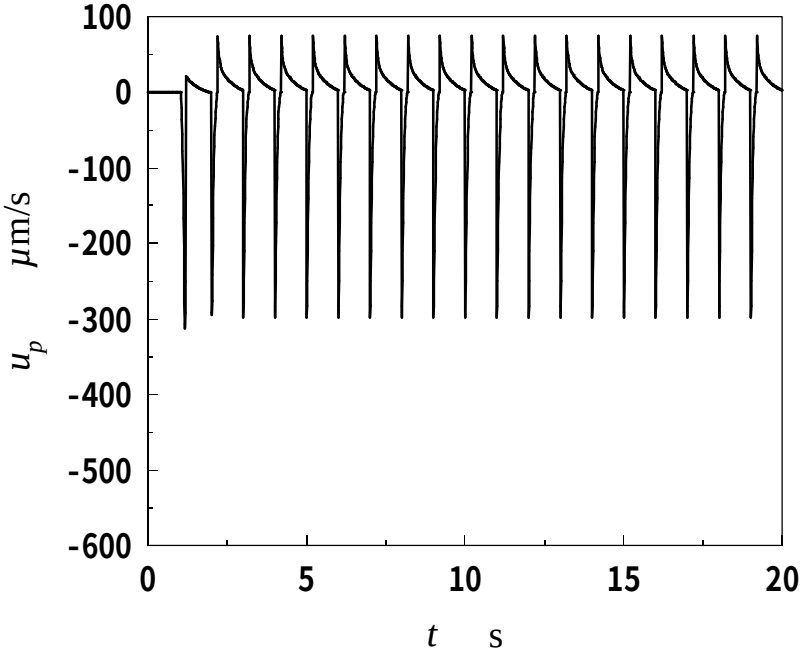

Fig. 5-9 Time change of the velocity with constant electric field (H = 60μm)

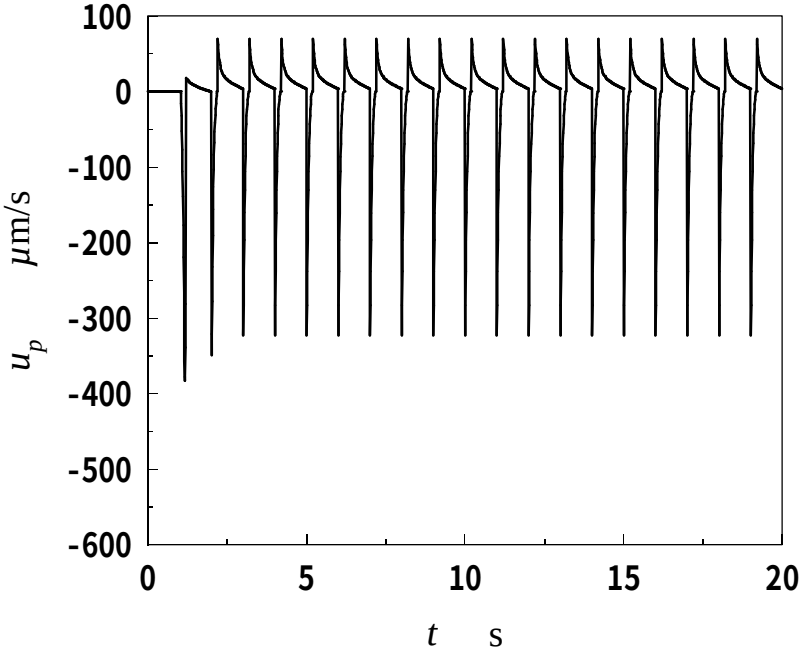

Fig. 5-10 Time change of the velocity with constant electric field (H = 70μm)

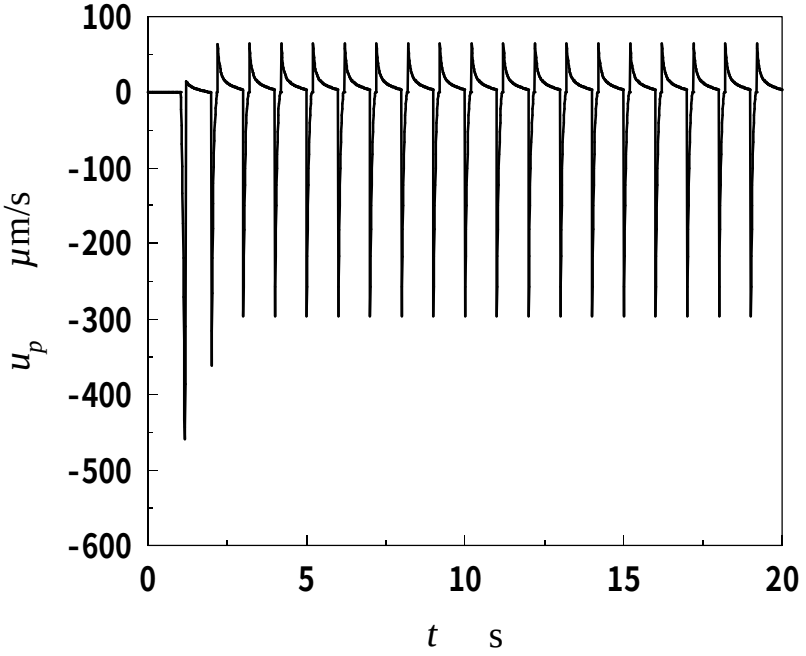

Fig. 5-11 Time change of the velocity with constant electric field (H = 80μm)

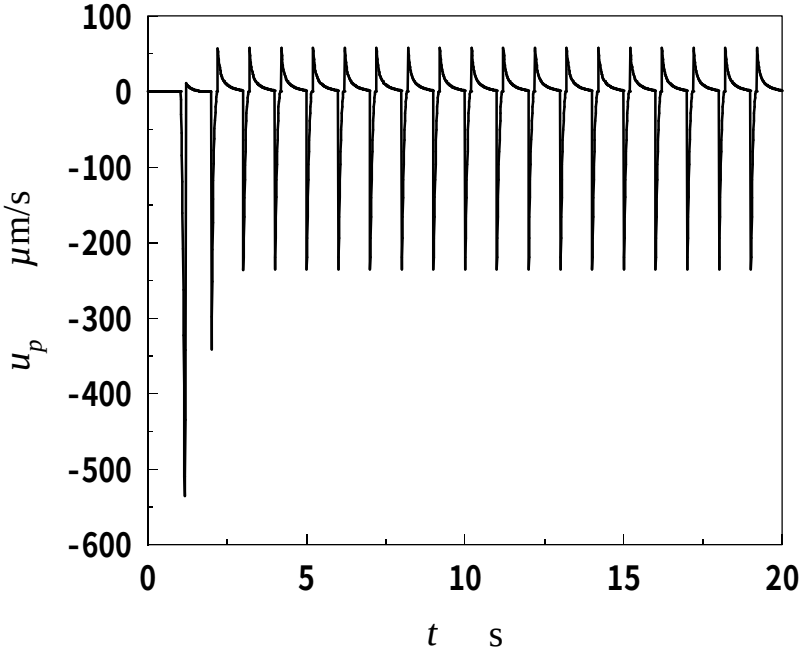

Fig. 5-12 Time change of the velocity with constant electric field (H = 90μm)

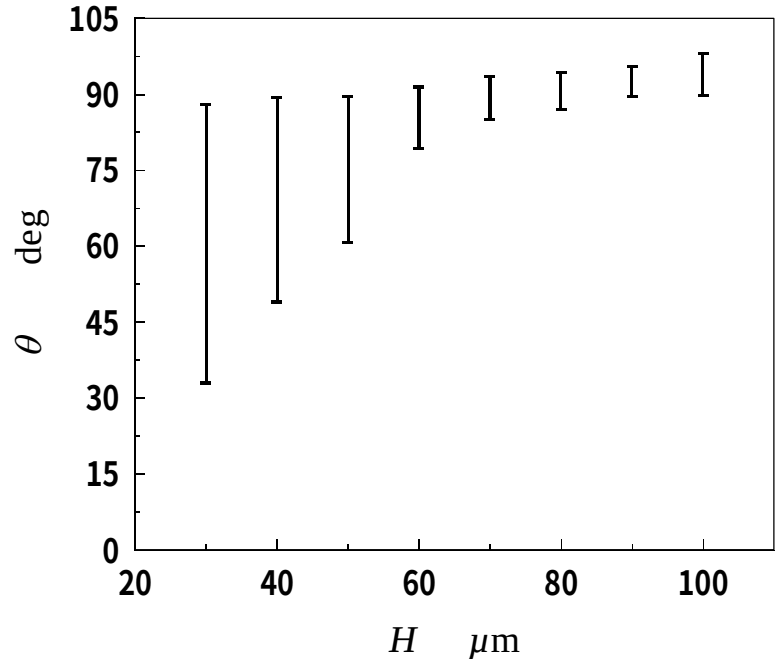

Fig. 5-13 Effect of the gap on the rotate angle range

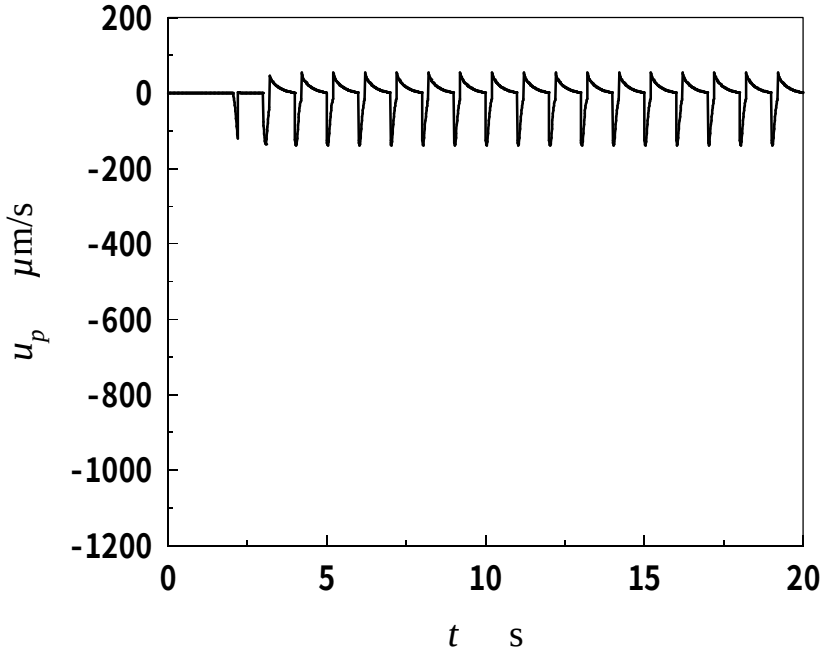

Fig. 5-14 Time change of the velocity with constant gap (E = 4V)

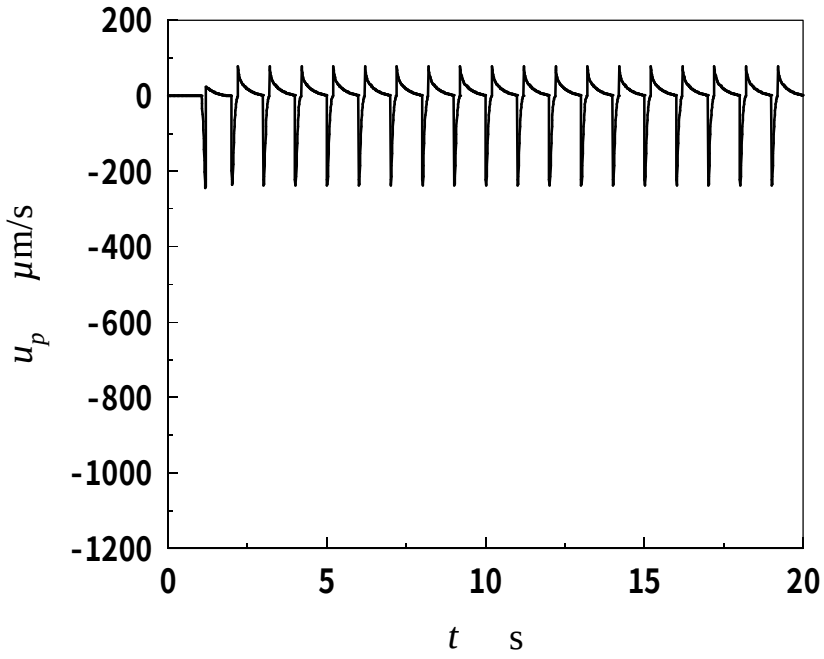

Fig. 5-15 Time change of the velocity with constant gap (E = 5V)

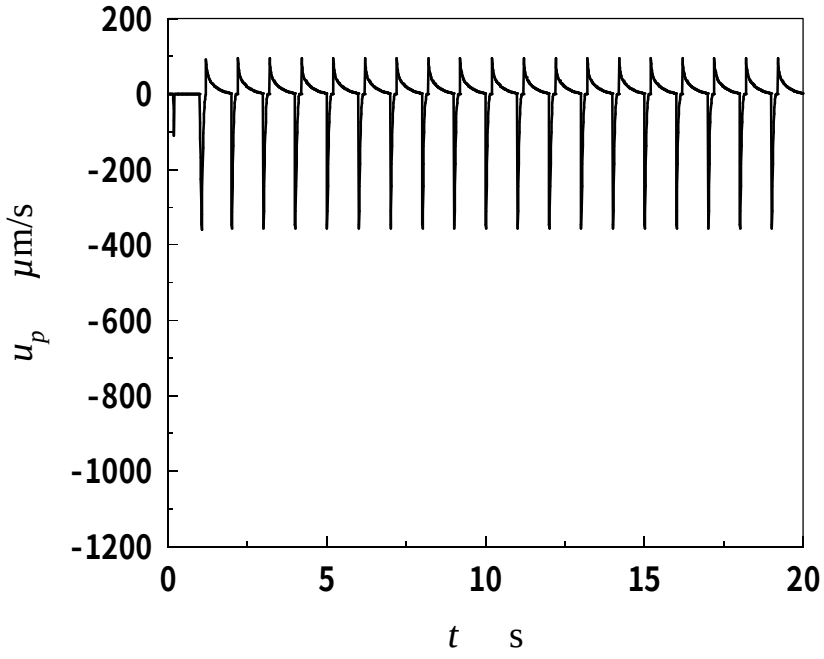

Fig. 5-16 Time change of the velocity with constant gap (E = 6V)

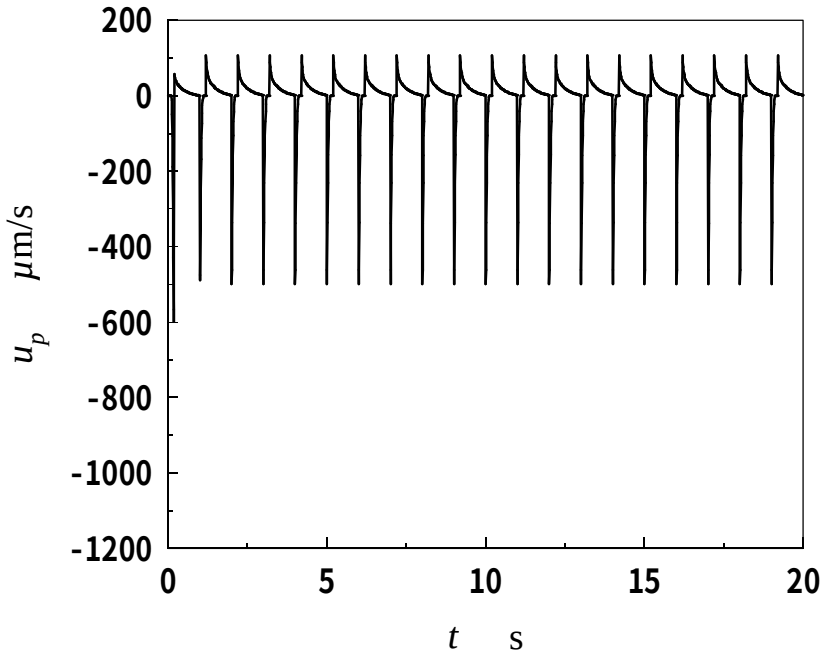

Fig. 5-17 Time change of the velocity with constant gap (E = 7V)

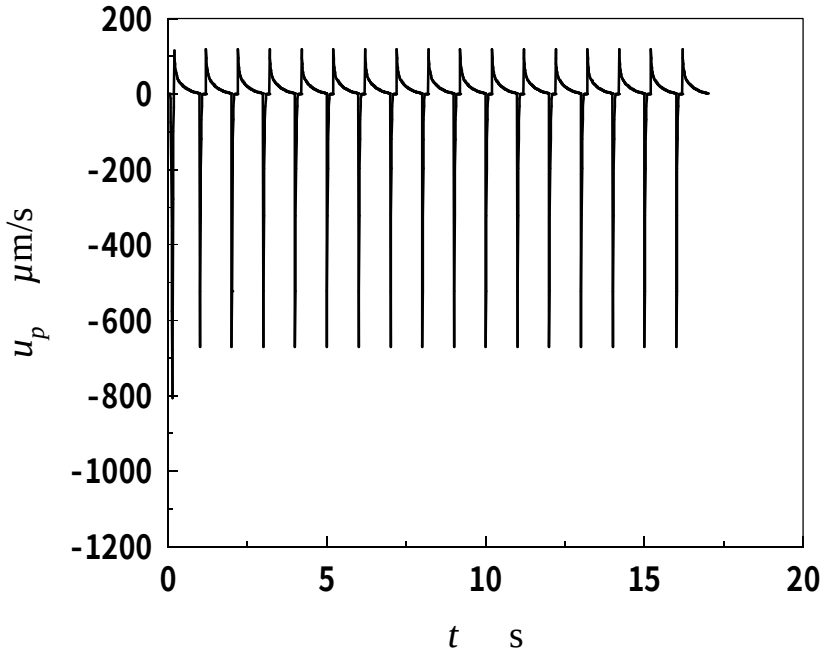

Fig. 5-18 Time change of the velocity with constant gap (E = 8V)

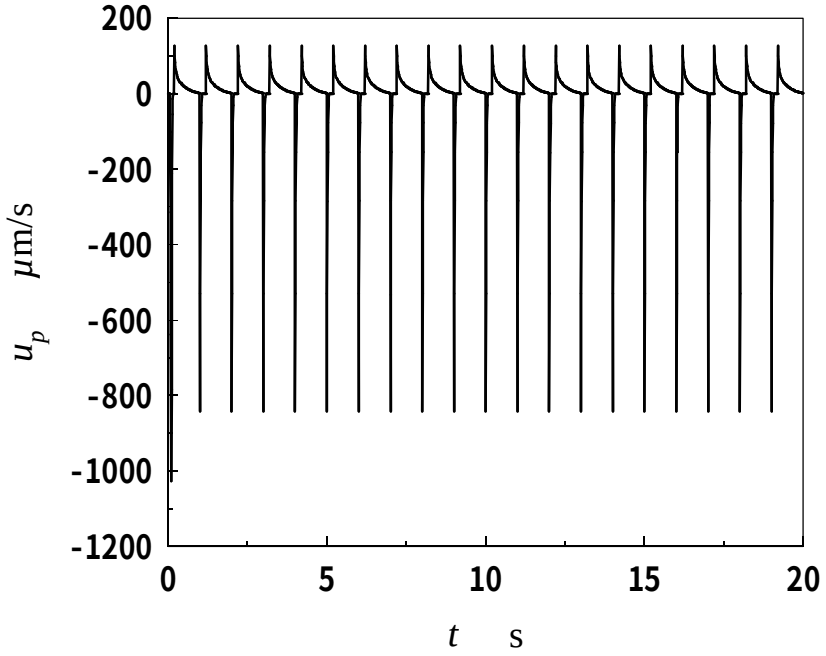

Fig. 5-19 Time change of the velocity with constant gap (E = 9V)

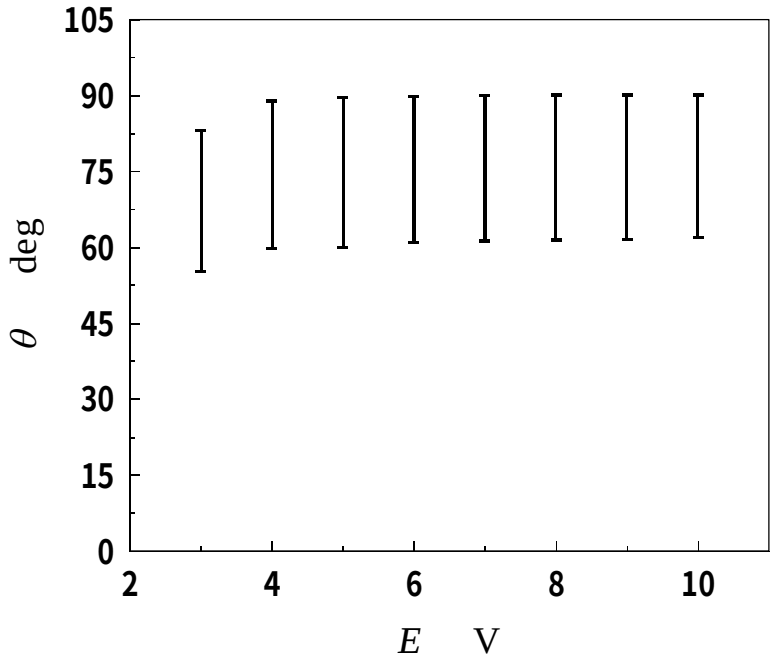

Fig. 5-20 Effect of the voltage on the rotate angle range

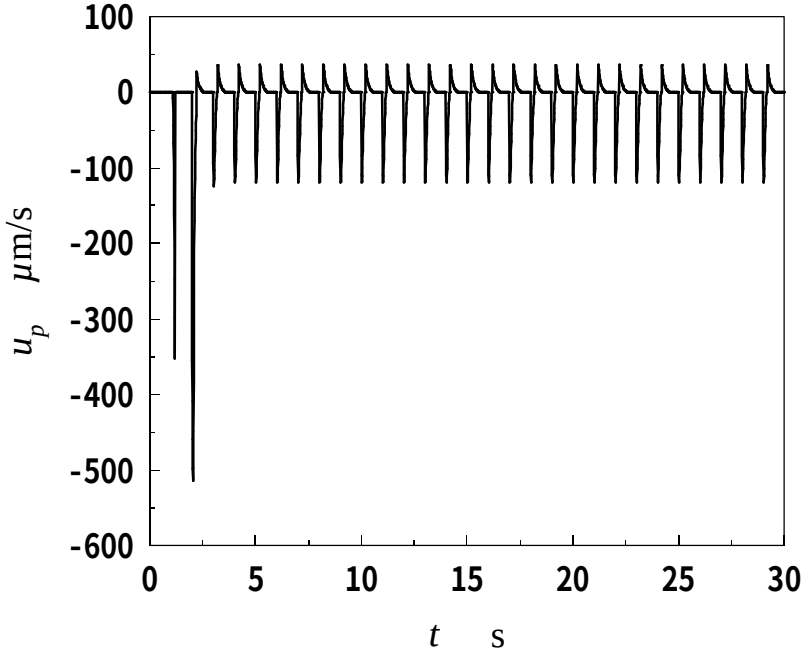

(a) Time change of the velocity

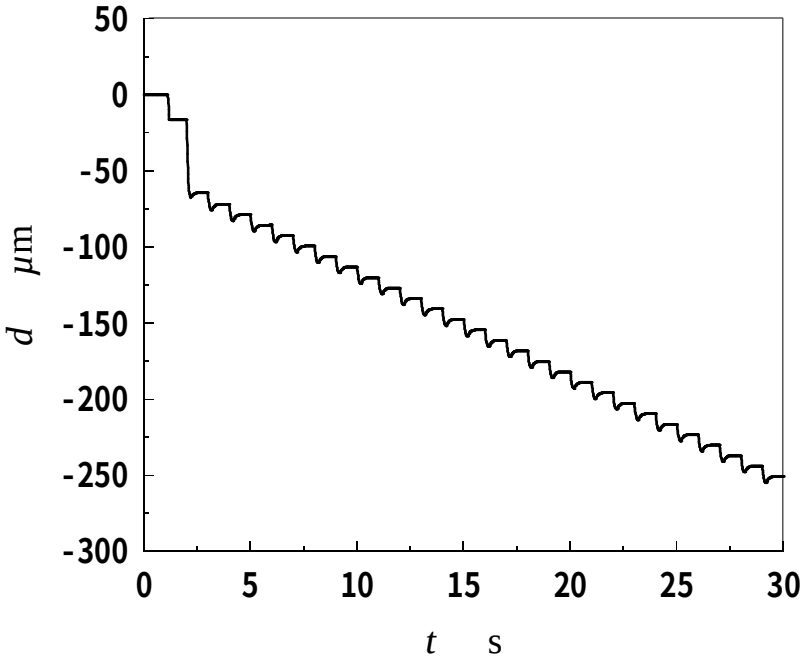

(b) Time change of the moved distance

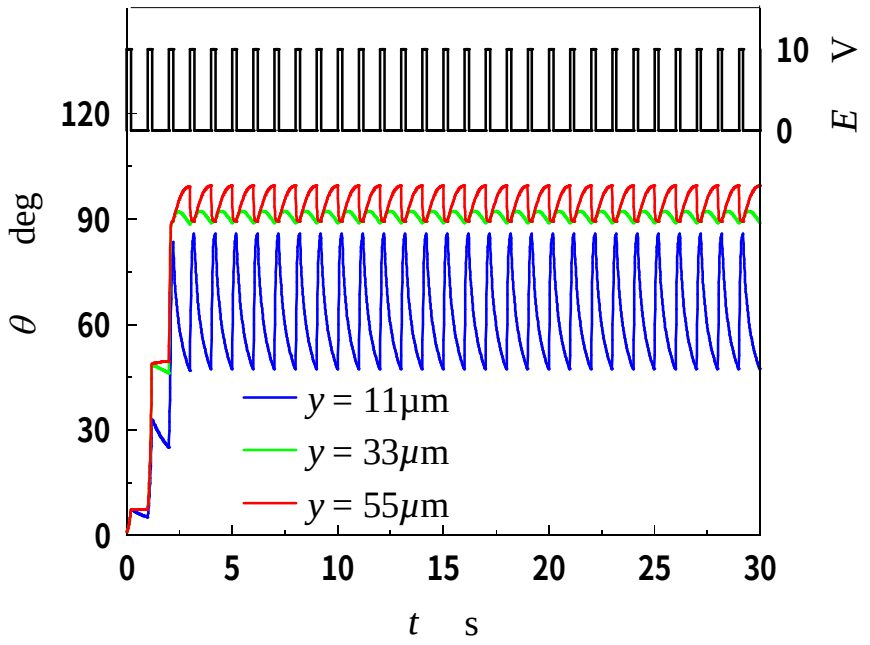

(c) Time change of orientation angle

Fig. 5-21 Time changes of typical quantities

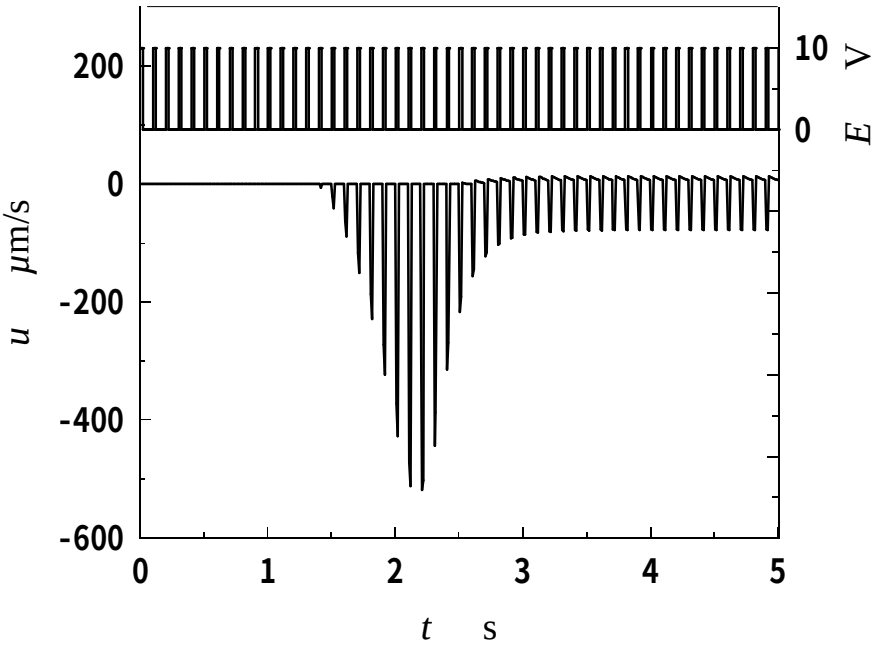

(a) Time change of the velocity

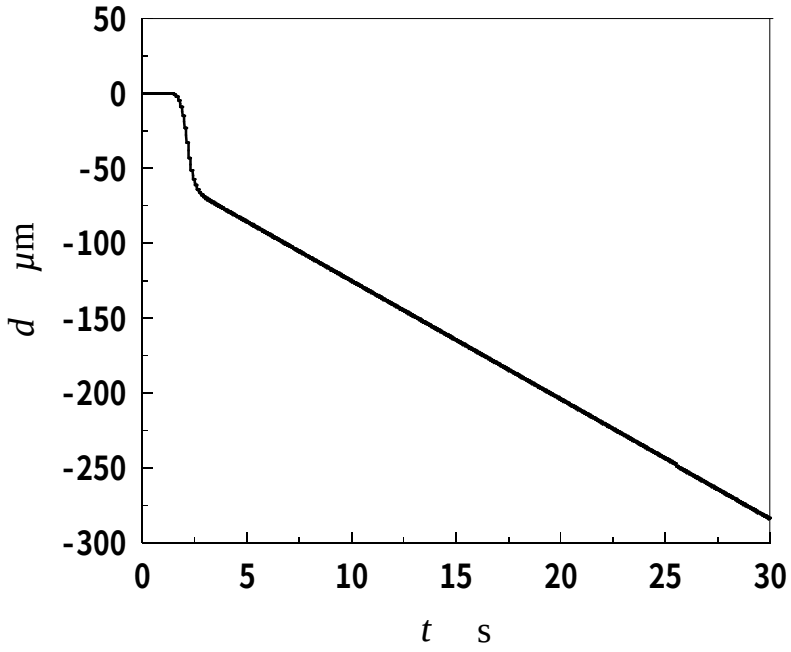

(b) Time change of the moved distance

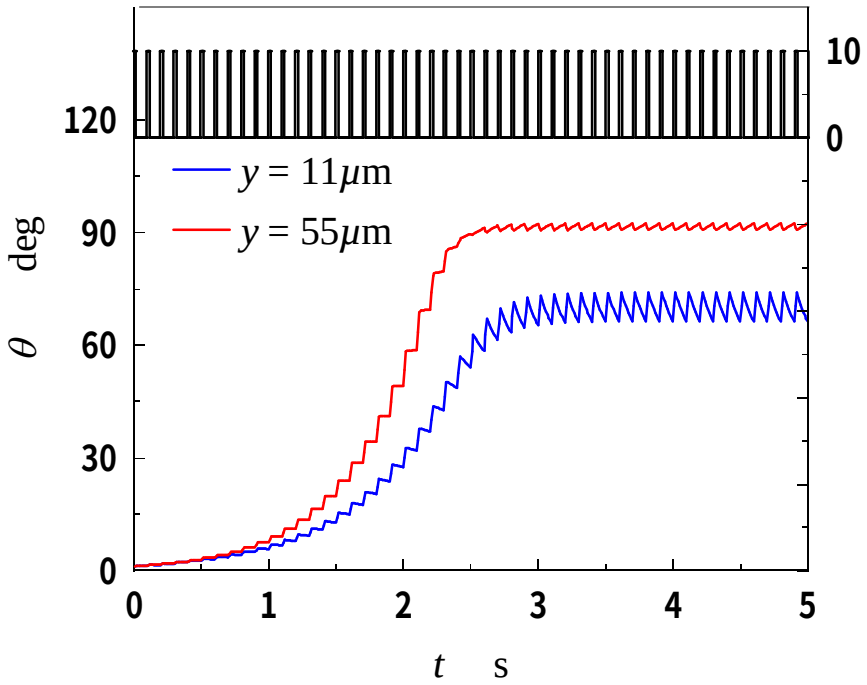

(c) Time change of the rotate angle

Fig. 5-22 Time change of typical quantities

Compare with the experimental results

Compare of the simulation and experiment results is shown in figure 5-23, both simulation and experiment were done under same initial conditions of gap 110 μm, voltage 10V with 1 Hz frequency and 20% ratio duty, we can see that the simulation result is in agreement with the experimental result.

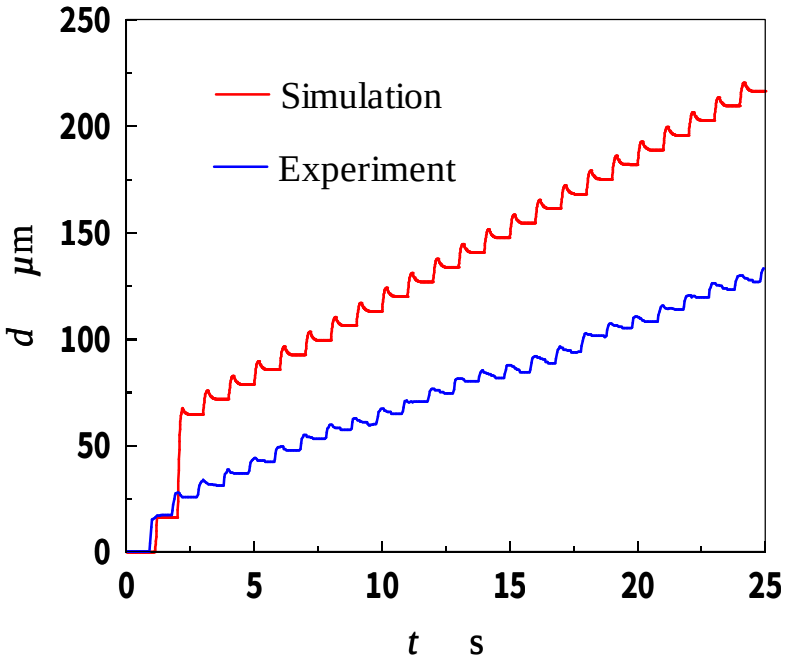

Fig. 5-23 Contrast of the simulation and experiment results

Chapter 6: Conclusions

We propose novel micro-actuators driven by liquid crystalline materials. Because of the fluidity of liquid crystals, there is no constraint on size and shape of the liquid crystalline actuators. To design and develop an optimized actuator, fundamental researches are required. In this dissertation, as fundamental research to develop the micro-actuator, transient behaviors of a nematic liquid crystal between two parallel plates under an electric field have been investigated numerically by using the Leslie-Ericksen theory as a constitutive equation. Applied voltage, gap of the plates, and twist and tilt angles have been selected as computational parameters. We have used the Crank-Nicolson scheme for the time integration, and a finite difference scheme for spatial discretization. The material constants, such as viscosity coefficients, elastic constants, and dielectric constants of 5CB (4-n-pentyl-4'- cyano-biphenyl) have been employed in this computation.

Imposition of an electric field on a liquid crystal induces flow (so called back-flow), whose profile and magnitude depend strongly on the twist angle of the director; when the twist angle is 0 deg, the induced flow is planar and the velocity profile between plates is S-shaped and anti-symmetric with respect to the center plane of the two plates. With increasing the twist angle, the flow has an out of plane component, and finally the profile becomes unidirectional when the twist angle reaches 180 deg.

With the increment of the applied voltage, the shear stress acting on the plate, the velocity, and the flow rate are increased and the response is improved. The effect of the gap of the plates is large; when the gap is reduced to 5 μm, for example, the response is so high that the physical quantities become maxima within a couple of milliseconds. However, if the electric field intensity is kept constant, the effect of the gap is negligible. The tilt angle has comparatively little effect.

In order to develop actuator, it is necessary to induce continuous flow with liquid crystal, and the simplest way to take the force out of the liquid crystal is through the bounding plate, so as a next step, one of the plates of the cell is set to be free, thus the upper plate will move freely when the induced liquid crystalline flow shear stress is exerted on it. In addition to this, this time, we use AC power supply in stead of the DC one in the last step, from the results it can be say that the upper plate is driven to move continuously by the induced liquid crystalline flow, and by controlling the frequency and ratio duty of the AC power supply, the smooth moving of the upper plate can be

achieved. When the gap is smaller than 60 μm, the rotate angle range of the director can be controlled by the selecting parameters such as the voltage, the frequency, etc, but in the case the gap is larger than 60μm, it is impossible to do this.

It is found from the results obtained in this study that liquid crystalline micro-actuators with arbitrary characteristics can be developed by controlling properly applied voltage, size of actuators, and anchoring conditions.

Reference

1. S.Chandrasekhar, Liquid Crystals (second edition), Cambridge University Press 1992
2. Ronald G. Larson, The structure and Rheology of Complex Fluids, Oxford University Press, 1999
3. Matsumoto, S. and Tsunoda, I., Liquid crystals fundamentals and applications, (1996), p. 1, Kogyo Chosakai
4. Koyama, K. ed., Development of electro-rheological (ER) fluids, (1999), CMC
5. Tsuji, T. and Chono, S., Numerical simulation of nematic liquid crystalline flow between parallel plates under a magnetic field, Transactions of the Japan Society of Mechanical Engineers, Series B, Vol.69, No.688(2003) pp.2649-2656
6. Brochard, F., Backflow effects in nematic liquid crystals, Mol. Cryst. Liq. Cryst., Vol. 23 (1973), pp. 51-58
7. Berreman, D.W., Liquid-crystal twist cell dynamics with backflow, J.Appl. Phys., Vol. 46 (1975), pp. 3746-3751
8. Daniel Lhuillier and Alejandro D. Rey, Nematic liquid crystals and ordered micropolar fluids, J. of Non-Newtonian Fluid Mechanics, Volume 120, Issues 1-3, 1 July 2004, pp. 169-174
9. Riger G. Gilbertson and John D. Busch, A Survey of Micro-Actuator Technologies for Future Spacecraft Missions, The Jounral of the British Interplanetary Society, Vol. 49, pp. 129-138, 1996
10. Chono, S. and Tsuji, T., Development of Micro-actuators Driven by Liquid Crystals, Transactions of the Japan Society of Mechanical Engineers, Series B, Vol. 75, No. 715(2006), pp.96-101(in Japanese)
11. C.W. Oseen, Trans, Raraday Soc., 29, 883 (1933)
12. H. Zöcher, Trans, Faraday Soc., 29, 945 (1933)
13. F. C. Frank, Disc. Faraday Soc., 25, 19 (1958)
14. A. Anzelius, Uppsala Univ. Arsskr., Mat. Och Naturvet, 1, (1931)
15. J. L. Ericksen, Arch. Rational Mech. Anal., 4, 231 (1960)
16. J. L. Ericksen, Trans. Soc. Rheol., 5, 23 (1961)
17. F. M. Leslie, Quart. J. Mech. Appl. Math., 19, 357 (1996); Arch. Rational Mech. Anal., 28, 265 (1968); Advances in Liquid Crystals, Vol. 4 (ed. G. H. Brown), p.1 Academic, New York (1979)
18. Leslie, F.M., Some constitutive equations for liquid crystals, Arch. Ration. Mech. Anal., Vol. 28 (1968), pp. 265-283

19. Karat, P.P. and Madhusudana, N.V., Elasticity and orientational order in some 4'-n-alkyl-4-cyanobiphenyls, Mol. Cryst. Liq. Cryst., Vol. 49 (1977), pp. 239-245
20. de Gennes, P. G. and Prost, J., The physics of liquid crystals, 2nd ed., (1993), p. 1, Oxfor Clarendon Press
21. Hieber C A and Shen S F, A finite-element/finite-different simulation of the injection-molding filling process, *J. Non-Newtonian Fluid Mech.* 1982, **7**1–32
22. M.J.Crochet, A.R.Davies, and K.Walters, Numerical simulation of Non-Newtonian flow, 1984, ELSEVIER SCIENCE B.V
23. Fehlberg, E. 1969 Low-order Classical Runge-Kutta Formulas with Stepsize Control and Their Application to Some Heat Transfer Problems, NASA Technical Report, NASA TR R-315
24. Numerical Methods Natural Sciences Tripos 1B Lecture Notes Lent Term 1998, Lecture Notes: http://www.damtp.cam.ac.uk/user/fdl/people/sd103/lectures/
25. Editors for handbook of liquid crystals, Handbook of liquid crystals, (2000), pp. 209, Maruzen.
26. Shigeomi CHONO and Tomohiro TSUJI. Computer simulation of flow and defect of nematic liquid crystal, EKISHO(in Japanese), Vol. 3, N0.2, 1999, 107-116
27. Marifi Güler, Symbolic evaluation of the Ericksen-Leslie equations in the computation domain, J. Non-Newtonian Fluid Mech., 52 (1994) pp.309-321
28. Chono, S. Tsuji, T. and Denn, M. M., Spatial development of director orientation of tumbling nematic liquid crystals in pressure-driven channel flow, J.Non-Nertonian Fluid Mech., Vol. 79(1998), pp. 515-527
29. Jianjun Tao and James J. Feng, Effects of elastic anisotropy on the flow and orientation of sheared nematic liquid crystals, J. Rheol. 47~4!, 1051-1070 July/August ~2003
30. Joe F. Thompson, Z. U. A. Warsi, and C. Wayne Mastin, Numerical Grid Generation: Foundations and Applications, 1985, Elsevier Science Publishing Co., Inc.
31. Rey, A.D. and Denn M.M., Jeffrey-Hamel flow of Leslie-Ericksen nematic liquids, J.Non-Newtonian FluidMech., Vol. 27(1998), pp.375-401
32. Rong-Yeu Chang, Fu-Chia Shiao, and Wen-Lii Yang, Simulation of director orientation of liquid crystalline polymers in 2-D flows, J. Non-Newtonian Fluid Mech., 55 (1994) pp.1-20
33. J.N. Baleo, M. Vincent, and P. Navard, Finite-element simulation of flow and director orientation of viscous anisotropic fluids in complex 2D geometries, J. Rheol. 36 (4), May 1992, pp.663-701

34. Kneppe, H., Schneider, F. and Sharma, N. K., Acomparative study of the viscosity coefficients of some nematic liquid crystals, Ber. Bunsenges. Phys. Chem., Vol. 85 (1981), pp. 784-789
35. Ericksen, J. L., Anisotropic fluids, Arch. Ration. Mech. Anal., Vol. 4 (1960), pp.231-237
36. Tomas Carlsson and Christian Högfors, Theoretical analysis of the stability of shear flow of nematic liquid crystals with a positive Leslie viscosity α_3, J. of Non-Newtonian Fluid Mechanics, Volume 119, Issues 1-3, 1 May 2004, pp. 25-37
37. Chono, S., Tsuji, T. and Denn, M.M., Numerical simulation of planar contraction flow of nematic liquid crystals, Transactions of the Japan Society of Mechanical Engineers, Series B, Vol. 60, No. 574(1994), pp.1944-1950
38. M. Cengiz Altan, S. Subbiah, Selcuk I. Gücerl and R. Byron Pipes, Numerical Prediction of three-dimensional fiber orientation in Hele-Shaw flows, Polym. Eng. Sci., July 1990, Vol 30, No. 14, pp.848-859
39. Alejandro D. Rey and Morton M. Denn, Analysis of converging and diverging flow of nematic liquid crystal polymers, Mol. Cryst. Liq. Cryst., 1987, Vol. 153, pp. 301-310
40. C.L. Choy, W.P. Leung and K.W. Kwok, Thermal diffusivity of an injection-moulded liquid crystalline polymer by flash radiometry, Polym. Commun. 1991, Vol. 32, No. 9, pp 285-288
41. I. Heynderickx, W. Potze, E.J.W. Ter Maten, Influence of a temperature gradient on the simple shear flow of a nematic liquid crystal, J. Non-Newtonian Fluid Mech., 55 (1994) pp.137-161.
42. Suresh G. Advani, Flow and rheology on polymer composites manufacturing, 1994, ELSEVIER SCIENCE B.V.
43. XuefengWang, Jonathan Engel and Chang Liu, Liquid crystal polymer (LCP) for MEMS: processes and applications, J. Micromech. Microeng. 13 (2003) pp.628–633
44. Chono, S. and Tsuji, T., Liquid crystal flow forming mechanism, method of forming same, and object moving mechanism using liquid crystal flow, Japan Patent No.3586734 (Aug. 20, 2004)
45. A. M. Sonnet, P. L. Maffettone and E. G. Virga, Continuum theory for nematic liquid crystals with tensorial order, J. of Non-Newtonian Fluid Mechanics, Volume 119, Issues 1-3, 1 May 2004, pp. 51-59

Acknowledgments

It is my great honor to give my super thanks to my supervisor Professor Shigeomi Chono for his continuous support in the Ph.D. program. Professor Chono is always there to listen and give me advices, not only on research but also on life. And a special thanks goes to my co-supervisor Professor Tomohiro Tsuji, who is very responsible for helping me to become a real doctor.

Besides my supervisors, I would like to thank all the members in our lab for the help on my research and Japanese study.